Development and metamorphosis in the male pedipalp of the cob-web spider *Parasteatoda tepidariorum.*

Dissertation

for the award of the degree

"Doctor rerum naturalium" (Dr.rer.nat.)

of the Georg-August-Universität Göttingen

within the doctoral program Grundprogramm Biologie

of the Georg-August University School of Science (GAUSS)

submitted by

Felix Simon Christian Quade

from Husum

Göttingen 2019

für meine Familie

Thesis Committee

Prof. Dr. Nikola-Michael Prpic-Schäper,
Justus-Liebig-Universität Gießen, AG Zoologie mit Schwerpunkt Molekulare Entwicklungsbiologie, Institut für Allgemeine und Spezielle Zoologie

Prof. Dr. Ernst Wimmer
Abteilung Entwicklungsbiologie, Johann-Friedrich-Blumenbach-Institut für Zoologie und Anthropologie

Members of the Examination Board

Reviewer:

Prof. Dr. Nikola-Michael Prpic-Schäper

Justus-Liebig-Universität Gießen, AG Zoologie mit Schwerpunkt Molekulare Entwicklungsbiologie, Institut für Allgemeine und Spezielle Zoologie

Second Reviewer:

Prof. Dr. Ernst Wimmer

Abteilung Entwicklungsbiologie, Johann-Friedrich-Blumenbach-Institut für Zoologie und Anthropologie

Further members of the Examination Board:

Prof. Dr. Tim Salditt
Institut für Röntgenphysik

Dr. Wiebke Möbius
Abteilung Elektronenmikroskopie, Max-Planck-Institut für Experimentelle Medizin

Prof. Dr. Christoph Bleidorn
Abteilung Evolution und Biodiversität der Tiere, Johann-Friedrich-Blumenbach-Institut für Zoologie und Anthropologie

Dr. Sven Bradler
Abteilung Evolution und Biodiversität der Tiere, Johann-Friedrich-Blumenbach-Institut für Zoologie und Anthropologie

Date of oral examination:

Declaration

Herewith I ensure, that the thesis “Development and metamorphosis in the male pedipalp of the cob-web spider *Parasteatoda tepidariorum*” has been written independently and with no other sources and aids than quoted.

Felix Quade

Publications that are part of this thesis:

Quade, F.; Preitz, B.; Prpic-Schäper, N.-M. (2018): A perforated anodised aluminium slide for improved specimen clearing and imaging for confocal laser scanning microscopy. BMC Research Notes, 11, 716.

Töpperwien, M.; Krenkel, M.; **Quade, F.**; Salditt, T. (2016): Laboratory-based x ray phase-contrast tomography enables 3D virtual histology, Proceedings of SPIE, 9964, 99640I.

“When the going gets weird,

the weird turn pro”

Hunter S. Thompson

Dankssagung

Mit dem Ende meiner Doktorarbeit möchte ich mich bei einer großen Anzahl an Menschen aufrichtig für ihre Hilfe und Unterstützung bedanken. Ohne euch wäre diese Arbeit nicht möglich gewesen.

Als Erstes möchte ich meinem Doktorvater Nikola-Michael Prpic-Schäper danken, dass er mich Morphologen in sein Team aufgenommen hat. Danke für die Freiheit und das Vertrauen in mich, sodass ich meine Projekte und Kollaborationen selbständig und eigenverantwortlich gestalten konnte, aber stets Unterstützung bekam, wenn ich sie benötigte. Ich hatte immer das Gefühl, dass meine Arbeit wertgeschätzt wird. Ich schätze Dich, als Person und Wissenschaftler, sehr.

Tim, ohne deine Unterstützung hätte ich meine Doktorarbeit nicht durchführen können. Du hast mit dem Institut für Röntgenphysik ein wahrlich interdisziplinäres Institut geschaffen. Deine Motivationsfähigkeit und Dein umfassendes Wissen haben mich außerordentlich beeindruckt. Ich danke auch Mareike, Martin, Marina und Jasper für ihre großartige Hilfe bei meinen Tomografie Experimenten.

Danke an das komplette Lab 2, ich habe meine Zeit bei euch unglaublich genossen. Natascha, Nico, Beate, Micael, Montse und Elisa ich kann von euch nicht mehr nur als Kollegen sprechen, sondern empfinde euch als Freunde. Ihr habt mich herzlich aufgenommen und auch in schwierigen Zeiten ein Ohr und gute Ratschläge für mich gehabt. Danke Dir Nico, für Deine unglaublich herzliche Art und Deinen Einsatz, dieses Labor zu einem großartigen Arbeitsplatz zu formen. Beate, danke für das viele Wissen, Dein Vertrauen in mich und deine Unterstützung.

Ich danke Ernst Wimmer und Gregor Bucher für eine sehr angenehme Arbeitsatmosphäre, die sie in unserer Abteilung geschaffen haben. Sie haben in meinen Progress Reports durch kritische Fragen und Diskussion der präsentierten Ergebnisse dafür gesorgt meine Projekte aus einem anderen Blickwinkel zu betrachten. Zudem habe ich stets genossen mit ihnen interessante und zum Teil aufgeheizte Diskussionen und Gespräche zu führen.

Zudem möchte ich mich bei allen Mitgliedern der Abteilung, unseren Technische Assistenten, den Gruppenleitern und den ehemaligen wie derzeitigen Doktoranden und Studenten dafür bedanken, dass es immer ein harmonisches Umfeld gab und ich immer sofort Unterstützung erhielt. Ich habe großartige Kollegen kennengelernt und dafür bedanke ich mich. Felix, Max, Elisa, Micael, Dominik, Hassan, Kolja, Dippel, Janna, Montse, Beni, Saleem, Ting, Beate, Nico, Niko, Sigrid, Dhaval, Benni, Christoph Vera, Schorsch, Musa, Attika, Bicheng, Yongang, Elke, Claudia,

Helma, Marita, Katrin, Birgit, Bettina und Merle, auch euretwegen bin ich wirklich gerne zur Arbeit gekommen. Auch möchte ich mich bei meinen beiden Bachelorstudentinnen Jana und Inna bedanken. Ihr habt einen super Job gemacht.

Wiebke, Torben und EM-Team, ihr habt im MPI-EM eine wirklich unglaublich großartige Facility aufgebaut. Ich bin euch für eure stets unkomplizierte Hilfe, die gute Zeit, die ich bei jedem Besuch bei euch hatte und dafür, dass ich eure großartige Infrastruktur so frei nutzen konnte, sehr dankbar.

Ein Riesendank geht an meine Freunde. Eure Freundschaft und Liebe und die großartige Zeit, die wir miteinander verbringen bedeutet mir unglaublich viel und war eine Quelle für Kraft, ohne die ich es nicht geschafft hätte. Tascha, Fothi, Erik, Gregor, Dirk, Luke, Hannes, Hendrik, Arne, Dani, Patrick, Fränze, Peter, Johanns und die Rostetaler, ihr seid die größten.

Als letztes möchte ich meiner Familie und meiner Partnerin Rosi bedanken. Ihr habt stets meine Neugier und meine Wissbegierde gefördert, habt mich unterstützt und getröstet, wenn es schwere Zeiten gab und euch mit mir gefreut und gefeiert. Ich durfte immer ich sein und habe mich immer geborgen gefühlt. Ihr habt euch die größte Mühe gegeben mir die Welt als einen großartigen, spannenden Ort zu zeigen und mir das Handwerkszeug dafür gegeben mich darin frei zu bewegen. Eure bedingungslose Liebe hat mich getragen und groß gemacht. Anne, Dieter, Martin, David, Marianne, Hans, Heiko, Edelgard, Gustav und ganz besonders Rosi, ohne euch wäre ich nicht wer ich bin.

Table of Contents

1. Summary

Tracing from marine ancestors, spiders have adapted to a terrestrial lifestyle independent from the insects. Many of the adaptations of spiders to life on land involve the shape and function of their appendages. From these appendage modifications, the transformation of the tarsal tip of the male pedipalp into an intromittent organ, the bulbus organ, is particularly interesting. Being an autapomorphy for spiders (*i.e.* a distinctive feature that is unique to a given taxon) the bulbus' role as intromittent organ for sperm transfer on land accounts for a large part of their evolutionary success. My research on the adult morphology and development of the bulbus organ of the theridiid spider model *Parasteatoda tepidariorum* has answered fundamental questions. It was confirmed that the adult bulbus is built up in a tripartite way, as described by Agnarsson and colleagues (2007). It is built of the subtegulum, tegulum and the embolic section which are connected through membranes, the haematodochae. The embolic section gives rise to the sclerites which are involved in the connection and penetration of the female during the copulatory act. The hitherto existing homology statements for two sclerites were corrected and the correct terms discussed. Furthermore, an innervation was found and a sensilla, which appears to be similar to that in the bulbus of *Philodromus cespitum* (Sentenská et al. 2017). The data on the development showed that the bulbus originates in the claw fundament and its primordium is already built in the stage before the penultimate moult. Through a newly discovered mechanism tibia and cymbium are built from scratch which involves coagulation of haemolymph and reorganisation of the coagulated material by histoblast-like cell clusters. Together these findings clearly show that a comprehensive analysis of the morphology over its ontogenesis yields deep insights. However, at the same time new questions arose which now must be answered with future research endeavours.

2. General Introduction

Sex on land is a complicated thing.

The origin of multicellular animals, the metazoa, began in the vast oceans. One major transition driving their evolution was the development of two sexes, males and females. The existence of sexes, referred to as anisogamy, is based on the presence of unequally sized gametes, *i.e.* bigger eggs holding most of the nutrition for the embryo and smaller sperm containing almost only genetic material (Parker et al. 1972; Parker 1984; Hoekstra 1987; Parker 2011). For fertilization it is essential that these two gametes meet and fuse to form the zygote. In marine habitats this process is much easier than on land. Because seawater is isotonic for gametes and zygotes of primary marine living organisms (Lasker and Theilacker 1962), they do not need special protection from osmotic pressure or desiccation. Thus, gametes can directly be released into the water, to disperse and fertilize externally, referred to as spawning. Sessile animals that live in colonies (*e.g.* corals), solely need to find common cues to arrange the time points of gamete release, *e.g.* dusk on a full- or new-moon night or signals transferred through water, like pheromones. In contrast, mobility allows males and females to meet each other in pairs or spawning groups. A prerequisite for successful terrestrialization and permanent conquest of more arid habitats was the entire uncoupling of their sexual reproduction from water bodies and therefore the protection of their gametes from the environment. Diverse mechanisms for internal fertilization and protected sperm transfer evolved, for example a sealed sperm package, the so called spermatophore, or via an intromittent organ, *i.e.* a structure that transfers the sperm directly into the female.

Arachnida have evolved a plethora of sperm transfer modes

The diversity and disparity of Arthropods with millions of species and various body forms is unrivalled in the animal kingdom. With their segmented body, protected by an outside armour made of chitin, and paired jointed appendages they are the evolutionary most successful group of animals. This success arose, among other things, through the ability to evolve a plethora of tools from their appendages allowing adaptation to almost every habitat (Angelini and Kaufman 2005; Prpic and Damen 2008).

Within the Arthropoda, the Chelicerata comprise the second largest group with around 120.000 described species (Sharma 2018). Arising out of the Chelicerata, with the sea living sea spiders (Pycnogonida) and horseshoe crabs (Xiphosura) as sister groups, the land living Arachnida comprises famous predators like scorpions (Scorpiones) and spiders (Araneae), blood sucking parasites and important disease vectors like ticks (Parasitiformes), the agricultural and medically important mites (Acariformes), the harvestmen ambiguously called daddy longlegs (Opiliones) and the less known but enigmatic taxa like sun spiders (Solifugae), whip scorpions or vinegaroons (Uropygi), short-tailed whipscorpions (Schizomida), whip spiders or tailless whip scorpions (Amblypygi), pseudoscorpions (Pseudoscorpiones) and hooded tickspiders (Ricinulei). Despite much progress through paleontological and molecular data analysis in the last years the number of convergent terrestrialization events is still under debate, Furthermore, the phylogenetic relationships of the different orders within this class, still not resolved (Dunlop and Webster 1999; Sharma et al. 2014; Sharma 2018).

With the conquest of land the Arachnida evolved a plethora of different sperm transfer modes, which can be roughly discriminated into three types; Type I: Indirect spermatophore transfer with pair formation (Acariformes, Pseudoscorpiones, Schizomida, Scorpiones, Amblypygi and Uropygi); Type II: Indirect spermatophore transfer without pair formation (Acariformes, Pseudoscorpiones); and Type III: Direct sperm(atophore) transfer (Opiliones, Acariformes, Ricinulei, Araneae, Solifugae, Parasitiformes) (Thomas and Zeh 1984). Whereas type I represents the ancestral mode from which the others evolved, type III is especially interesting concerning evolution of appendage modification, because this type convergently evolved many different intromittent organs, ranging from a real penis in harvestmen to diverse conversions of walking legs and mouthparts to transfer sperm in spermatophores or fluids.

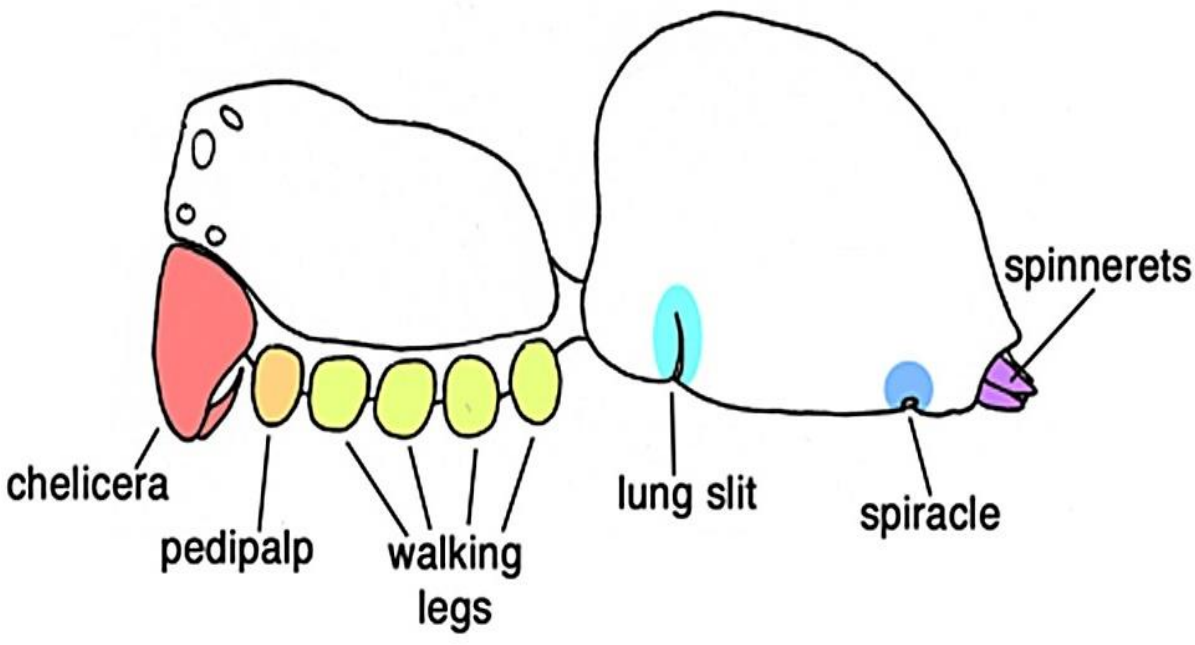

Figure 1: Body plan of a higher spider, lateral view. Prosoma containing six appendage pairs, the chelicerae (red), pedipalps (orange) and four pairs of walking legs (yellow). The Opisthosoma bears the internalized book lungs (their postion is only visible by a slit (turquoise)), the opening of the thrachea system, the spiracle (blue) and the spinnerets (pink). Leg-like appendages have been omitted for better oversight. Modified after Pechmann et al. 2010

The bulbus organ of spiders is unique

With currently almost 50.000 described species (World Spider Catalog (2018)) spiders are the evolutionary most successful chelicerates. As in the ground pattern of chelicerates their body is divided into two major units, the opisthosoma harbouring respiratory, circulatory, digestive and reproductive organs and the prosoma harbouring the six appendages, the chelicerae, the pedipalps and the four pairs of walking legs (Figure 1). Their evolutionary success is fuelled by mesmerising modifications of the appendages: On the opisthosoma evolved the spinnerets, modified appendages combined with glands, producing the most durable threats in the animal kingdom, spider silk. The chelicerae were transformed in dagger-like fangs and equipped with venomous glands to capture prey. The pedipalps could be named the “swiss army knife” with various functions like sensory input, prey handling, extraintestinal digestion, courtship and copulation (Prpic and Damen 2008; Foelix 2010).

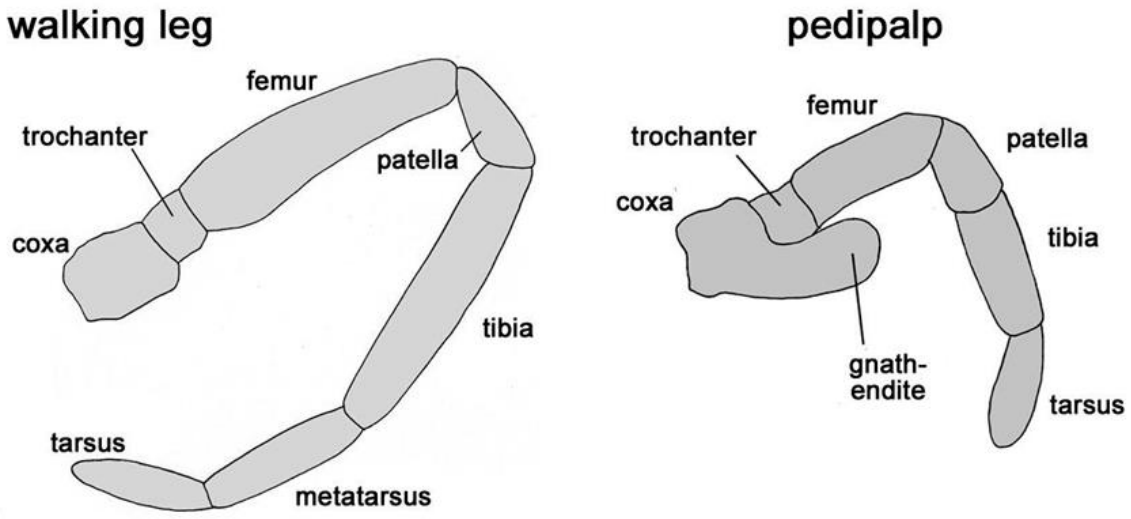

Figure 2: Schematic drawings of a walking leg (a) and a pedipalp (b). Note the superficial morphological similarity, the pedipalp is only missing the metatarsus and the coxa bears an outgrowth, the gnathendite. The gnathendite holds a role in extraintestinal digestion. Modified after Pechmann et al. (2010)

From these appendage modifications, the transformation of the tarsal tip of the male pedipalp into an intromittent organ, the bulbus organ, is considered unique in several aspects. Its species-specific structures are an adaption for direct sperm transfer into the corresponding female copulatory structures. Superficially, the main organization of the spider pedipalps is morphologically similar to the walking legs, but shorter as they lack one segment, the metatarsus (Figure2). During postembryonic development the pedipalp of spider males transforms in a metamorphosis-like manner. During this transition the pedipalp tip swells into a club-like cuticle bubble in which then the bulbus organ develops. After the final moult the functional structure is everted.

The bulbus organ is a pipette-like copulatory organ used by the males to draw up their own sperm, store it, and then inject it into the sperm storing organs of the female (Austad 1984; Foelix 2010; Pechmann et al. 2010). To get the sperm into the bulbus, a process called sperm induction, males produce a specialized web into which they ejaculate the sperm from the gonopore, which lies on their opisthosoma. From this web they draw up the sperm, by dipping the tip of the embolus, which holds the opening of the sperm storing organ, *i.e.* the spermophor (Foelix 2010). The bulbus organ morphology ranges from a simple pear-shaped protrusion to extremely complex, sclerite equipped structures (Figure 3). These sclerites have species-specific shapes and fit into the female genital opening like a key into a lock (Pechmann et al. 2010) and evolution lead to an excess of different sclerite morphologies (Figure 4) which is frequently used by taxonomists for species identification.

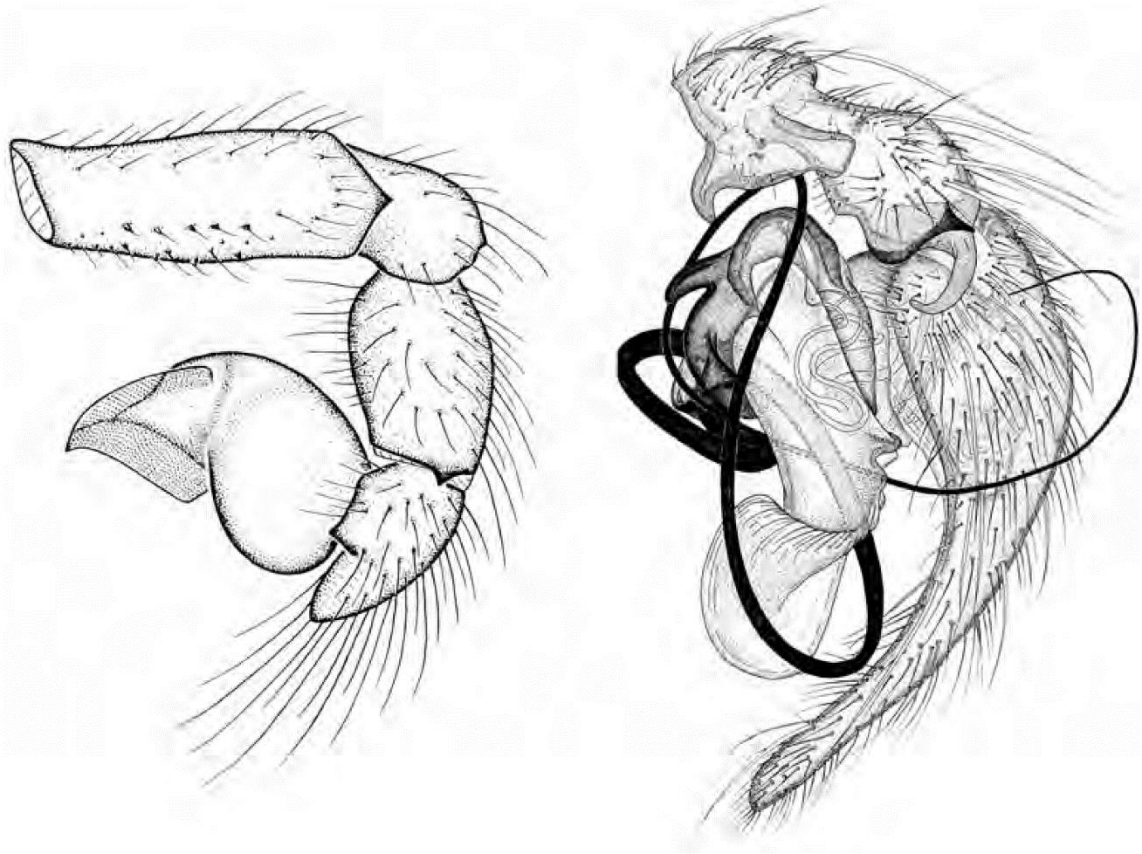

Figure 3: Drawings of spider bulbus organs. The very simple bulbus of *Segestrioides tofo* on the left and in contrast the highly complex bulbus of *Histopona torpida* in the right. Adapted from Eberhard and Huber (2010)

In the highly complex bulbus organs the sclerites are connected by membranes, so called haematodochae. These membranes can be inflated by haemolymph-pressure and by that move the sclerites. Through diverse morphologies of these haematodochae, like a composition of fibres of different elasticity or an irregular and twisted folding, these membranes can produce complex movements of the sclerites (Eberhard and Huber 2010).

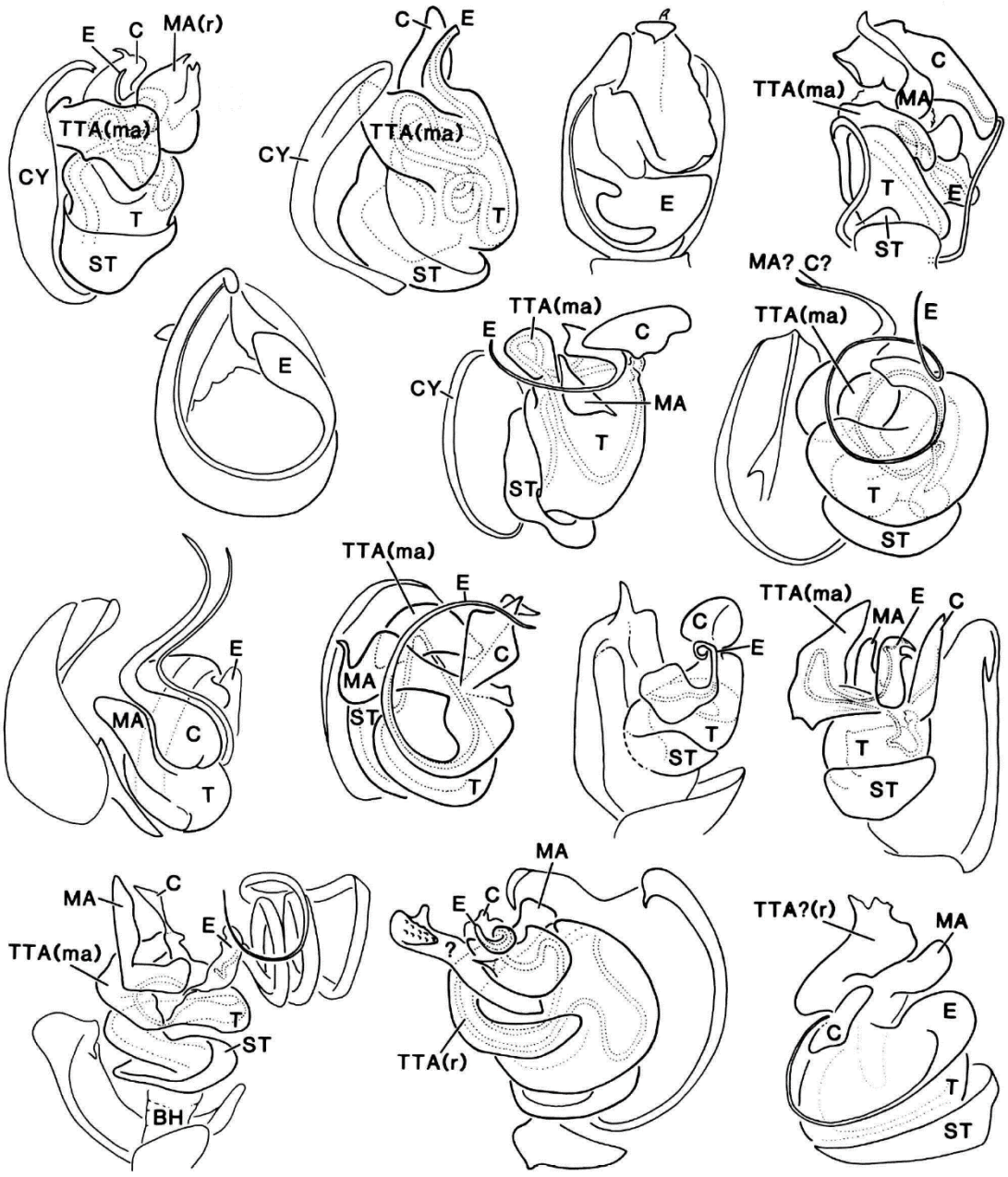

Figure 4: Drawings of bulbus organs of theridiid spiders depicting the incredible disparity of morphology. Even regarding only the embolus, i.e. the sclerite penetratig the female, shows the different morphological setups. Abbreviations for the sclerite nomenclature C= conductor, Cy= cymbium, E= embolus, MA= median apophysis, ST= subtegulum, T=tegulum TTA= theridioid tegular apophysis. Modified after Coddington (1990)

The correct fit of the bulbus to the female genital opening is essential to ensure the sperm is properly disposed in the female sperm storing organ, *i.e.* the spermatheca. Without proper placement, the sperm cannot be used in the internal fertilization process. For

copulation, the embolus, *i.e.* the sperm transferring sclerite, is inserted into the gonoduct/copulatory duct. The sperm is deposited into the spermatheca and then used by the female to fertilize her eggs (Austad 1984; Foelix 2010). Spiders transfer their sperm in an inactive state. It is packaged in a proteinaceous sheathing in two different forms: The single packed Cleistospermia (Michalik et al. 2013) or in small spermatophores, so called Coenospermia. Coenospermia represent the ancestral mode, found in the most basal branching taxa Mesothelae and Mygalomorphae (Eberhard and Huber 2010). To activate the sperm, the sheathing needs to be removed, a process happening in the spermatheca (Vöcking et al. 2013).

Spiders generally have two different female genital morphologies both generally corresponding to the morphology of the bulbus organ. Haplogynae and Orthognatha have a rather simple morphology and Entelegynae tend to higher complexity. The Haplogynae morphology has only a gonopore and no extra copulatory duct. One or two spermathecae are situated laterally to the gonoduct and have a cul-de-sac morphology. The Entelegynae morphology shows a central gonopore which is only used for oviposition. In front of this gonopore lies a specialised copulatory organ, the epigynum, which is a sclerotized plate with several cuticular infoldings. Two of these orifices lead to the sclerotized copulatory ducts, which end in the spermatheca. From the spermatheca the sperm is transferred to the eggs through a fertilization duct (Foelix 2010). Female Spiders store the sperm for months and can fertilize several batches of eggs after a single copulation (Uhl 1993; Albo and Costa 2017). Because of the sclerotization of the copulatory duct in the Entelegynae-setup, the penetrating male sclerite, *i.e.* the embolus, needs to fit its shape closely. Without a close fit the placement of sperm into the spermatheca will not be effective.

Research on the evolution of the bulbus organ had to fight an obstacle for a long time. The bulbus containing no muscle to move (Huber 2004) was thought to be a numb structure. In spite of many approaches (Osterloh 1922; Harm 1931; Lamoral 1973; Eberhard and Huber 1998), no innervation could be found and the consequences have been described in a nice comparison: “Because of the lack of nerves in the palpal bulb, the challenges faced by a male spider attempting to copulate can be likened to those of a persona attempting to adjust a complex, delicate mechanism in the dark using an elongate, elaborately formed fingernail” (Eberhard and Huber 2010). This opinion changed, with the findings of a nerve, innervation of the accessory glands and a proposed proprioceptive organ of the spermophor in *Hickmania troglodytes*, a basal branching spider (Lipke et al. 2015). These findings were corroborated, and a sensory organ was found on the base of the embolus of the derived species *Philodromus cespitum* (Sentenská et al. 2017). These new findings require an entirely new appraisal of the function of the bulbus organ and will provide novel insight into the evolution of this unique structure.

The bulbus organ of Parasteatoda tepidariorum

As mentioned above, the bulbus organ is morphologically very diverse, which drove the desire to clarify its evolution for almost one century (Barrows 1925; Coddington 1990; Huber 1994; Haupt 2002; Agnarsson 2004; Huber 2004; Agnarsson et al. 2007; Eberhard and Huber 2010). The adult bulbus organ is not only diverse, but also morphologically complex and comparisons between species are therefore difficult. However, this complex organ is the product of a postembryonic developmental process, and insight into the formation of the bulbus organ during development is expected to also provide a better

understanding how the morphology of the spider pedipalp bulbus has evolved and has adapted to its functions in sperm transfer. To investigate the developmental processes and their gene regulatory networks, it requires a suitable model organism. Genomic and transcriptomic resources are beneficial to study such networks via molecular techniques like gene expression pattern and gene function analyses, because they can aid in identifying genetic factors and interactions. In addition, to have a detailed description of the morphological changes during development and a reconstruction of the adult morphology is a prerequisite to investigate the underlying molecular genetic processes. Without this knowledge, it is difficult to identify the right timing and crucial time-points of development for investigation, and it is also difficult to interpret morphological changes after functional tests: even if one could guess the involved genes and right time-points to knock down the gene products it would be impossible to understand and interpret the resulting phenotype correctly. To successfully combine these methodological approaches, a well-established model species is required. The entelegyne theridiid spider *Parasteatoda tepidariorum* as long been used to study embryonic appendage development with a set of well-established molecular techniques like gene expression pattern and gene function analyses. It is the best-established spider model and therefore represents a mandatory candidate to investigate bulbus development. Even though there is much known about appendage development in *P. tepidariorum* there is almost no knowledge about its bulbus organ and only superficial studies have been conducted (Agnarsson 2004; Agnarsson et al. 2007). To fill this gap in the knowledge about this spider species, I have studied the adult morphology of the bulbus organ with a multimodal imaging approach, combining high resolution phase contrast micro-computed-

tomography (Töpperwien et al. 2016) with serial semi-thin sectioning for transmitted light microscopy.

Despite the amount of research conducted on the evolution of the bulbus organ, almost nothing is known about bulbus development. The reason for this might be that it develops post-embryonically as a complex three-dimensional structure, which is difficult to dissect, analyse and describe. Additionally, it is surrounded by a mostly opaque cuticle bubble, which hinders direct investigation. These obstacles are probably the cause why few morphological investigations of bulbus development have been conducted so far (Barrows 1925; Gassmann 1925; Harm 1931; Harm 1934; Bhatnagar and Rempel 1962; Bhatnagar and Sadana 1971; Sadana 1971). This lack of morphological research on bulbus development precluded work to dissect its genetic mechanisms. Embryonic data suggest that the underlying genetic network steering the development of the pedipalp, which harbours the bulbus organ, is not much different from that of the walking legs (Prpic and Damen 2004; Pechmann and Prpic 2009; Prpic and Damen 2009; Pechmann et al. 2010). Thus, it appears that embryonic development is not playing a crucial role in bulbus development, but its origin rather lies in postembryonic development.

I investigated the development of the bulbus organ of *P. tepidariorum* with a multimodal imaging approach. In addition to micro-computed tomography, I devised a protocol for bleaching and clearing the pedipalp harbouring the developing bulb and a perforated anodised aluminium slide to image the autofluorescence with confocal laser scanning microscopy.

The following results chapter is divided into four parts. In the first chapter different algorithms for phase contrast micro-computed tomography are described and evaluated. For this an iodine-stained critical-point-dried male *P. tepidariorum* was imaged with an inhouse laboratory tomography setup. Phase-retrieval from the measured intensity images makes it possible to increase soft-tissue contrast and resolution. Different algorithms for phase-retrieval from the measured images were tested and their results evaluated with respect to resolution and of the reconstructed image stacks. In the second chapter an anodised aluminium object-slide to scan specimen in the confocal laser scanning microscope is described. This slide improves the procedure of specimen clearing and mounting. The slide is perforated, and specimens can be mounted in holes dimensioned to their size in the clearing and mounting medium. The slide is equipped with cover slips on both sides adding to the convenience. The third chapter delivers a description of the adult morphology of the bulbus organ of *P. tepidariorum*. Through virtual dissection of the bulbus organ each sclerite, the connecting membranes and some details of the contained soft-tissue, are depicted and described. Based on this data the homology hypotheses of the sclerites are discussed. In a fourth chapter the development of the bulbus organ is investigated. The duration of the morphogenesis, the origin of the bulbus organ primordium and the differentiation is described. From these results a staging scheme is developed.

3. Results

Every chapter within the results starts with a one-page description of

- the main aim of the particular manuscript in the context of the complete thesis
- the authors and their contributions to the practical work, and
- the status of the manuscript.

3.1. Laboratory-based x-ray phase-contrast tomography enables 3D virtual histology

In this part, different phase retrieval algorithms were evaluated, to find the best suited for our laboratory setup. Therefore, a male *Parasteatoda tepidariorum* spider was prepared for µCT-imaging and imaged on the laboratory setup. Afterwards different phase retrieval algorithms were evaluated for soft tissue visualisation and resolution.

Töpperwien, Mareike, Krenkel, Martin, **Quade, Felix,** Salditt, Tim

Author contributions to practical work:

Mareike Töpperwien: Construction of the laboratory setup, evaluation of the algorithms

Martin Krenkel: Construction of the laboratory setup, evaluation of the algorithms

Felix Quade: Fixation, dehydration, contrasting and critical point drying of the test-specimen

Status: Published in Proceedings of SPIE, 9964, 99640I. http://doi.org/10.1117/12.2246460

Laboratory-based x-ray phase-contrast tomography enables 3D virtual histology

Mareike Töpperwien[1], Martin Krenkel[1], Felix Quade[2], and Tim Salditt[1]

[1]Institute for X-Ray Physics, Friedrich-Hund-Platz 1, Göttingen, Germany
[2]Johann-Friedrich-Blumenbach Institute for Zoology and Anthropology, Department of Developmental Biology, Justus-von-Liebig-Weg 11, Göttingen, Germany

ABSTRACT

Due to the large penetration depth and small wavelength hard x-rays offer a unique potential for 3D biomedical and biological imaging, combining capabilities of high resolution and large sample volume. However, in classical absorption-based computed tomography, soft tissue only shows a weak contrast, limiting the actual resolution. With the advent of phase-contrast methods, the much stronger phase shift induced by the sample can now be exploited. For high resolution, free space propagation behind the sample is particularly well suited to make the phase shift visible. Contrast formation is based on the self-interference of the transmitted beam, resulting in object-induced intensity modulations in the detector plane. As this method requires a sufficiently high degree of spatial coherence, it was since long perceived as a synchrotron-based imaging technique. In this contribution we show that by combination of high brightness liquid-metal jet microfocus sources and suitable sample preparation techniques, as well as optimized geometry, detection and phase retrieval, excellent three-dimensional image quality can be obtained, revealing the anatomy of a cobweb spider in high detail. This opens up new opportunities for 3D virtual histology of small organisms. Importantly, the image quality is finally augmented to a level accessible to automatic 3D segmentation.

Keywords: laboratory-based x-ray phase contrast, propagation-based imaging, tomography, 3D virtual histology

1. INTRODUCTION

X-ray computed tomography is a powerful tool for non-invasive imaging of optically opaque samples, revealing the three-dimensional density distribution of the examined object. Due to the large penetration depth and small wavelength of hard x-rays, imaging of relatively large objects with high resolution is theoretically possible. In classical tomography, also used in daily clinical practice, contrast formation is based on absorption of the x-rays while passing through the specimen. This enables sufficient contrast for absorbing structures like bones while soft tissue shows almost no absorption, leading to a decrease in resolution. However, when considering the x-ray index of refraction $n(\mathbf{r}) = 1 - \delta(\mathbf{r}) + i\beta(\mathbf{r})$ it becomes evident that not only the absorption of the beam, characterized by the extinction coefficient $\beta(\mathbf{r})$, but also the phase shift, induced by the much larger decrement $\delta(\mathbf{r})$, can be used for imaging, leading to an increased contrast in soft tissue. As it is not possible to directly measure the phase of the x-ray beam, several methods exist to make this phase shift visible in the measured intensity images, e.g., Zernike based phase contrast,[1] Talbot interferometry,[2] edge-illumination[3,4] or speckle-based phase contrast.[5] Well suited for high spatial resolution, we here use propagation-based phase contrast in which free space propagation behind the object leads to measurable intensity modulations in the detector plane.[6–8] Subsequently, the phase distribution of the object has to be reconstructed from the measured intensity images using suitable phase-retrieval algorithms.[9] Note that propagation-based imaging can be applied over a wide range of resolution and field of view, spanning macroscopic down to nanoscopic length scales, with best resolution values reported at about 25 nanometers in two dimensions.[10]
Due to the necessity of a sufficient degree of spatial coherence, this method was first only implemented at

Further author information: (Send correspondence to M.T. or T.S.)
M.T.: mtoeppe@gwdg.de
T.S.: tsaldit@gwdg.de

Advances in Laboratory-based X-Ray Sources, Optics, and Applications V, edited by Ali M. Khounsary, Gert E. van Dorssen, Proc. of SPIE Vol. 9964, 99640I · © 2016 SPIE · CCC code: 0277-786X/16/$18 · doi: 10.1117/12.2246460

synchrotron facilities. However, with the invention of new microfocus x-ray sources the required partial coherence combined with a high flux can also be reached at the laboratory, enabling propagation-based imaging of relatively fast degrading biological samples with high throughput.[11,12]
In the following we demonstrate the capabilities of our laboratory setup consisting of a liquid-metal jet source by imaging an iodine stained cobweb spider, revealing the anatomy with high resolution in 3D. We compare different widely used phase-retrieval algorithms and evaluate the results with respect to resolution and quantitativeness of the reconstructed volumes.

2. PHASE-RETRIEVAL ALGORITHMS

In the following, we recall the fundamentals of phase-retrieval algorithms based on the Transport of Intensity Equation (TIE), as the starting point for the phase-retrieval schemes used in this work. The TIE describes the propagation of a paraxial monochromatic wave[13]

$$\nabla_\perp \left[I_z(\mathbf{r}_\perp) \nabla_\perp \phi_z(\mathbf{r}_\perp) \right] = -\frac{2\pi}{\lambda} \frac{\partial}{\partial z} I_z(\mathbf{r}_\perp) \,, \tag{1}$$

where $\phi_z(\mathbf{r}_\perp)$ is the phase and $I_z(\mathbf{r}_\perp)$ the measured intensity of the beam at distance z behind the object and $\mathbf{r}_\perp = (x, y)$ denotes the plane perpendicular to the optical axis. Note that in the following, $I_z(\mathbf{r}_\perp)$ represents the intensity distribution corrected by the intensity distribution I^{in} of the incident radiation. As the laboratory CT setup used in this work exhibits a very uniform illumination function, this empty beam or flat field correction is straightforward and without problems, unlike the typical situations encountered for focused synchrotron radiation.[14]

Modified Bronnikov Algorithm (MBA) Under the assumption of a small propagation distance z' the partial derivative can be approximated as $\frac{\partial}{\partial z} I_z(\mathbf{r}_\perp) \approx \frac{I_{z=z'}(\mathbf{r}_\perp) - I_{z=0}(\mathbf{r}_\perp)}{z'}$, leading to the following expression for the intensity distribution

$$I_{z=z'}(\mathbf{r}_\perp) = I_{z=0}(\mathbf{r}_\perp) - \frac{\lambda z'}{2\pi} \nabla_\perp \left(I_{z=0}(\mathbf{r}_\perp) \nabla_\perp \phi(\mathbf{r}_\perp) \right) , \tag{2}$$

where $\phi(\mathbf{r}_\perp)$ denotes the (projected) phase function of the object, i.e. the phase of the wave in the object's exit plane $z = 0$. For weakly absorbing objects we can set $\nabla_\perp I_{z=0}(\mathbf{r}_\perp) \approx 0$, leading to

$$I_{z=z'}(\mathbf{r}_\perp) = I_{z=0}(\mathbf{r}_\perp) \left[1 - \frac{\lambda z'}{2\pi} \nabla_\perp^2 \phi(\mathbf{r}_\perp) \right] \,. \tag{3}$$

From this result we can infer that the weak intensity distribution imparted on the wave by the object does not undergo diffraction within the given assumptions (weak absorption, small propagation distance z'), while the second derivative of the phase creates intensity variations increasing with propagation distance. In this so-called *direct contrast regime*, the phase contrast is hence visible in form of an edge-enhancement, as given by the laplacian of the object's projected phase function. For a pure phase object, this further simplifies to $I_{z=z'}(\mathbf{r}_\perp) = 1 - \frac{\lambda z'}{2\pi} \nabla_\perp^2 \phi(\mathbf{r}_\perp)$, as the intensity distribution directly behind the object is unity in this case. For phase retrieval one can exploit the fact that the laplacian can be inverted in Fourier space via a filter of the form $-\frac{1}{|\mathbf{k}_\perp|^2}$ with $\mathbf{k}_\perp = (k_x, k_y)$ the lateral reciprocal coordinates. In order to avoid the singularity at $|\mathbf{k}_\perp| = 0$, a regularization parameter α can be added to the denominator of the filter, leading to the following reconstruction formula for the phase function of the object, known as the *Modified Bronnikov Algorithm*[15]

$$\phi(\mathbf{r}_\perp) = \frac{2\pi}{\lambda z'} \cdot \mathcal{F}^{-1} \left[\frac{\mathcal{F} \left[I_{z=z'}(\mathbf{r}_\perp) - 1 \right]}{|\mathbf{k}_\perp|^2 + \alpha} \right] . \tag{4}$$

The regularization parameter α also accounts for the object's residual absorption which amplifies low spatial frequencies in the image. Hence, applying an unregularized filter would inevitably corrupt these Fourier components and yield strong artifacts and blurring. Therefore, α must be chosen sufficiently high, depending on the (residual) absorption of the object. At the same time this compromises the correct filtering for the phase and may result in incomplete inversion of the edge-enhancement.

Bronnikov Aided Correction (BAC) To avoid this dilemma, objects with non-negligible absorption can be treated by a further reconstruction step, resulting in a sharp image of the intensity distribution $I_{z=0}(\mathbf{r}_\perp)$ directly behind the object. According to Eq. 3, the pure absorption image can be calculated from the measured intensity image $I_{z=z'}(\mathbf{r}_\perp)$ at distance z' and the phase information of the object. Taking the phase $\phi^\dagger(\mathbf{r}_\perp)$, reconstructed via the MBA scheme, as an approximation of the real phase function $\phi(\mathbf{r}_\perp)$, this leads to[16]

$$I_{z=0}(\mathbf{r}_\perp) = \frac{I_{z=z'}(\mathbf{r}_\perp)}{1-\gamma\nabla_\perp^2\phi^\dagger(\mathbf{r}_\perp)}, \tag{5}$$

where the coefficient $\frac{\lambda z'}{2\pi}$ was replaced by a an α-dependent regularization parameter γ to avoid residual edge-enhancement (γ too small) or an inversion of the edges (γ too large). This scheme is called Bronnikov Aided Correction.[16] As we show in this work experimentally, this seems to conglomerate both absorption and phase contrast in a suitable way, in particular for laboratory CT, where many more rigorous approaches fail.

Single Material Object (SMO) Instead of the assumption of a weakly absorbing object another widely used approximation is that the the object is composed of a single material with constant ratios of extinction coefficent β and decrement δ.[17] The absorption as well as the phase modulation of the beam when going through the object are therefore only dependent on an effective projected thickness $T(\mathbf{r}_\perp)$ of the object. According to Lambert-Beer's law of absorption, the intensity of the beam directly behind the object is given by $I_{z=0}(\mathbf{r}_\perp) = e^{-2k\beta T(\mathbf{r}_\perp)}$, whereas the phase function of a sufficiently thin object is proportional to the projected thickness with $\phi(\mathbf{r}_\perp) = -k\delta T(r_\perp)$. Inserting this into the original expression of the TIE in Eq. 1 and rearranging the result using the identity $\exp(f(x))\nabla_\perp f(x) = \nabla_\perp \exp(f(x))$ yields

$$\left(-\frac{\delta}{2k\beta}z'\nabla_\perp^2 + 1\right)e^{-2k\beta T(\mathbf{r}_\perp)} = I_{z=z'}(\mathbf{r}_\perp). \tag{6}$$

By again inverting the laplacian in Fourier space, leading to a filtering with the function $-\frac{1}{|\mathbf{k}_\perp|^2}$, the phase can be retrieved via

$$\phi(\mathbf{r}_\perp) = \frac{\delta}{2\beta}\ln\left(\mathcal{F}^{-1}\left[\frac{\mathcal{F}[I_{z=z'}(\mathbf{r}_\perp)]}{\frac{\delta}{2k\beta}z'|\mathbf{k}_\perp|^2+1}\right]\right), \tag{7}$$

where the relation between the projected thickness $T(\mathbf{r}_\perp)$ and the object phase function $\phi(\mathbf{r}_\perp)$ given above was used. For weak absorbing objects the logarithm can be approximated by its first order Taylor expansion,[18] leading to the same expression as in Eq. 4 if $\alpha = \frac{4\pi}{\lambda z'}\frac{\beta}{\delta}$.

3. METHODS

Laboratory micro-CT setup The laboratory setup (Fig. 1a and b) consists of a liquid-metal jet microfocus source (Excillum, Stockhom, Sweden) which enables sufficiently small spot sizes to achieve the partial coherence needed for propagation-based imaging while on the other hand delivering a relatively high photon flux. The anode material is Galinstan, an alloy consisting of gallium, indium and tin which is liquid at room temperature. The peak energy of the source is at 9.25 keV. Downstream of the source the sample is positioned on a motorized sample tower including one rotation for tomographic measurements and three translations for sample alignment with respect to the tomographic axis. Below the rotation stage two additional translations perpendicular to the optical axis are installed to adjust the source-sample-distance z_1 and to align the position of the rotation axis. At some distance z_2 behind the sample, a detector is placed on a motorized stage with two perpendicular translations to align the pitch angle and the zero position of the rotation axis.
Due to the cone-beam geometry of the setup, the source can be operated in two different configurations by either implementing a high geometrical magnification M ($z_1 \ll z_2$) leading to a small effective pixel size $\mathrm{d}x_{\mathrm{eff}} = \frac{\mathrm{d}x}{M}$ or by implementing a low magnification ($z_1 \gg z_2$) while simultaneously using a high resolution detector. In the first case the resolution is limited by the spot size whereas in the second case the point spread function of the detector is the limiting factor.[11] As the minimal spot size of the source lies in the range of 4 μm we turn to the

second approach for highest resolution measurements. To this end, the lens-coupled single crystal scintillator CCD camera XSight (Rigaku, Prague, Czech Republic) is installed in the setup which has a pixel size of 540 nm. In two dimensions this configuration can reach a resolution in the range of 800 nm, as revealed by an absorbing test pattern, and is at the moment limited by vibrations.

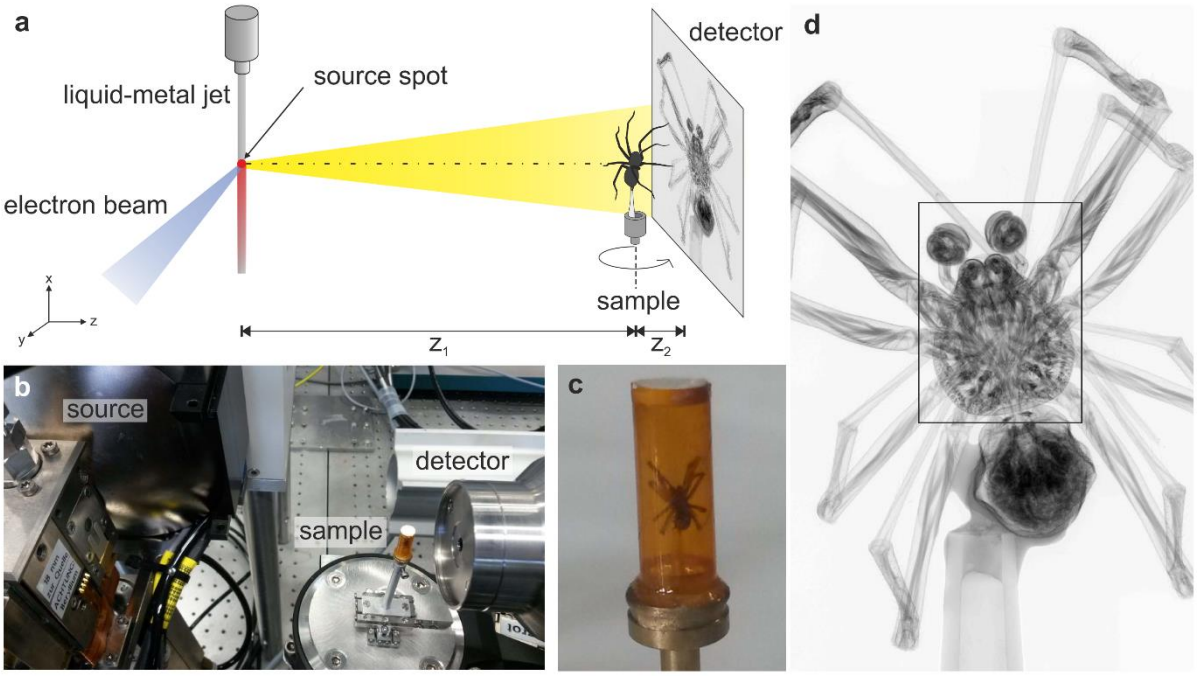

Figure 1. Experimental setup. **a** Sketch of the laboratory setup consisting of a liquid-metal jet source, the sample on a motorized sample tower and the detector some distance z_2 behind the object. **b** Photograph of the setup. **c** Photograph of the sample. The spider is glued to a pipette tip and put in a Kapton tube to prevent sample changes due to atmospheric differences. **d** Stitched projection of the sample from 28 single projection images. The approximate position of the two neighboring tomograms (presented below) is indicated.

Sample preparation A wild type cobweb spider (*Parasteatoda tepidariorum*) is sacrified by putting it into the freezer for 20 minutes and subsequently fixing it in 4% para-formaldehyde (PFA) for 1 hour at room temperature. It is dehydrated via an ascending ethanol series (70%, 80%, 90% ethanol, 95% and pure ethanol each for 30 minutes) and stained with iodine to increase the contrast for x-ray imaging. To this end, it is stored in pure ethanol with 1% iodine for 1 day and afterwards rinsed three times with pure ethanol. In order to minimize absorption of the x-rays the liquid is removed by critical point drying of the spider (CPD300, Leica, Austria) using the same settings as in[19] except for the exchange speed which was set to 5. Finally, the dried spider is glued on a pipette tip and enclosed by a Kapton tube, which is sealed with hematocrit, to prevent sample changes due to atmospheric differences (see Fig. 1c).

4. RESULTS

For a first evaluation of the imaging system and the different phase-retrieval methods, a two-dimensional empty-beam corrected projection of the spider is considered. This is acquired at a source-to-sample distance $z_1 = 158.75\,\mathrm{mm}$ and a sample-to-detector distance $z_2 = 22.5\,\mathrm{mm}$, leading to an effective pixel size of $0.47\,\mu\mathrm{m}$ and a field of view of $1.18 \times 1.57\,\mathrm{mm}^2$. In order to image the entire spider, 28 projections at different positions on the sample are recorded with an exposure time of 50 s each and virtually stitched together (see Fig. 2). To achieve a higher signal-to-noise ratio the projection is resampled by a factor of 2, resulting in an actual pixel size of $0.95\,\mu\mathrm{m}$.

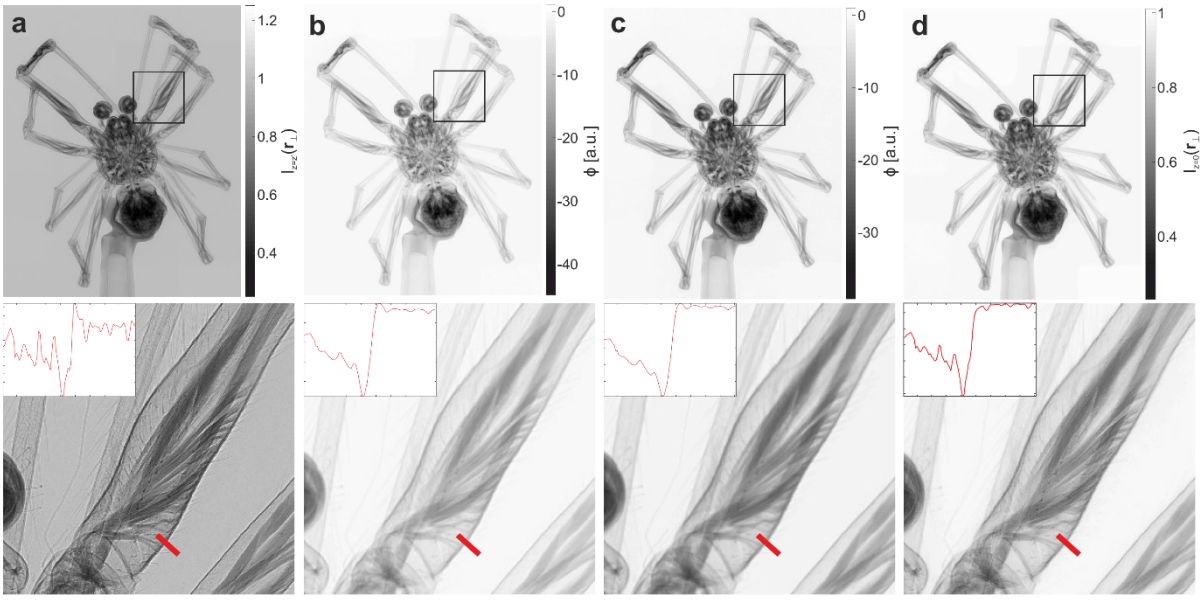

Figure 2. Comparison of the different phase-retrieval algorithms, applied to the stitched 2D projection of the whole spider. **a** Raw projection without the application of a phase-retrieval algorithm. The rectangle marks a region shown in higher detail in the lower row. The inset shows a line profile along the red line indicated in the zoomed image. The typical edge-enhancement can be seen visually in the projection as well as in the profile. **b** Reconstructed phase using the SMO method with a β/δ-ratio of 0.015. The edge-enhancement is compensated as can be seen in the projection image and the line profile, but the reconstructed phase seems blurred in comparison to the raw data. **c** Reconstructed phase using the MBA algorithm with a regularization parameter of 0.04. As in the SMO case, the edge-enhancement can be reduced but also here the reconstruction seems blurred compared to the raw data. **d** Reconstructed intensity distribution in the object plane using the BAC algorithm with the parameters $\alpha = 0.02$ and $\gamma = 0.15$. The edge-enhancement is again removed by applying the reconstruction algorithm, but in contrast to the SMO and MBA methods, the reconstructed image looks almost as sharp as the raw data.

Figure 2a shows the raw projection without the application of any phase-retrieval algorithm. The inset displays part of a leg in higher magnification revealing the muscles inside the leg as well as hairs on top of it in high detail. The typical edge-enhancement is clearly visible in the two-dimensional image but can also be recognized in the line profile shown below. The result after applying the SMO algorithm with a $\frac{\beta}{\delta}$-ratio of 0.015 is shown in Fig. 2b. The ratio is chosen in a way that the edge-enhancement is removed while keeping the reconstruction as sharp as possible. The projection as well as the line profile over the edge of a leg show that on the one hand the edge-enhancement is compensated while on the other hand also the signal-to-noise ratio is improved. However, the inset of the reconstructed projection seems blurred compared to the raw image especially when considering small structures like the roots of the hairs. The reconstructed phase using the MBA scheme with a regularization parameter $\alpha = 0.04$ is shown in Fig. 2c. As in the SMO case the edge-enhancement is removed and the signal-to-noise ratio is higher. But also here, the inset reveals that the projection is slightly blurred in contrast to the raw data. As a last phase-retrieval algorithm the BAC is applied with the regularization parameters $\alpha = 0.02$ and $\gamma = 0.015$. The result is shown in Fig. 2d. As in the previous cases the edge-enhancement is removed and the signal-to noise ratio is higher, although it is not as high as for the SMO and the MBA. In exchange, the reconstruction seems almost as sharp as the raw data.

To evaluate the imaging capabilities of the setup in three dimensions, two tomographic measurements at adjacent positions in height are recorded and virtually stitched together to achieve a higher field of view. The approximate position of both tomograms is indicated in Fig. 1d. For each tomogram 1000 projections over 180° were recorded with an exposure time of 20 s per projection. Before reconstructing the three-dimensional volume with the cone-beam reconstruction algorithm of the ASTRA toolbox,[20,21] the phase-retrieval algorithms are applied on each projection with the parameters given above.

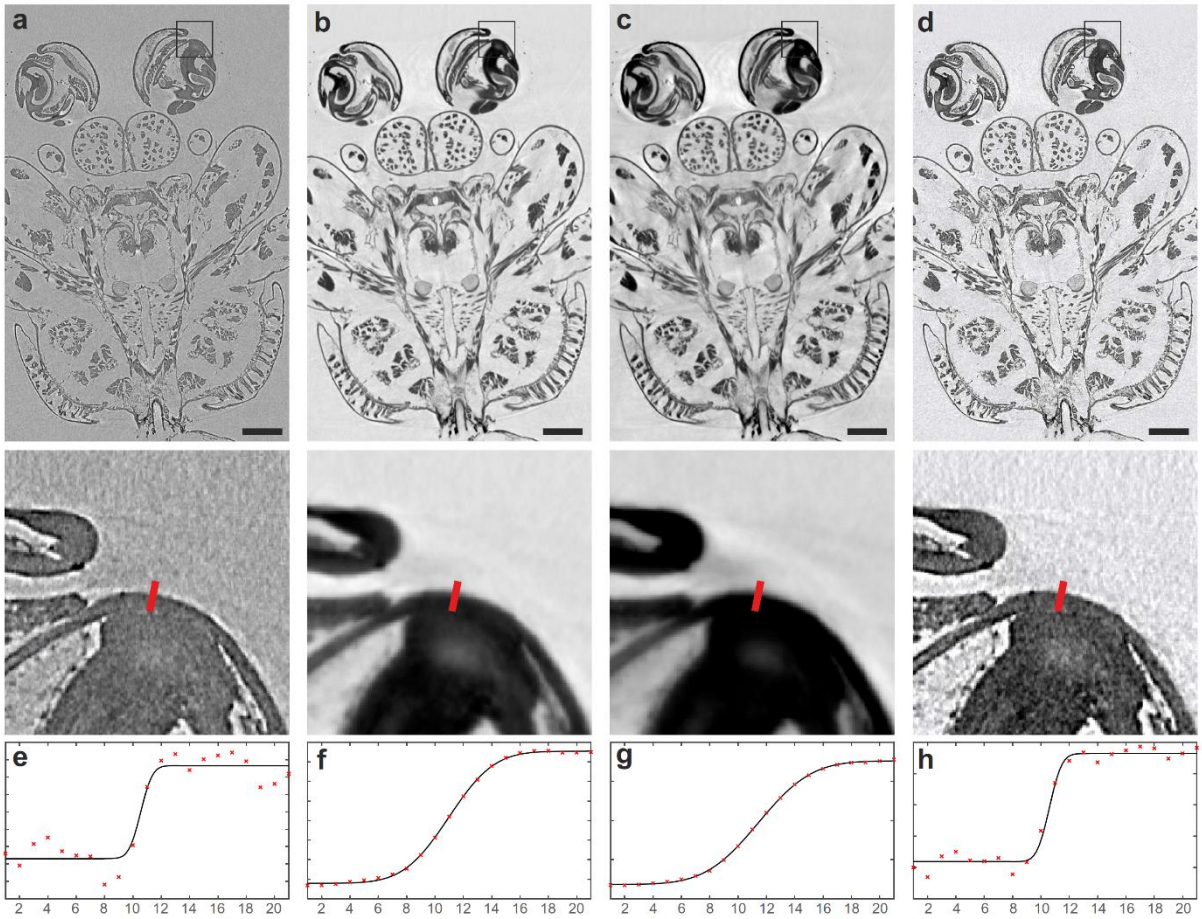

Figure 3. Comparison of the phase-retrieval algorithms by slices of the reconstructed volumes. **a** Longitudinal slice through the reconstructed and stitched volumes corresponding to the raw data (no phase retrieval). The capability to stitch the two volumes without introducing artifacts proves the stability of the entire imaging system. The rectangle marks the region which is shown in higher detail in the bottom row. The red line indicates the position of the line profile shown in e. **b** Corresponding slice through the SMO reconstruction, using the same parameter as in Fig. 2b. Compared to the result from the raw projections, the edge-enhancement is removed and the reconstructed densities are quantitative in such a way that areas with same composition have the same gray values. **c** Slice through the volume of the MBA reconstruction. As in the SMO case, phase retrieval removes the edge-enhancement and makes the reconstruction quantitative. However, some artifacts can be seen in the slice which are caused by the object not being a pure phase object as assumed in the derivation of the MBA algorithm. **d** Corresponding slice through the BAC reconstruction. The edge-enhancement is removed while at the same time the reconstructed volume is sharp with quantitative gray values. **e** Line profile of the raw data at the position indicated above. To estimate the resolution an error function is fitted to the data with an FWHM of $1.22\,\mu$m. Due to the edge-enhancement, the error of the fit is quite large ($1.2\,\mu$m). **f** The same curve and fit for the data treated by the SMO method, leading to an FWHM of $4.7(3)\,\mu$m. **g** The fit to the line profile of the MBA data gives an FWHM of $5.5(2)\,\mu$m. **h** The same fit for the BAC data leads to an FWHM of $1.3(6)\,\mu$m. Scalebars: 200μm

Visualization of the three-dimensional datasets Fig. 3 shows a longitudinal slice through the reconstructed and stitched volume for each reconstruction scheme as well as the raw images. The stitching of the volumes is performed with the software *Avizo* (FEI Visualization Sciences Group, Burlington, USA) which is also used for the visualization of the three-dimensional data. The absence of artifacts due to the stitching proves the stability of the setup despite the total measurement time on the order of 15 hours. The slice reconstructed from the raw data is depicted in Fig. 3a, revealing a sharp reconstruction but lacking quantitativeness of the

gray values. This is especially apparent at the edges of large areas consisting of the same material as the gray values get darker towards the edges while outside of the object the edge-enhancement leads to brighter values. An estimate of the resolution can be performed by looking at the edge spread function along the line indicated in red. The profile as well as an error function fit are shown in e, revealing an FWHM of 1.22 μm. Note that due to the edge-enhancement, the profile does not follow a perfect error function, leading to a relatively large uncertainty of the fit of approximately 1.2 μm. The reconstructed slice from the SMO projections is shown in Fig. 3b. In contrast to the reconstruction from the raw data the gray values are quantitative as parts of the sample which have the same density show similar gray values without a gradient towards the edges. However, already by visual inspection of the small structures in the slice, it is apparent that the resolution decreases. This can also be confirmed by the line profile shown in f. The error function fit gives an FWHM of 4.7(3) μm which is a factor of 4 larger compared to the raw data. The reconstruction from the MBA projections in Fig. 3c shows a similar result. The gray values are quantitative but the reconstruction seems blurred. The line profile reveals an FWHM of 5.5(2) μm which is even slightly worse than in the SMO case. Also the reconstruction shows more artifacts which are, e.g., visible in the non-uniformity of background. As a last result, the slice of the BAC reconstruction is shown in Fig. 3d, revealing a sharp object and quantitative gray values without any residual edge-enhancement. The same level of detail as in in the reconstruction from the raw data can be reached, though not with the same signal-to-noise ratio as in the SMO and MBA case. The error function fit to the line profile shown in h confirms the high resolution, as it reveals an FWHM of 1.3(6) μm which lies in the same range as for the raw data.

For a better visualization of the three-dimensional density of the object, automatic volume renderings are performed based on the gray values of the reconstructions. For these renderings the reconstructed density values belonging to the background are displayed in transparent while each density value inside the spider is displayed in a different shade of gray. Figure 4 shows the results for all datasets with cuts through the volume to obtain a better view of the anatomy of the spider. In the case of the raw data, the spider can be rendered in high detail as seen, e.g., at the hairs on the outside as well as the muscle strands inside the spider's legs and body. However, due to the missing quantitativeness, homogeneous parts of the spider are not displayed in the same gray values and seem to consist of different materials. This can be especially recognized in the inset on the right side of the figure which shows muscle strands from the inner part of the spider. Accordingly, the muscles seem to be hollow inside. The SMO and MBA reconstructions show these muscles with the same gray values throughout the volume but the edges of the sample are blurred and the inner structure of the muscle strands is not resolved, as can be especially observed in the inset of both datasets. Only the volume rendering of the BAC reconstruction shows the object in the same level of detail as the raw data while providing a rendering of homogeneous parts of the spider with uniform and quantitative gray values.

5. DISCUSSION

The imaging results obtained for an iodine stained fixated spider clearly demonstrate the potential of propagation-based laboratory CT when optimizing experimental setup and phase-retrieval methods. In this case, sharp quantitative reconstructions of the three-dimensional object density are obtained at an image quality which outpasses many synchrotron results of similar objects. They also show that the phase retrieval is a crucial step in order to enable automatic renderings and segmentations of specific parts of the sample. However, due to the different assumptions in the derivation of the phase-retrieval algorithms, the applicability and achievable resolution of each case depend on the characteristics of the examined objects and the experimental setup.

Because of the staining with iodine, for example, the assumption of an object consisting of a single material is relatively well fulfilled, leading to a satisfactory performance of the SMO approach. This results in an artifact-free reconstruction of the density with quantitative gray values and a good signal-to-noise ratio. However, the resolution is lower compared to the raw unreconstructed data. In the case of the MBA reconstruction, the assumption of a pure phase object or an object with negligible absorption is not fulfilled due to the iodine stain, leading to blurred reconstructions and artifacts in the three-dimensional volume. Hence, the SMO approach is clearly more suitable for the present object, and in this case the difference between these very similar algorithms becomes evident. However, in order to achieve highest resolution and to fully exploit the optimized experimental setup, we find that the phase reconstruction has to be performed following the BAC algorithm, as solely this reconstruction scheme provided quantitative images without loss of resolution compared to the raw data.

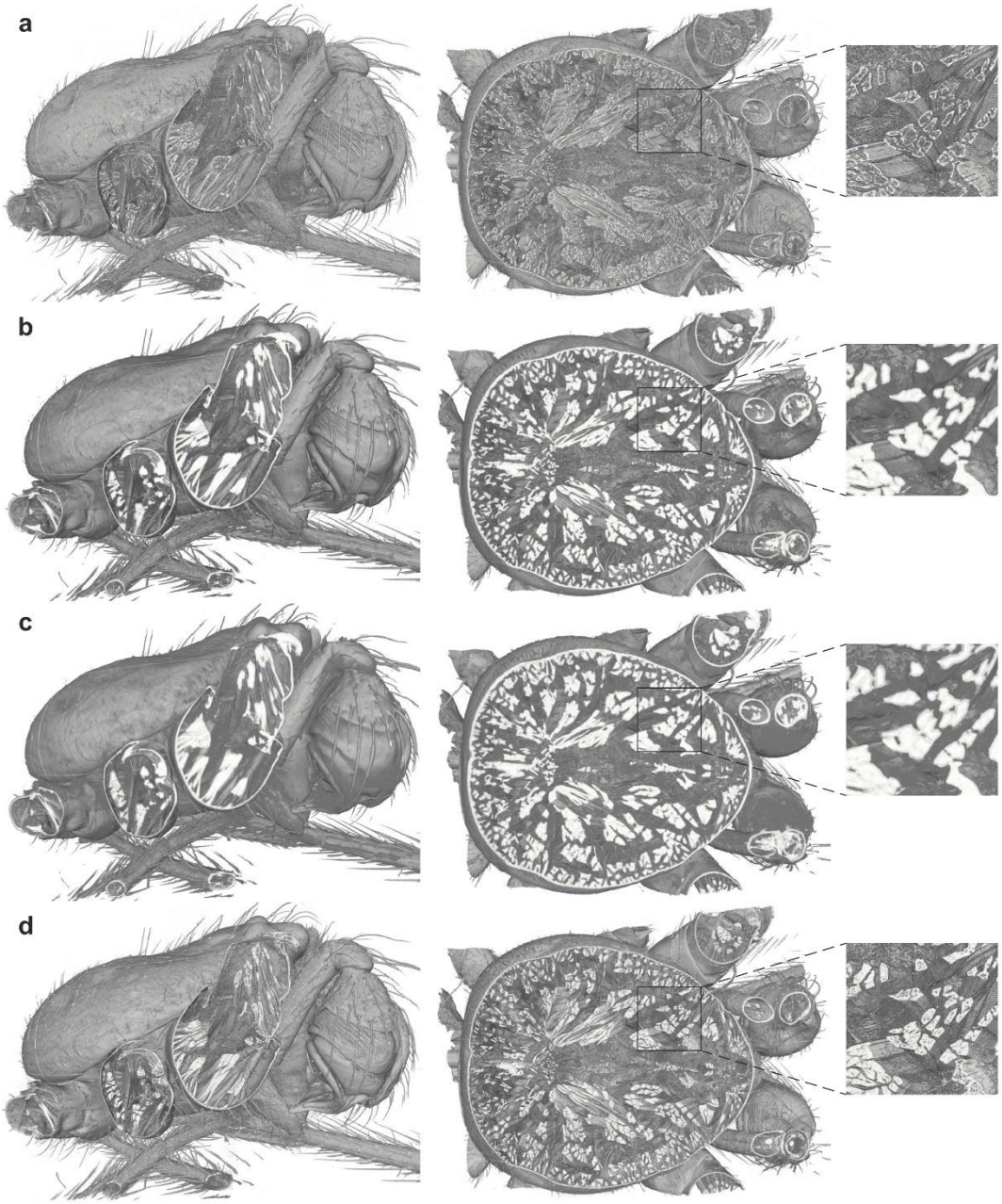

Figure 4. 3D visualization of the reconstructed volumes. Automatic renderings of the data are shown for volumes obtained from (**a**) the raw projections, (**b**) the reconstructed projections using the SMO method, (**c**) the MBA phase retrieval and (**d**) the BAC algorithm. Cuttings into the volume give an insight into the anatomy of the spider. In the case of the raw images, the resolution is sufficient to reveal ,e.g., the muscle strands in high detail, but the quantitativeness is missing as muscles do not have the same gray value throughout the volume. This is given in the case of the SMO and MBA phase retrieval but at the cost of resolution. Only the BAC algorithm provides results which are quantitative and show the same material with uniform gray values, while maintaining the same level of detail as the raw data.

All in all it has to be noted that due to the projection over an extended object, the differences in performance of the three reconstruction algorithm are particularly well visualized in the retrieved three-dimensional density distributions. In two dimensions, the respective differences can also be found, but require a more experienced eye. More importantly, the resolution cannot be properly quantified by considering the line profiles of the projection data (Fig. 2, bottom), and the edge spread function over the edge of the spider leg shows a similar slope for all cases.

In summary, we have shown an application of propagation-based phase-contrast tomography at the laboratory, enabling the imaging of the inner structure of small biological specimens at high resolution. Using the capabilities of the setup together with suitable sample preparation and phase-retrieval algorithms, in particular the BAC reconstruction scheme, a kind of virtual histology becomes possible, revealing the three-dimensional architecture of the organism and its constituent tissues at micrometer resolution, without the need for slicing the specimen.

Acknowledgments

We thank Willem Jan Palenstijn for excellent support regarding the ASTRA toolbox. Financial support by the Cluster of Excellence 171 *Nanoscale Microscopy and Molecular Physiology of the Brain* and the Collaborative Research Center 755 *Nanoscale Photonic Imaging* of the German science foundation (DFG) is greatly acknowledged.

REFERENCES

[1] Stampanoni, M., Mokso, R., Marone, F., Vila-Comamala, J., Gorelick, S., Trtik, P., Jefimovs, K., and David, C., "Phase-contrast tomography at the nanoscale using hard x rays," *Phys. Rev. B* **81**(14), 140105 (2010).

[2] Weitkamp, T., Diaz, A., David, C., Pfeiffer, F., Stampanoni, M., Cloetens, P., and Ziegler, E., "X-ray phase imaging with a grating interferometer," *Opt. Express* **13**(16), 6296–6304 (2005).

[3] Munro, P. R., Ignatyev, K., Speller, R. D., and Olivo, A., "Phase and absorption retrieval using incoherent x-ray sources," *Proceedings of the National Academy of Sciences* **109**(35), 13922–13927 (2012).

[4] Hagen, C., Munro, P., Endrizzi, M., Diemoz, P., and Olivo, A., "Low-dose phase contrast tomography with conventional x-ray sources," *Medical physics* **41**(7), 070701 (2014).

[5] Zanette, I., Zhou, T., Burvall, A., Lundström, U., Larsson, D. H., Zdora, M., Thibault, P., Pfeiffer, F., and Hertz, H. M., "Speckle-based x-ray phase-contrast and dark-field imaging with a laboratory source," *Phys. Rev. Lett.* **112**(25), 253903 (2014).

[6] Cloetens, P., Ludwig, W., Baruchel, J., Van Dyck, D., Van Landuyt, J., Guigay, J. P., and Schlenker, M. a., "Holotomography: Quantitative phase tomography with micrometer resolution using hard synchrotron radiation x rays," *Appl. Phys. Lett.* **75**(19), 2912–2914 (1999).

[7] Lagomarsino, S., Cedola, A., Cloetens, P., Di Fonzo, S., Jark, W., Soullie, G., and Riekel, C., "Phase contrast hard x-ray microscopy with submicron resolution," *Appl. Phys. Lett.* **71**(18), 2557–2559 (1997).

[8] Paganin, D. and Nugent, K. A., "Noninterferometric Phase Imaging with Partially Coherent Light," *Phys. Rev. Lett.* **80**, 2586–2589 (1998).

[9] Paganin, D. M., [*Coherent X-Ray Optics*], New York: Oxford University Press (2006).

[10] Bartels, M., Krenkel, M., Haber, J., Wilke, R. N., and Salditt, T., "X-ray holographic imaging of hydrated biological cells in solution," *Phys. Rev. Lett.* **114**, 048103 (2015).

[11] Bartels, M., Hernandez, V. H., Krenkel, M., Moser, T., and Salditt, T., "Phase contrast tomography of the mouse cochlea at microfocus x-ray sources," *Appl. Phys. Lett.* **103**(8), 083703 (2013).

[12] Krenkel, M., Töpperwien, M., Dullin, C., Alves, F., and Salditt, T., "Propagation-based phase-contrast tomography for high-resolution lung imaging with laboratory sources," *AIP Advances* **6**(3), 035007 (2016).

[13] Teague, M. R., "Deterministic phase retrieval: a greens function solution," *JOSA* **73**(11), 1434–1441 (1983).

[14] Homann, C., Hohage, T., Hagemann, J., Robisch, A.-L., and Salditt, T., "Validity of the empty-beam correction in near-field imaging," *Phys. Rev. A* **91**, 013821 (2015).

[15] Groso, A., Abela, R., and Stampanoni, M., "Implementation of a fast method for high resolution phase contrast tomography," *Opt. Express* **14**(18), 8103–8110 (2006).

[16] Witte, Y. D., Boone, M., Vlassenbroeck, J., Dierick, M., and Hoorebeke, L. V., "Bronnikov-aided correction for x-ray computed tomography," *J. Opt. Soc. Am. A* **26**(4), 890–894 (2009).
[17] Paganin, D., Mayo, S. C., Gureyev, T. E., Miller, P. R., and Wilkins, S. W., "Simultaneous phase and amplitude extraction from a single defocused image of a homogeneous object," *J. Microsc.* **206**(1), 33–40 (2002).
[18] Gureyev, T. E., Paganin, D. M., Myers, G. R., Nesterets, Y. I., and Wilkins, S. W., "Phase-and-amplitude computer tomography," *Appl. Phys. Lett.* **89**(3), 034102 (2006).
[19] Leika Mikrosysteme GmbH, "Application Note: Micro-CT of Insect Brain Protocol," (January 2015).
[20] Palenstijn, W., Batenburg, K., and Sijbers, J., "Performance improvements for iterative electron tomography reconstruction using graphics processing units (gpus)," *Journal of structural biology* **176**(2), 250–253 (2011).
[21] van Aarle, W., Palenstijn, W. J., De Beenhouwer, J., Altantzis, T., Bals, S., Batenburg, K. J., and Sijbers, J., "The astra toolbox: A platform for advanced algorithm development in electron tomography," *Ultramicroscopy* **157**, 35–47 (2015).

3.2. A perforated anodised aluminium slide for improved specimen clearing and imaging for confocal laser scanning microscopy

In this chapter an anodised aluminium object-slide to scan specimen in the confocal laser scanning microscope is described. This slide improves the procedure of bulbus organ clearing and mounting for confocal laser scanning microscopy. The slide is perforated, and specimens can be mounted in holes dimensioned to their size in the clearing and mounting medium. The slide is equipped with cover slips on both sides adding to the convenience.

Felix Quade, Beate Preitz, Nikola-Michael Prpic

Author contributions to practical work:

Felix Quade: Designed the slide, Fixation, bleaching, clearing and imaging of the specimens.

Beate Preitz: Designed the slide

Status: Published in BMC Research Notes (2018) 11,1 pp.716 DOI: 10.1186/s13104-018-3826-3

Quade, F. S. C., Preitz, B., & Prpic, N.-M.. A perforated anodised aluminium slide for improved specimen clearing and imaging for confocal laser scanning microscopy. BMC Research Notes,.

Quade *et al. BMC Res Notes (2018) 11:716*
https://doi.org/10.1186/s13104-018-3826-3

BMC Research Notes

RESEARCH NOTE

Open Access

A perforated anodised aluminium slide for improved specimen clearing and imaging for confocal laser scanning microscopy

Felix Simon Christian Quade[1,2], Beate Preitz[1,2] and Nikola-Michael Prpic[1,2,3*]

Abstract

Objective: The bleaching, clearing and handling of tiny specimens with soft tissue and cuticular components for confocal laser scanning microscopy is difficult, because after cuticle bleaching and tissue clearing the specimens are virtually invisible. We have adjusted the design of the specimen container described by Smolla et al. (Arthropod Struct Dev 43:175–81, 2014) to handle tiny specimens.

Results: We describe a perforated and anodised aluminium slide that was designed to hold the distal tips of the pedipalp appendages of the spider *Parasteatoda tepidariorum* during clearing, and that can then be used directly for confocal laser scanning microscopy. We believe that this slide design will be helpful for others who want to visualise specimens between 500 and 800 µm with confocal laser scanning microscopy.

Keywords: Confocal laser scanning microscopy, Tissue clearing, Imaging

Introduction

Confocal laser scanning microscopy (CLSM) is a widely used visualisation technique in biology. Its major advantage is the capability to produce precise optical sections of a specimen, and these sections can be assembled into three dimensional reconstructions of the specimen using image processing software (e.g. Amira). The major limitation of CLSM is that the specimen has to be transparent to allow the laser to penetrate into the specimen. Thus, CLSM is mainly used for biological samples that are transparent or only slightly pigmented (e.g. embryos, many larval types). Many arthropods, however, have a strongly pigmented cuticle that prevents laser beams to enter the inside of the body. Smolla et al. [1] have devised a method to bleach the pigmented cuticle of insects and at the same time preserve and clear the soft tissue of the specimen. This method thus makes both the cuticle and the soft tissue fully transparent and allows the in situ documentation of internal soft tissue as well as cuticle with CLSM. We have transferred this method to the common house spider *Parasteatoda tepidariorum* and have applied it to the heavily pigmented pedipalp of the male. The protocol by Smolla et al. [1] worked very well, but we had difficulties with the handling of our tiny specimens (approx. 500–800 µm) after they had been fully bleached and cleared, because they were virtually invisible in the clearing medium and the 1 cm container described by Smolla et al. [1] proved too large for our specimens.

Main text

We have devised a perforated aluminium slide that allows us to perform the clearing of several tiny specimens already on the slide that is also used for CLSM and therefore renders the further handling of the hardly visible specimens unnecessary. The slide was manufactured in our in-house precision mechanics workshop. It is made of aluminium alloy (DIN AlMgSi1) and has the dimensions of a regular glass microscope slide, approximately 75 mm × 25 mm × 0.5 mm (Fig. 1a). The slide was precut from the metal sheet using a Festool Cs70 EB bench

*Correspondence: nikola-michael.prpic-schaeper@allzool.bio.uni-giessen.de
[3] Justus-Liebig-Universität Gießen, Allgemeine Zoologie und Entwicklungsbiologie, Carl-Vogt-Haus, Heinrich-Buff-Ring 38, 35392 Gießen, Germany
Full list of author information is available at the end of the article

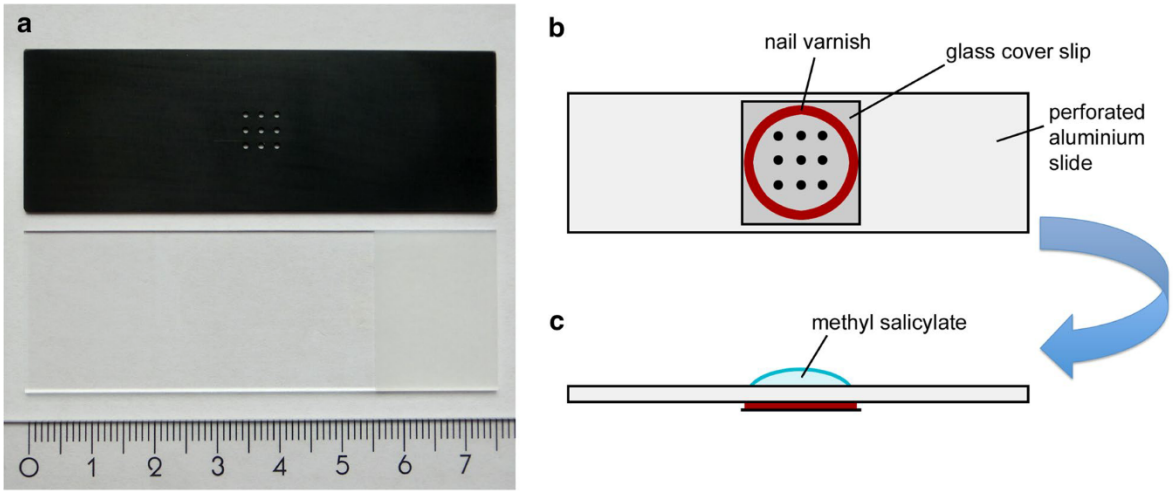

Fig. 1 A perforated anodised aluminium slide for clearing and CLSM imaging of small specimens. **a** The anodised slide is shown at the top; note the holes that serve as containers for the specimens. A conventional glass microscope slide and a ruler (in cm) are shown below the slide for comparison. **b** Preparation of the aluminium slide for tissue clearing. A ring of nail varnish (denoted in red) and a cover slip are placed over the perforated area. **c** The slide is then turned upside down to place the specimens into the holes and to place a drop of methyl salicylate (denoted in blue) on the perforated area

saw and was then milled to its final size using a milling machine (Deckel Maho DMU 50 T, CNC-controlled) equipped with an end-mill cutter of 4 mm diameter. In the centre of the aluminium slide we drilled 9 holes arranged in three rows. The diameter of the holes is 0.9 mm. The holes were drilled with the Deckel Maho DMU 50 T machine equipped with a twist drill bit (diameter 0.9 mm). These holes hold the specimens during clearing, but also allow the penetrance of the laser during imaging. In our experience in an untreated aluminium slide the laser light is reflected to a certain degree due to the small diameter of the holes. This laser reflection is problematic during imaging and reduces the image quality. We have therefore anodised the aluminium, so that the slide and, most importantly, the inside of the holes is lustreless and completely black. For anodising we used the Colinal technique ("**col**our **in al**uminium"; electrolytic colouring with Tin(II) sulfate) and the maximum colour depth EURAS C-35 ("black"). The process of electrolytic colouring has been performed in the central workshop for precision mechanics, Department of Physics, Göttingen. The black surface of the aluminium entirely prevented laser light reflection during imaging.

For tissue clearing, the slides were prepared as follows (Fig. 1b): around the square of 9 holes in the slide a ring of nail varnish was applied with a varnish brush. Then a square glass cover slip (18 mm × 18 mm × 0.17 mm) was placed on the nail varnish (lower the cover slip carefully, so that no nail varnish is pressed into the holes; the holes must remain entirely clean). After a few minutes the nail varnish has dried and fixes the cover slip tightly to the aluminium slide. The aluminium slide can then be turned upside down (Fig. 1c). The dehydrated specimens were then placed in the holes (one specimen per hole) and a sufficient drop of methyl salicylate was applied onto the specimens. The methyl salicylate should be added slowly and carefully to avoid washing out the specimens and to ensure that enough methyl salicylate enters the holes without air bubbles. After all holes were filled with methyl salicylate, a second glass cover slip was placed on top of the methyl salicylate in the perforated area, and excess methyl salicylate was carefully wiped away with an ethanol soaked, lint-free cloth. After an incubation time of approximately 60 min, the specimens were cleared (Fig. 2a, b) and the aluminium slide with the cleared specimens in the 9 holes was directly used for CLSM (Fig. 2c). Importantly, after the incubation time, the slide can also be turned upside down to scan the specimens from the other side. This facilitates the scanning of objects that are too deep to be scanned from one side only.

Limitations

The basis for our perforated anodised aluminium slide is the specimen chamber described by Smolla et al. [1], which proved to be too large for our purpose of clearing the tiny pedipalp tips of *P. tepidariorum*. The slide described in this note is therefore specially designed for tiny specimens, of about 500–800 µm. Larger specimens

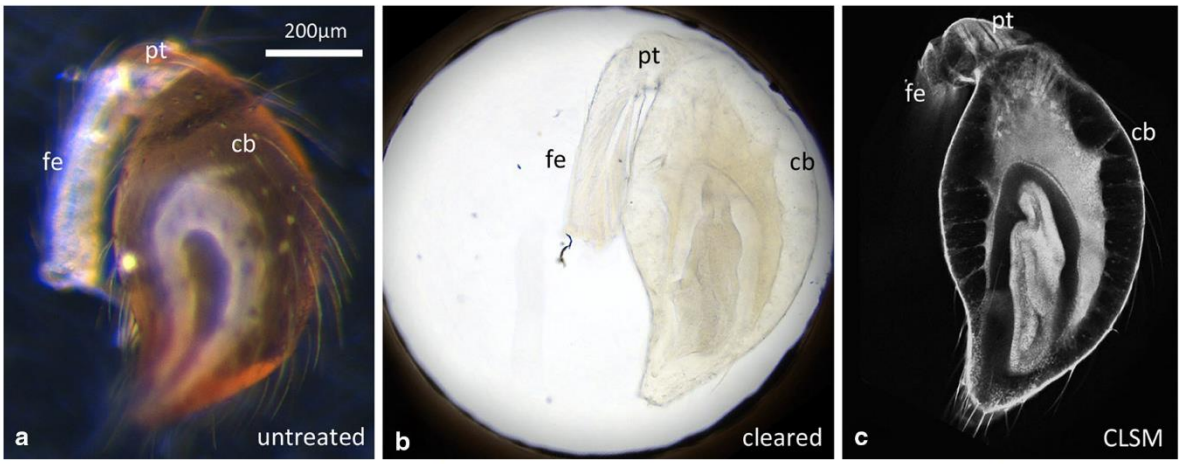

Fig. 2 Specimen bleaching and CLSM imaging using the perforated anodised aluminium slide. **a** An untreated subadult pedipalp tip. The distal end comprises the segments femur (fe), patella (pt), and the club (cb). The club is surrounded by dark brown cuticle and contains internally (not visible) the primordium of the tibia, cymbium and the male copulatory organ (bulb). **b** A pedipalp tip fully cleared embedded in a hole of the perforated aluminium slide. The cuticle and the internal tissue are transparent. **c** CLSM image showing an optical section through the pedipalp tip. Internal anatomy of the club is well preserved (the primordium of tibia and cymbium surrounding the bulb organ). Scale bar: 200 µm (for all panels)

are better handled in the specimen chamber as described by Smolla et al. [1]. We have no experience with specimens smaller than 500 µm, but we believe that the diameter of the holes can be made less than 0.9 mm to suit smaller specimens, if the inside of the holes is properly anodised to prevent laser light reflections.

Authors' contributions
Designed the slide described in this note: FSCQ, BP. Devised the project: NMP. Wrote the manuscript: NMP. All authors read and approved the final manuscript.

Author details
[1] Georg-August-Universität Göttingen, Johann-Friedrich-Blumenbach-Institut für Zoologie und Anthropologie, Abteilung für Entwicklungsbiologie, Justus-von-Liebig-Weg 11, 37077 Göttingen, Germany. [2] Göttingen Center for Molecular Biosciences (GZMB), Ernst-Caspari-Haus, Justus-von-Liebig-Weg 11, 37077 Göttingen, Germany. [3] Justus-Liebig-Universität Gießen, Allgemeine Zoologie und Entwicklungsbiologie, Carl-Vogt-Haus, Heinrich-Buff-Ring 38, 35392 Gießen, Germany.

Acknowledgements
We thank Tobias Mühmer and Sven Neumann (precision mechanics workshop, Johann-Friedrich-Blumenbach-Institute, Göttingen) for help with the manufacturing of the aluminium slides, and Christof Schmidt and Alexander Gehrt (central workshop for precision mechanics, Department of Physics, Göttingen) for help with anodising.

Competing interests
The authors declare that they have no competing interests.

Availability of data and materials
All data generated or analysed during this study are included in this published article.

Consent for publication
Not applicable.

Ethics approval and consent to participate
Not applicable.

Funding
This work was funded by the Deutsche Forschungsgemeinschaft [DFG; Grant Numbers PR1109/6-1 and PR1109/6-2 (to NMP)]. Additional financial backing has been received from the Göttingen Center for Molecular Biosciences (GZMB), Göttingen University (GAU), and Justus-Liebig-University Gießen (JLU). The funders had no role in study design, data collection and analysis, decision to publish, or preparation of the manuscript.

Publisher's Note
Springer Nature remains neutral with regard to jurisdictional claims in published maps and institutional affiliations.

Received: 10 August 2018 Accepted: 8 October 2018
Published online: 10 October 2018

Reference
1. Smolla M, Ruchty M, Nagel M, Kleineidam CJ. Clearing pigmented insect cuticle to investigate small insects' organs in situ using confocal laser-scanning microscopy (CLSM). Arthropod Struct Dev. 2014;43:175–81.

3.3. Morphology of the pedipalp tip in adult *Parasteatoda tepidariorum*

This chapter delivers a description of the adult morphology of the bulbus organ of *Parasteatoda tepidariorum*. Through virtual dissection of the bulbus organ each sclerite, the connecting membranes and some details of the contained soft-tissue are depicted and described. Based on this data the function of the blind sperm duct and the homology hypotheses of the sclerites are discussed.

Felix Quade, Jasper Frohn, Mareike Töpperwien, Torben Ruhwedel, Wiebke Möbius, Tim Salditt, Nikola-Michael Prpic

Author contributions to practical work:

Felix Quade:	Preparation of bulbus organs for µCT, reconstruction and segmentation of the µCT-image-stack, Fixation, serial-semi-thin sectioning, staining of bulbus organs and imaging of the sections
Mareike Töpperwien:	Development of the script for µCT-reconstruction
Jasper Frohn:	Development of the µCT-imaging setup
Torben Ruhwedel:	Resin embedding for serial-semi-thin sectioning of the bulbus organs

Status: First draft of the manuscript

Morphology of the pedipalp tip in adult Parasteatoda tepidariorum

Introduction

Some arachnid groups have evolved specialised genital organs in the male, e.g. the penis in harvestmen (Opiliones). By contrast, spider have modified the tip of the second appendage, the pedipalp, to serve as an intromittent organ. Similar to the female pedipalp, the male pedipalp is a segmented appendage, similar to the walking legs, but usually shorter and thinner. In the male, the distalmost segment, the tarsus, is flattened and broadened. It bears at its ventral side an outgrowth, the bulbus organ, which is used to take up the sperm that is discharged from the male genital opening, store it, and transfer it into the female genital opening during copulation.

In basally branching spiders, this bulbus organ is a simple sac, often likened to a pipette that just aspirates and ejects the seminal fluid. However, in the majority of spiders the bulbus organ has an intriguingly complex shape, with a number of specially formed hard parts (sclerites). This complex morphology of the male bulbus organ is mirrored in a similarly complex shape of the female genitalia (epigyne). The male and the female genitalia apparently form a functional unit, similar to a key and a lock. The purpose of this complexity is still unclear, but it is generally assumed that the exact fitting of the male bulbus into the female epigyne is necessary for safe sperm transfer, prevention of sperm loss, and the recognition of species (by prezygotic isolation). Indeed, bulbus morphology is highly species specific and is widely used in taxonomy as a key character to distinguish between closely related species.

This complexity and diversity make the identification of corresponding parts in different species difficult and has led to a number of conflicting hypotheses about the homology of the different bulbus organ components among diverse spider groups. The homology of sclerites between different spider families is still controversial, but progress has been made within some spider groups. For the family Theridiidae (cob-web spiders) the work by Agnarsson et al. (2007) provides a thorough review and synthesis of previous views of sclerite homology among Theridiidae, and also provides a solid framework for homology hypothesis testing. The spider species studied in this work, *Parasteatoda tepidariorum*, belongs to this spider family.

Because of the complexity of the bulbus organ, a detailed description of its components is difficult and usually relied on destructive methods (e.g. sectioning, dissection) that provided some insight, but at the same time destroyed the three-dimensional aspects and relationships of the components. Non-destructive methods like diffusible iodine-based contrast-enhanced micro computed tomography (dice-μCT) now contribute significantly to our understanding of the morphology of complex biological structures therefore, I have applied these methods to the study of the morphology of the adult bulbus organ of *P. tepidariorum*. This work supports the vast majority of the homology hypotheses by Agnarsson et al. (2007), but also provides an update especially on the interplay of the sclerites and previously unrecognized membranes between them. Therefore, two homology hypotheses are not supported, especially the notion that *P. tepidariorum* is lacking the theridioid tegular apophysis (TTA, see explanation below).

My results are also a strong basis for future analyses of functional morphology and developmental genetic studies. Especially the search for genes involved in the morphology of the bulbus organ requires a solid understanding of the morphology of the wildtype, in order to correctly interpret possible phenocopies and phenotypes.

Material and Methods

Parasteatoda tepidariorum husbandry

Our *P. tepidariorum* husbandry is kept at controlled temperature (25 °C) and dark/light cycle (10 hours of light). The animals are kept separate in plastic vials sealed with styrene foam plugs and are supplied regularly with water and food. Juveniles are fed with *Drosophila melanogaster* flies, older stages and adults are fed with larger flies (*Musca domestica* and *Lucilia caesar*) or juvenile crickets (*Acheta domesticus*). Water is provided by humid soil.

Specimen fixation

The spiders to be studied by histology and diffusible iodine-based contrast-enhanced micro computed tomography (dice-µCT) were anaesthetised at -20°C for 7-10 minutes. Then the opisthosoma was removed and only the prosoma was placed in Karlsson and Schultz phosphate buffer (13mM sodium dihydrogen phosphate monohydrate, 85mM di-sodium hydrogen phosphate dehydrate, 85mmol NaCl, 2,5% glutaraldehyde, 4% formaldehyde in water) at 4°C over night. After fixation, the pedipalps were separated

from the spider. Treatment for dice-µCT involved dehydration, iodine staining and critical point drying (see below).

Histology

Pedipalp tips were embedded in epoxy resin. Semi-thin sections (0.5µm) were prepared (Leica RM 2155, using a diamond knife Histo HI4317, Diatome) and stained with a mixture of 1% toluidine blue and azur II–methylene blue for 1 min at 60 °C. Microscopic images were collected using an Axio Imager 2 microscope (Zeiss) equipped with Axiocam 305 color and Axiocam 506 mono (Zeiss) respectively and zen blue 2018 software.

Dehydration and iodine staining for dice-µCT

An ethanol series was performed comprising the following steps for at least 30 min each: 30%, 50%, 70%, 80%, 90%, and 95% ethanol in water. Then the pedipalps were incubated twice in 100% ethanol for half an hour each. After the dehydration was complete the pedipalps were stained with iodine (in ethanol) to increase contrast. Iodine changes the interaction of the specimen with the x-rays, through an increase of phase shift and absorption. A solution of 1% iodine in ethanol was added to the vial with fully dehydrated samples overnight, then the samples were rinsed three times with 100% ethanol to remove excess iodine.

Critical point drying

An automatic critical point dryer (Leica EM CPD300) was used to perform critical point drying. After the samples were dehydrated and iodine stained, they were transferred into a microporous container to avoid losing it due to its very small size. These containers were placed into a larger container filled with 100% ethanol and placed in the critical point

dryer. 18 cycles of ethanol/liquid carbon dioxide (CO_2) exchange were performed to quantitatively remove the ethanol. The CO_2 was then slowly heated to 31°C with a pressure of 74 bar. It is essential to perform this phase transfer of CO_2 very slowly in order to avoid capillary forces or volume changes that would damage delicate morphological structures inside the forming pedipalps.

Diffusible iodine-based contrast-enhanced micro computed tomography (dice-µCT)

To achieve proper resolution of the soft tissue portions of the samples a self-commissioned laboratory-based X-ray phase-contrast tomography setup was used for dice-µCT imaging[24]. To reach a high resolution of approximately 1 µm despite a relatively high focal spot size of the X-ray source (70 µm) an inverse geometry (source-to sample distance >> sample-to-detector distance) in combination with the high-resolution detector XSight (Rigaku, Prague, Czech Republic) was used. The resolution of this setup is limited to the detector point spread function (0.54 µm) due to negligible optical magnification. The detector´s field of view is 1.8 x 1.4 mm, but we chose as the maximum sample dimensions 0.8 x 0.5 x 0.5 mm, because this makes it much easier to perform tilt corrections in the reconstruction step. A detailed setup description has been published previously[24]. For tomographic reconstruction 25 dark-field images, 25 flat-field images and 1000 projections over 180° were recorded with an exposure time of t = 40 s each. To increase the signal to noise ratio, each empty-beam corrected projection was binned by a factor of 2. To retrieve the phase information the Bronnikov-Aided-Correction algorithm (BAC) was applied on each projection[25,26]. The tomographic reconstruction was performed

with the (cone-beam) filtered back-projection implementation of the ASTRA toolbox[27,28,29].

Image segmentation and processing

dice-µCT 3D-stacks were processed in Amira 5.4.1 (FEI SAS, France, www.vsg3d.com). Structures of interest were marked with the brush or magic wand tool in the segment editor. With the brush tool individual or groups of pixels are marked by the user, and the magic wand is a grey value-based region growing algorithm, where the user sets the seeding points and is able to set limit lines to define borders for the growth. To insert scale bars the module scale was activated and for correct distances the orthographic camera was used in the viewer window. Images for figures were taken with the snapshot tool.

Results

Overview

The male pedipalp tip of *P. tepidariorum* is a morphologically complex structure. It comprises a number of parts that have all been adapted to aid in the main role of the male pedipalp: copulation. An overview of the main components of the distal pedipalp is shown in Figs. 1 and 2. The fundament of the pedipalp tip is the cymbium that gives rise to the bulbus organ and that at the same time holds this organ in place when it is not used. The bulbus itself comprises a "fleshy" portion that is sac-shaped and that supports on its surface a number of heavily-sclerotised sclerites. This bulbus organ also houses a number

of internal structures, e.g. a blind sac for sperm storage and several glands. In the following sub-chapters, I will describe the morphology of these components separately. Please note that I adopt the nomenclature by Agnarsson et al. (2007) for all morphological structures. However, the homology of some of the structures is unclear: this will be discussed in more detail in the discussion.

Cymbium

The cymbium is the distal-most segment of the male pedipalp. It is therefore homologous to the tarsus of the female pedipalp, but has been strongly modified morphologically, to support the role of the male pedipalp in copulation. The entire segment is broadened and flattened, and its ventral side is strongly concave ("scoop shaped") in order to hold the bulbus organ in this cavity. This concave side is sometimes called "alveolus". The bulbus is an outgrowth of the ventral side of the cymbium, that emerges from a site near the joint between the cymbium and the tibia. The bulbus is thus essentially a membranous sac formed by the ventral hypodermis of the cymbium. This sac produces a number of large sclerites that almost entirely surround the sac. Only a few spots of the sac are not covered by sclerites: these "naked" portions are termed haematodochae (see below).

The cymbium also plays an important part in the unique mechanism that locks the bulbus organ when it is not in use. It has a groove in the distal portion that interacts with the proximal embolus to secure the bulbus organ in its resting position (Fig. 3). This interaction is further explained in the sub-chapter that deals with the proximal embolus. The outer side of the cymbium bears approximately 90 sensory hairs (Fig. 4). Over most of the

surface these hairs are evenly spaced, thus indicating that there is some genetic spacing mechanism involved during the specification of these hairs during development (e.g. lateral inhibition). Near the distal tip the density of the hairs is highest, whereas the area near the cymbium-tibia joint does not bear any sensory hairs. The presence of the hairs on the cymbium indicates that the cymbium still serves the sensory function of the normal tarsus, despite its heavy modification for its main function in copulation.

Sclerites

a) Conductor

The conductor is the distalmost sclerite of the bulbus organ (Figs. 5 and 6). Its inner surface is concave ("scoop shaped") and this shape accommodates and guides the embolus (see next sub-chapter) when it is inserted into the female genital opening. On the outside (the convex side) there are a number of rows composed of scale-like structures. The role of these scales in not clear. However, similar scales are found in other species of the genus as well, indicating that the scales serve some evolutionarily conserved function.

b) Distal embolus

The embolus is a medium-sized sclerite and is clearly bipartite in *P. tepidariorum* (Fig. 7). The two parts are separated by a distinct suture. The distal part of the embolus has a spiral shape (Figs. 8, 9), tapering towards the tip. The bend of the embolus fits into the concave side of the conductor and is guided by the conductor when the embolus is inserted into the female genital opening. The distal tip of the embolus has an opening through which the male can take up its own sperm and ejaculate it into the female sperm storage organ.

The sperm is sucked up through the distal opening into a blind duct that end in a sac-shaped fundus. This blind sperm duct is described below in more detail.

c) Proximal embolus

The proximal part of the embolus is separated from the distal part by a deep furrow (Fig. 10) and has a characteristic outgrowth that serves as a hook that grips into a notch in the cymbium (Fig. 10). In this way the spider can control the expansion of the bulbus organ. Normally, the bulbus is safely locked in the concave side of the cymbium, by the insertion of the proximal embolus hook into the cymbal notch. However, if the male engages in copulation with a female, the male can also actively retract the hook from the notch, and in this way unfold the bulbus with its sclerites in order to attach it to the female genital opening.

d) Tegulum

The tegulum is a large sclerite that stabilises the soft portions of the bulbus. It is ring shaped and has an additional bar that divides the inner side of the ring into a smaller and a larger opening (Fig. 11-13). It sits on top of the subtegulum (see below). The blind sperm duct that comes from the inside of the distal embolus, enters the tegulum near the smaller opening. The duct then coils further and follows the ring structure of the tegulum for about 75% of its circumference, until it exits the tegulum towards the subtegulum. The tegulum thus shields and protects a significant portion of the blind sperm duct. In addition, the tegulum also protects two internal glands that follow the blind sperm duct (see below) (Fig. 14).

e) Subtegulum

Like the tegulum, the subtegulum is a strap that surrounds and stabilises the soft portions of the bulbus organ (Fig. 15). And like the tegulum, also the subtegulum is ring shaped. This enables haemolymph, innervation and a single blood vessel to enter the bulbus organ from the cymbium. In addition, the ring of the subtegulum houses and protects the blind end (fundus) of the blind sperm duct (see also below).

Connective membranes

a) Basal haematodocha

All sclerites are connected by membranous, "soft" areas. By far the largest of these membranes is the basal haematodocha (Fig. 16). It is the membrane between the subtegulum and the cymbium and thus is the connection between the cymbium and the entire bulbus organ. But in addition to this role in connecting the bulbus to the cymbium, the area of this membrane is also massively enlarged. Therefore, the major portion of the basal haematodocha does not fit into the gap between the subtegulum and the cymbium and is heavily wrinkled, folded in two layers and wrapped around the subtegulum. In the resting position of the bulbus organ, the subtegulum is therefore entirely covered by the basal haematodocha. The reason for the massive enlargement is that the folded haematodocha can be inflated by haemolymph pressure during copulation (Fig. 17). The male unlocks the hook of the proximal embolus from its notch in the cymbium, thus enabling the inflation of the basal haematodocha by the influx of high-pressure haemolymph. The expansion of the basal haematodocha moves the entire bulbus away

from its resting position in the concave side of the cymbium, and probably also provides pressure to expel the sperm stored in the blind sperm duct.

b) Median haematodocha

The median haematodocha is the membrane that connects subtegulum and tegulum (Fig. 18). It is inflatable as well but is not heavily folded. Its main function is to provide flexibility between the two sclerotised rings (tegulum and subtegulum) in order to allow a movement of the entire distal portion of the bulbus organ. This flexibility is necessary, because in the resting position all sclerites are placed closely together and this, of course, hinders their separate roles during copulation. The inflation of the basal and median haematodocha moves the sclerites apart and they become erect.

c) Embolic membrane

The embolic membrane is a narrow membrane that connects the entire embolus with the tegulum (Fig. 19). It appears that the embolic membrane extends to the suture between the distal and proximal embolus. In addition, the embolic membrane appears to be connected with the connective membrane (Fig. 20). However, a definite statement about the extensions of the embolic membrane requires additional work and more detailed microscopic three-dimensional data.

d) Connective membrane

The connective membrane is located between the tegulum and the conductor. Previously, it was believed that the conductor is a direct projection of the tegulum. However, a membrane is clearly present at the base of the conductor (Fig. 21, Fig. 22).

Internal soft structures

a) Blind sperm duct ("spermophor")

The blind sperm duct takes up the ejaculated sperm from the specially built net and stores it. It is connected with three glands that help to ejaculate the sperm and nourish them during storage (Foelix 2011).

It is built of three distinct parts (Figs. 23-25):

(1) a very thin distal part (diameter 5-10µm (Fig. 26)) starting at the embolus tip

(2) the middle part starting with a diameter of 15µm and expanding to approximately 50µm at the entrance to the last part the fundus

(3) the fundus, measuring approximately 100µm in diameter.

The first part describes a full counter-clockwise turn if viewed from ventral and in the first 3/4 turn it follows the rotation of the embolus. After leaving the embolus it crosses the tegulum until it goes over into the middle part. From the base of the embolus and during its crossing of the tegulum it is accompanied by gland #1. The middle part of the blind sperm duct follows the outer wall of the tegulum and is accompanied by the gland #3, which follows its path closely. In the last clockwise turn of the middle part lies the fundus gland (the second gland).

b) Glands

Three distinctive glands are associated with the blind sperm duct and are assumed to help with the process of sperm ejaculation (Foelix 2011). The first gland tightly surrounds about one third of the thin part of the duct (Fig. 27A). The second gland extends perpendicular to this gland and attaches to the transition between middle part and fundus (Fig. 27B). It is formed more globe-like and is connected to a large lacuna of secreted fluid directly above the sieve-like entrances to the fundus of the blind sperm duct. The third gland is attached to one side of almost the entire middle part of the duct (Fig. 27C). Cross sections through the glands (Figs. 28, 29) show that the gland tissue is connected to the lumen of the blind sperm duct via a sieve-like structure. This strongly suggests that the glands indeed empty their products into the blind sperm duct, but no further statements about the role of these secretions can be made at this point.

c) Innervation

The bulbus is innervated by a small nerve bundle closely joined by a blood vessel entering the bulbus through the duct built by the cymbium, basal haematodocha and subtegulum. From there it projects into the tegulum to build up a small ganglion situated near the gland at the blind sperm duct (between this gland and the fundus gland). At the base of the embolus a second ganglion is present which innervates at least one sensillum (Fig. 30) as described by Sentenská et al. (2017). Unfortunately, it is currently unclear what further structures are innervated by these small ganglia. Their location suggests that they at least innervate the associated glands, and/or some portions of the terminal sclerites that make

direct contact with the female genital opening. However, further work and higher resolution data will be required to answer these questions more definitely.

Discussion

a) Function of the blind sperm duct

The male stores its own sperm in the bulbus until it can be discharged into the female genital opening during copulation. The males of many spider species weave a specialized web (a so-called sperm web) in which they place a drop of sperm ejected from their genital opening at the ventral side of the opisthosoma. The male then dips its pedipalp tips into the sperm fluid and fills the blind sperm duct with sperm. This process of sperm fluid uptake is generally called "sperm induction", but the exact mechanism how the male sucks up its sperm into the bulbus is not clear. It is generally assumed that the sperm fluid enters the blind sperm duct via capillary forces, but alternative views include more active sucking forces like a pipette.

My results support the hypothesis that capillary forces enable the male to fill its blind sperm duct with sperm fluid. The distal part of the blind sperm duct is long and very thin. The diameter of this portion of the blind sperm duct as measured from µCT scans is only 10 µm. The capillary action of a glass capillary with this tiny diameter is enough to draw up water to approximately 1.4 meters (Wikipedia 2001ff). Of course, the walls of the thin portion of the blind duct are not as rigid as a glass capillary, and this will influence the capillary effect, but the capillary action should be strong enough to aspirate the sperm

liquid entirely, without the need of active sucking by compression of elements of the bulbus.

b) Homology of the sclerites

The shape of the sclerites of the male pedipalp bulbus organ is species specific, at least in higher spiders. Therefore, their morphology and function are highly diverse, and this makes homology statements between the sclerites of different spider groups quite difficult. *P. tepidariorum* belongs to the family Theridiidae. This family is characterized by a number of unique features that concern their bulbus sclerites (apomorphic characters), but the homology of the sclerites among the members of Theridiidae is still not entirely clear. Agnarsson et al. (2007) discuss the many homology hypotheses that have been proposed for the sclerites, and finally present a synthesis and new assessment for the bulbus sclerites in the Theridiidae. I adopt this scheme here, but two exceptions are explained below.

1) The embolus of *P. tepidariorum* is clearly separated into two separate sclerites. This fact alone suggests that only the distal embolus is homologous to the embolus in other species. The proximal portion, that is separated from the distal embolus by a deep suture and probably by an extension of the embolic membrane, is not actually a part of the embolus, and its homology is therefore unclear. However, this proximal portion plays an important function in the cymbium-bulbus locking mechanism described above. In other theridiid spiders, this role is played by a separate sclerite, the so-called median apophysis. Note, however, that the term "median apophysis" is used inconsistently in the literature,

which is a consequence of the complex morphology of the bulbus organ and the unclear homology relationships. Especially Levi (1961) uses the term "median apophysis" in an ambiguous way and the term may either denote soft parts ("distal haematodocha"), or different sclerites. I use the term here as defined by Agnarsson et al. (2007). In theridiid spiders the median apophysis is thought to be lacking (Saaristo 1976, Saaristo 2006) or at least lacking in some members of the genus *Parasteatoda* (Agnarsson et al. 2007). However, Yoshida (2008) regards the proximal portion of the "embolus" as the median apophysis, but without discussing the reasons why he thinks so. The facts that the sclerite proximally attached to the embolus is clearly separated from the embolus and, in addition, is the sclerite that functions as the locking sclerite, strongly support the notion by Yoshida (2008) that the proximal portion of the embolus is actually the median apophysis, and, therefore, a well-developed median apophysis is present in *P. tepidariorum*.

2) A unique sclerite of the Theridiidae (i.e. it is present only in Theridiidae), is the theridioid tegular apophysis (TTA) sensu Agnarsson et al. (2007). This sclerite is usually physically associated with the embolus and supports/stabilizes it in the resting position and also during copulation. The TTA also makes the first contact with the female during mating (Huber 1993). Although this sclerite is viewed as an apomorphy of the Theridiidae by Agnarsson et al. (2007), these authors write that some theridiid species lack the TTA sclerite, and among these species is *P. tepidariorum*. The function of the TTA as a support of the embolus makes it difficult to separate it from the conductor, that has the same function. Agnarsson et al. (2007) acknowledge this problem but provide a character to

distinguish between conductor and TTA: the conductor is always a direct outgrowth of the tegulum and therefore never connected via a membrane. The TTA, on the other hand, always has a membrane at the base that separates it from the tegulum. My data clearly show that the conductor is connected to the tegulum by a connective membrane. Therefore, the conductor of *P. tepidariorum* is not homologous to the conductor of other theridiid spiders. Rather, the conductor of *P. tepidariorum* is actually the TTA, and *P. tepidariorum* does not lack the TTA, but lacks an additional conductor.

References

Agnarsson, I., Coddington, J.A., Knoflach, B. (2007). Morphology and Evolution of Cobweb Spider Male Genitalia (Araneae, Theridiidae). J Arachnol 35, 334-395.

Foelix, R.F. (2011). Biology of Spiders. Third Edition. Oxford University Press, Oxford.

Huber, B.A. (1993). Genital mechanics and sexual selection in the spider Nesticus cellulanus (Araneae: Nesticidae). Canadian Journal of Zoology 71:2437–2447.

Saaristo, M.I. (1978). Spiders (Arachnida, Araneae) from Seychelles Islands, with notes on taxonomy. Annales Zoologici Fennici 15:99–126.

Saaristo, M.I. (2006). Theridiid or cobweb spiders of the granitic Seychelles islands (Araneae, Theridiidae). Phelsuma 14:49–89.

Sentenská, L., Müller, C. H. G., Pekár, S., & Uhl, G. (2017). Neurons and a sensory organ in the pedipalps of male spiders reveal that it is not a numb structure. Scientific Reports, 7, 12209.

Wikipedia (2001 ff.). Article "Kapillarität". URL: https://de.wikipedia.org/wiki/Kapillarit%C3%A4t (accessed on January 3, 2019).

Figures and figure legends

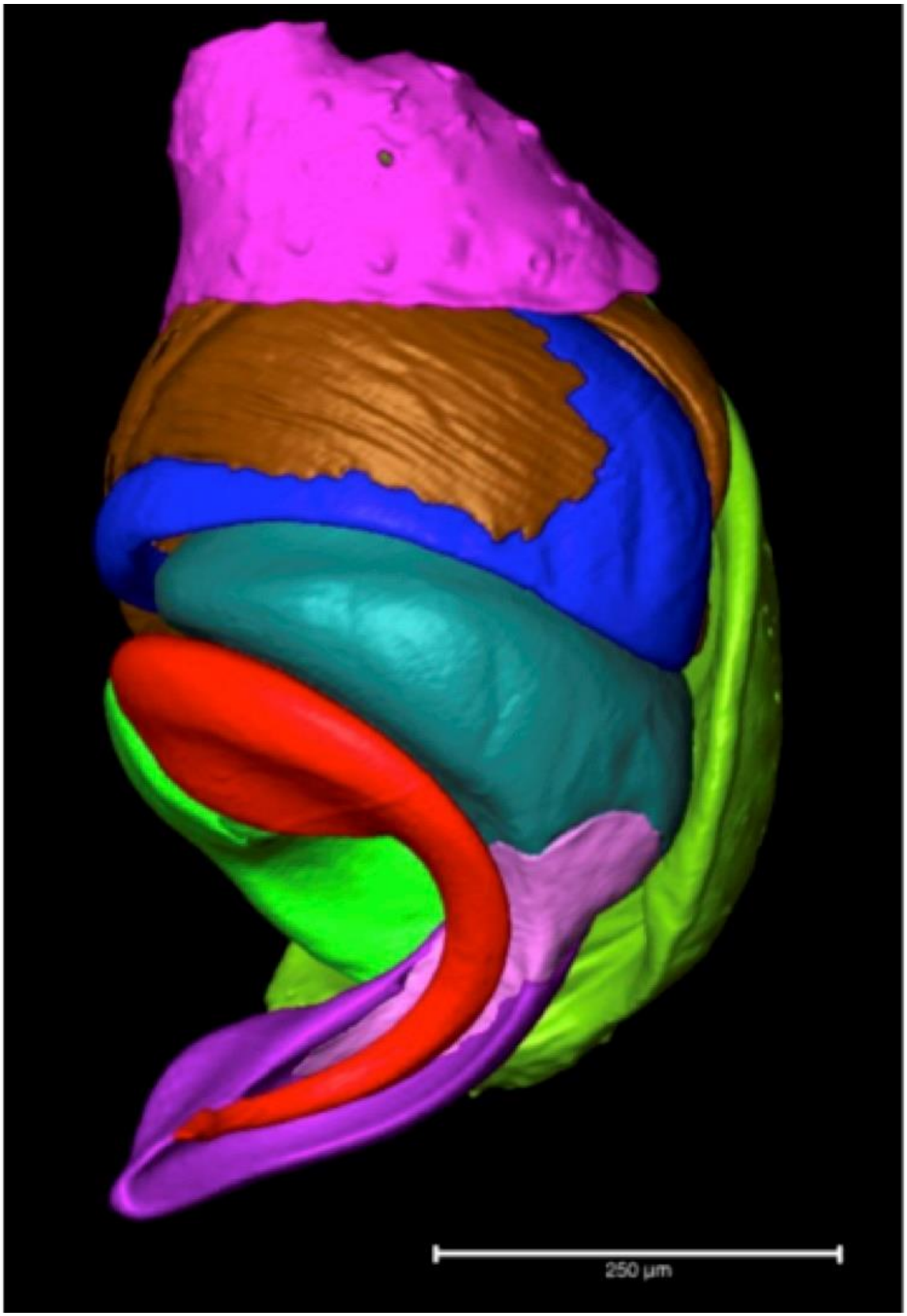

Figure 1. Overview of the distal tip of the male pedipalp of *Parasteatoda tepidariorum*. Shown is the right pedipalp tip in lateral-internal aspect. Colours indicate the following components: magenta=tibia; brown=basal haematodocha (between cymbium and subtegulum); blue=subtegulum; teal=tegulum; light green=cymbium; pink=connective membrane (between conductor and tegulum; red=distal embolus; green=proximal embolus; dark green=embolic membrane (between embolus and tegulum); purple=conductor. Scale bar: 250 μm.

Figure 2. Same specimen as in Fig. 1, but in lateral-external aspect. Scale bar: 250 µm.

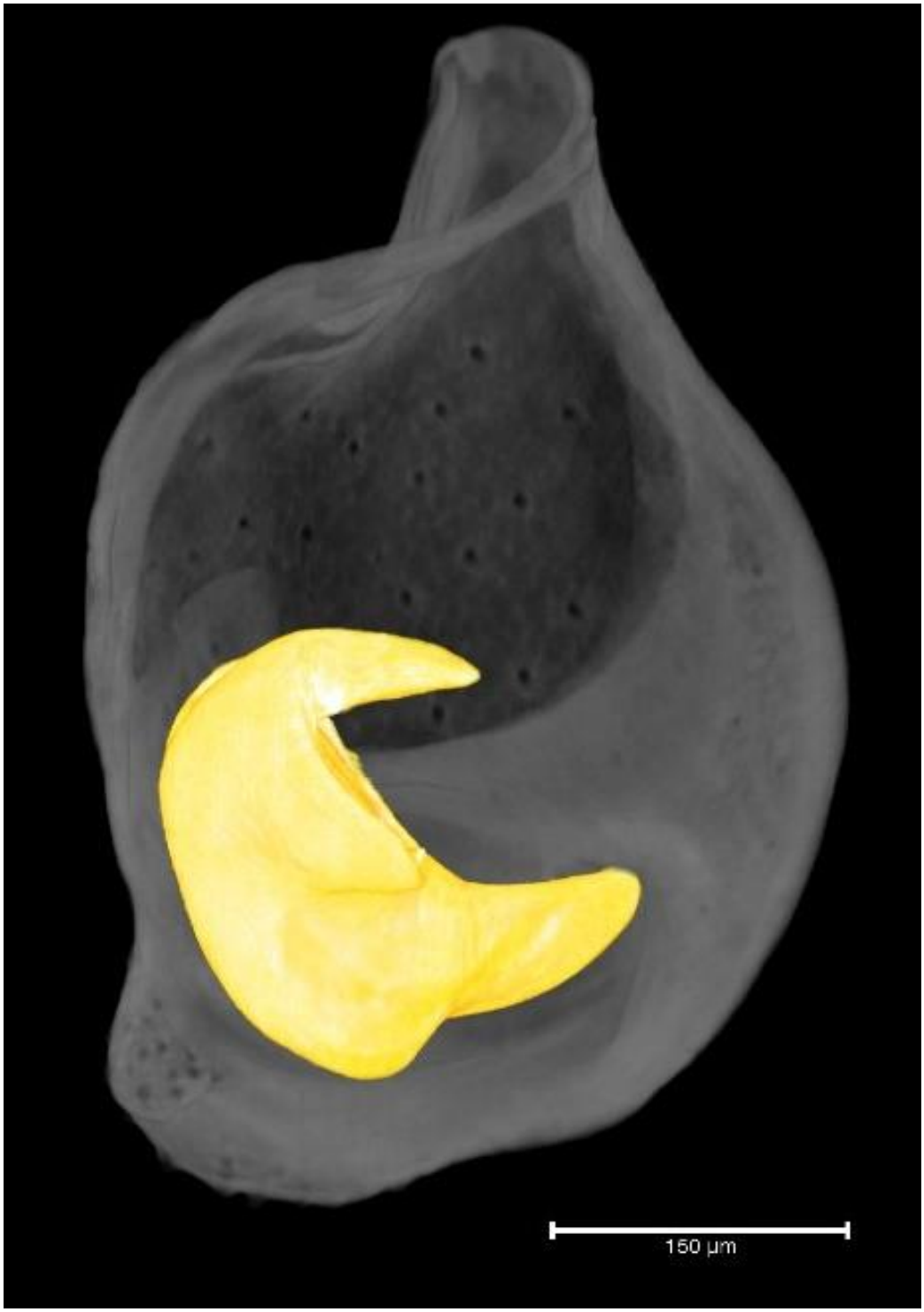

Figure 3. Ventral, semi-transparent aspect of the cymbium (gray) with proximal to the top, showing the location of the proximal embolus (yellow) with its hook inserted into the groove in the cymbium. Scale bar: 150 µm.

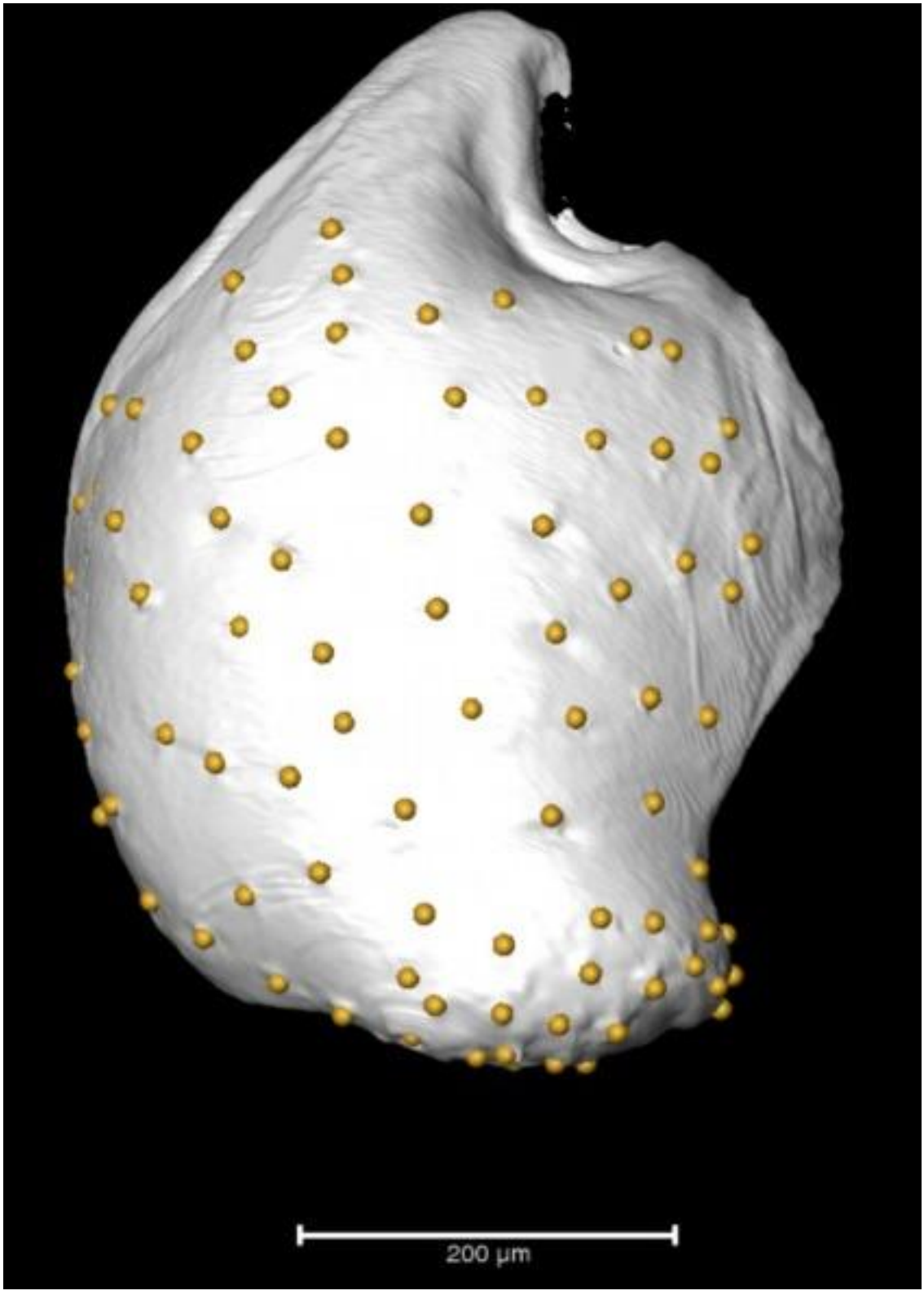

Figure 4. Surface scan of the cymbium in dorsal aspect, proximal is to the top. The location of the sensory hairs is indicated by yellow dots. Scale bar: 200 µm.


175 µm

Figure 5. Conductor viewed from the convex side. Distal is to the top. This aspect shows the scale-like structures that cover most of the distal surface. Scale bar: 175 µm.

Figure 6. Conductor viewed from the convex side. Distal is to the top. This aspect shows the scoop-shaped inner surface, that accommodates and guides the embolus. Scale bar: 175 µm.

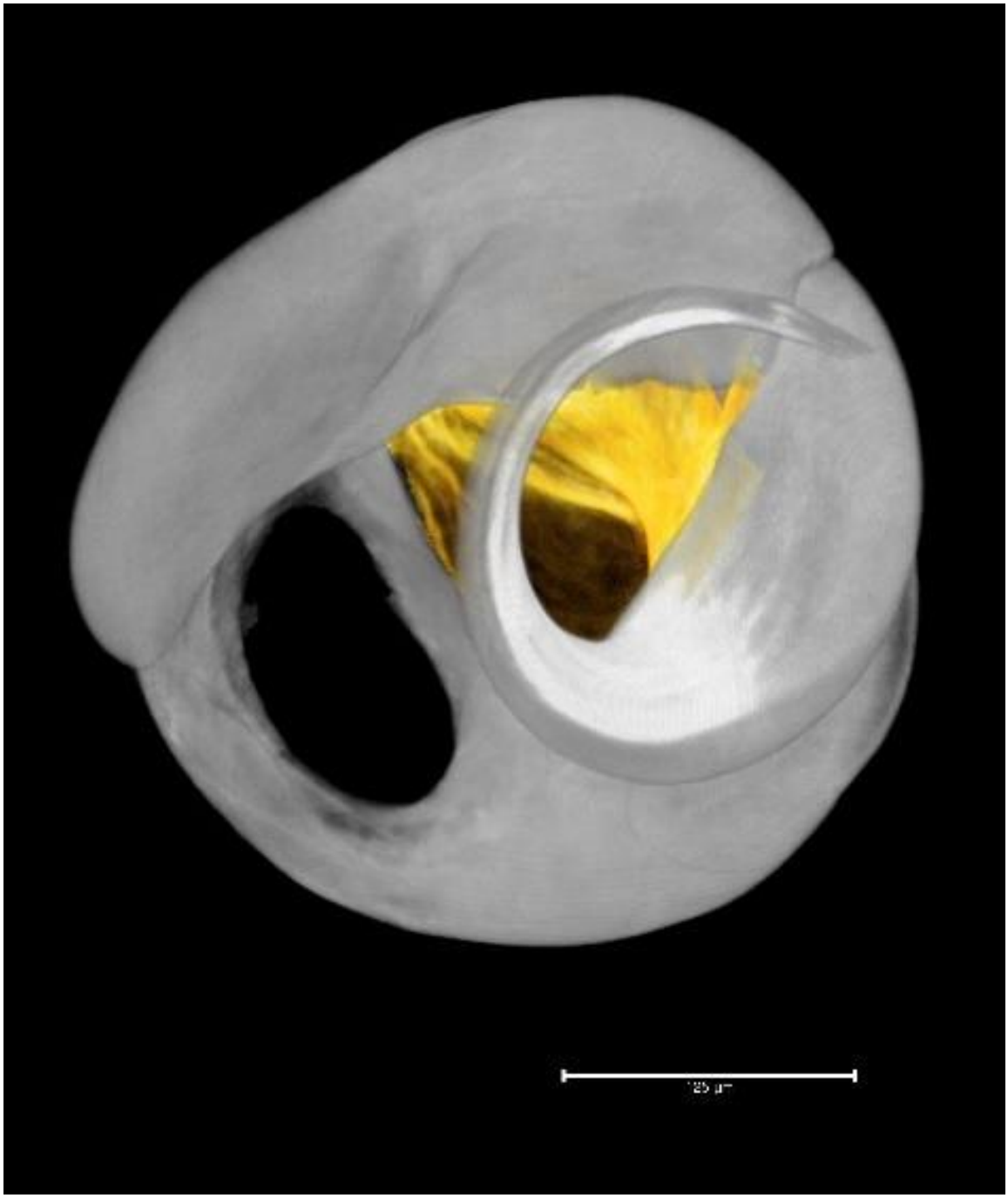

Figure 7. Embolus viewed from the distal end. The coiled distal embolus is right in the picture, and the suture between the distal and proximal embolus is clearly visible. The entire embolus sits on top of the tegulum. Scale bar: 250 µm.

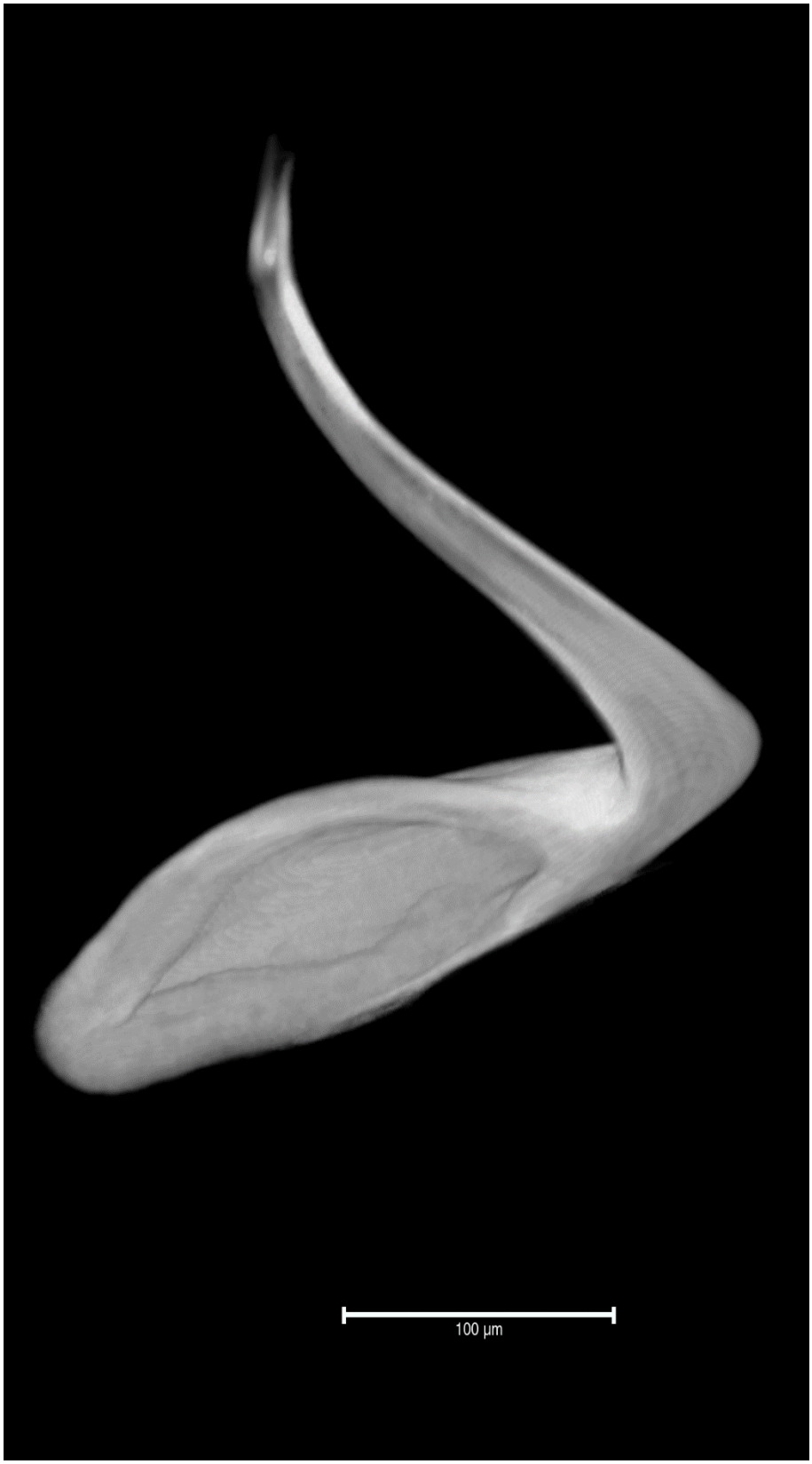
100 µm

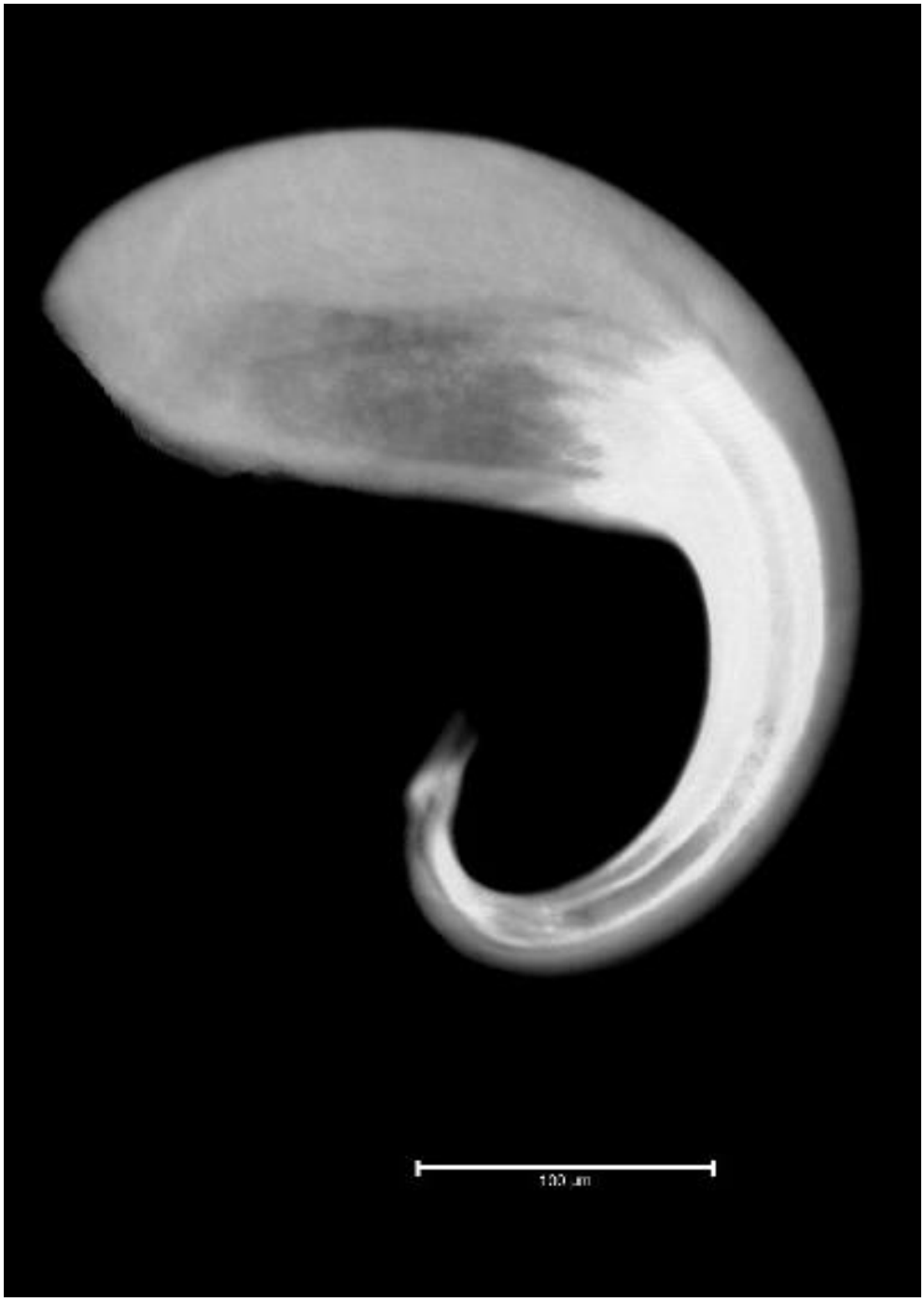

Figure 8. Distal embolus. Aspect of the surface that is attached to the proximal part of the embolus. Scale bar: 100 µm.

Figure 9. Distal embolus. Aspect of the outer surface of the distal embolus, to show the spiral shape of this sclerite. Scale bar: 100 µm.

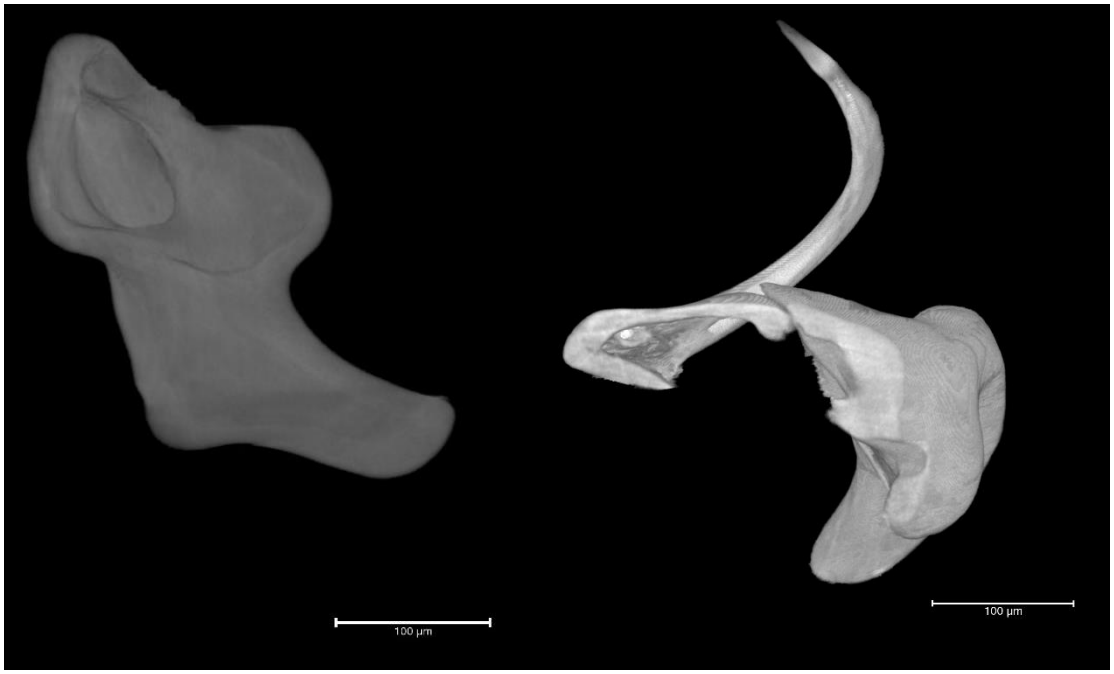

Figure 10. Proximal embolus. Left: Aspect of the surface that is attached to the distal part of the embolus. Note the outgrowth that interacts with the cymbium. Right: Aspect of the suture between distal and proximal embolus. The two sclerites are clearly separate. Scale bars: 100 µm.

Figure 11 and 12. Tegulum viewed from the top to show the ring-like shape and the internal subdivision. Scale bars: 100 µm

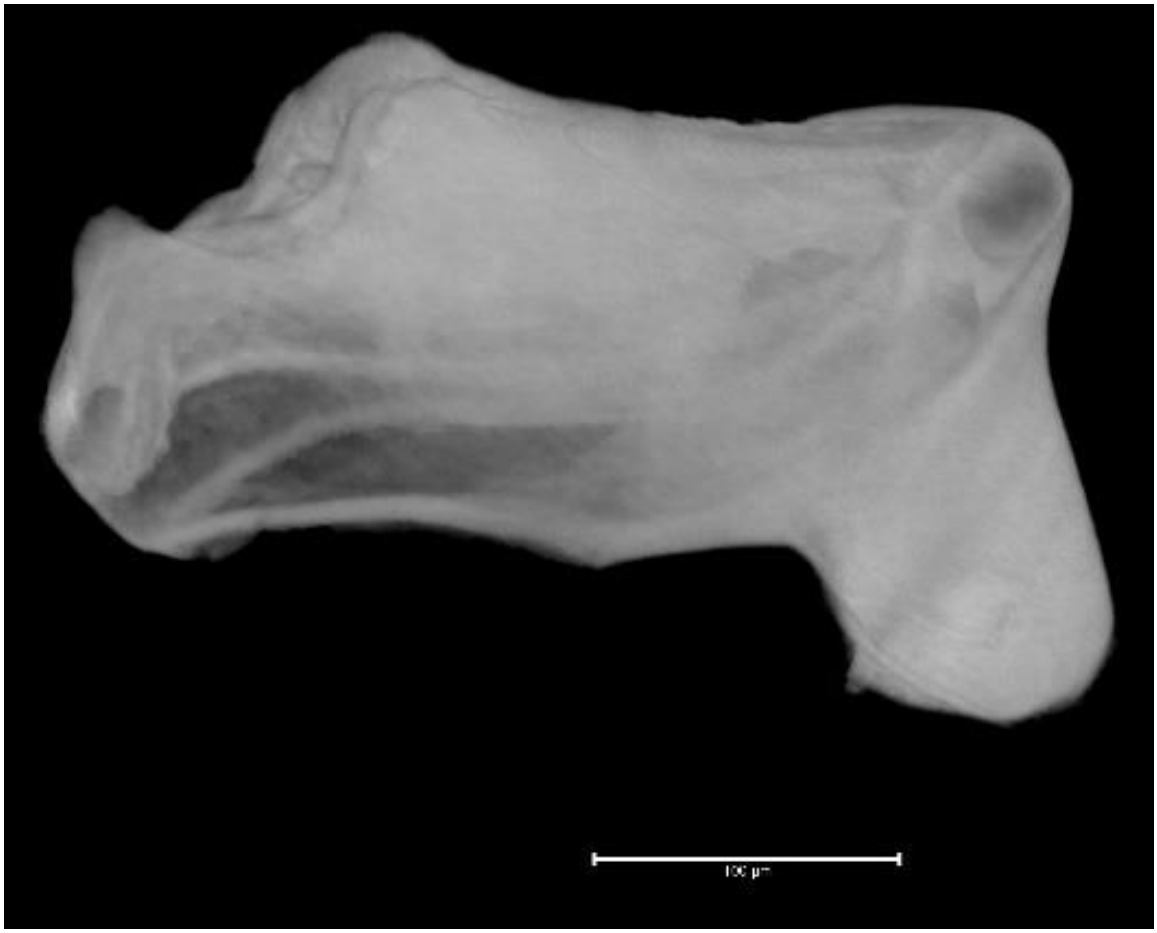

Figure 13. Tegulum viewed from the side. Scale bar: 100µm.

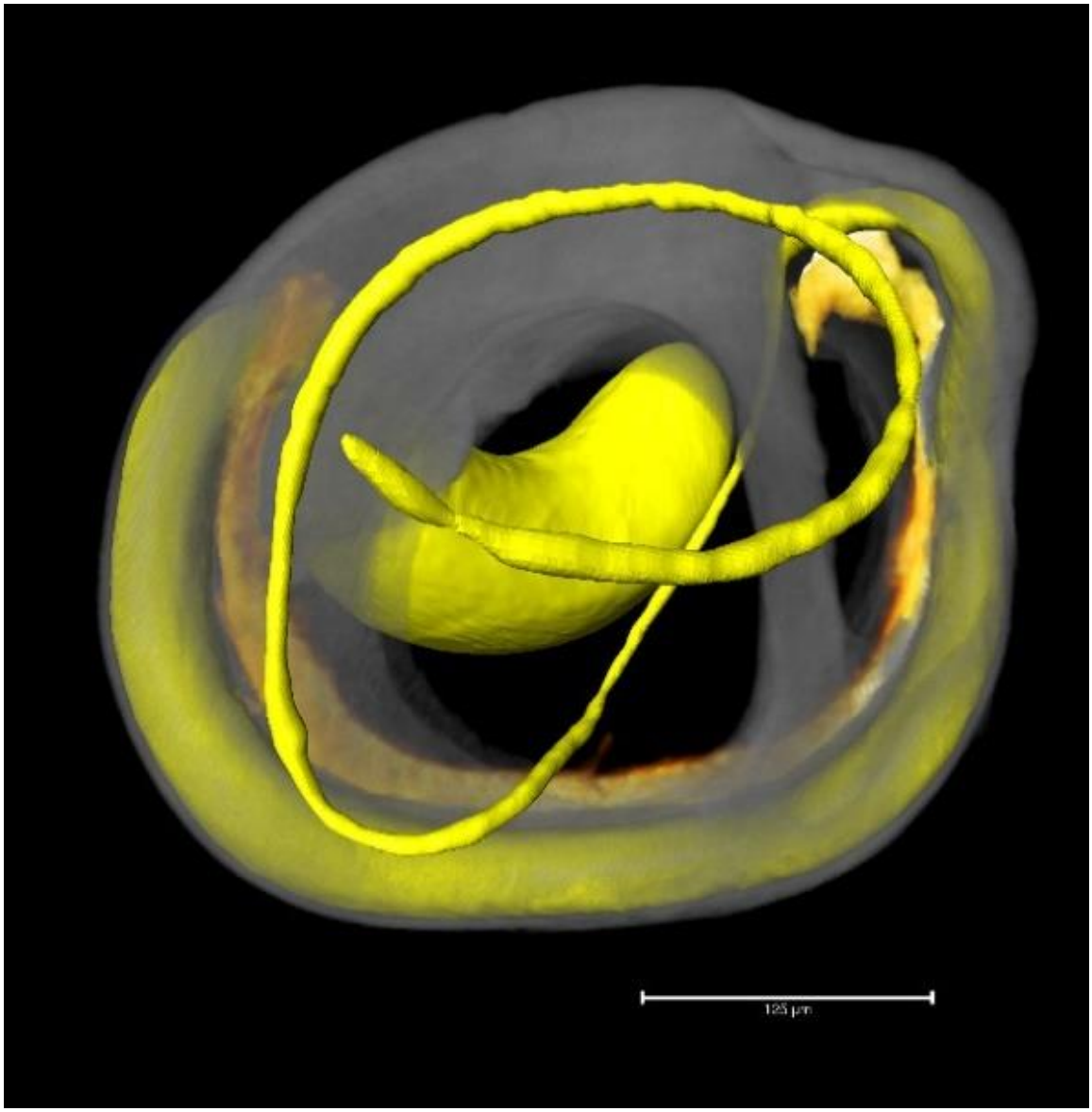

Figure 14. Distal view of the tegulum together with the blind sperm duct (yellow) and gland #3 (orange). Scale bar: 125 µm.

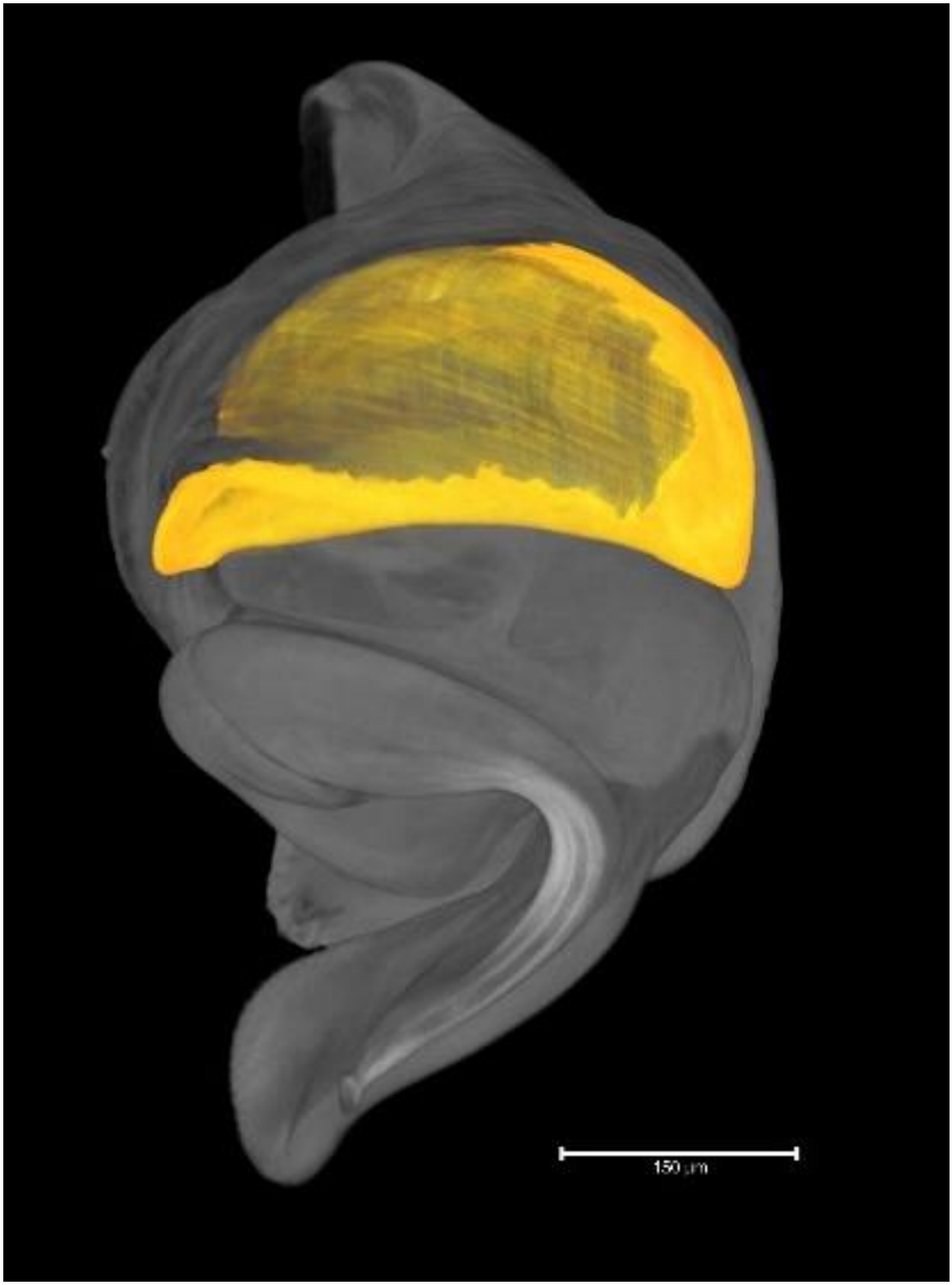

Figure 15. Position of the subtegulum (orange) in the entire pedipalp tip. Scale bar: 150 µm.

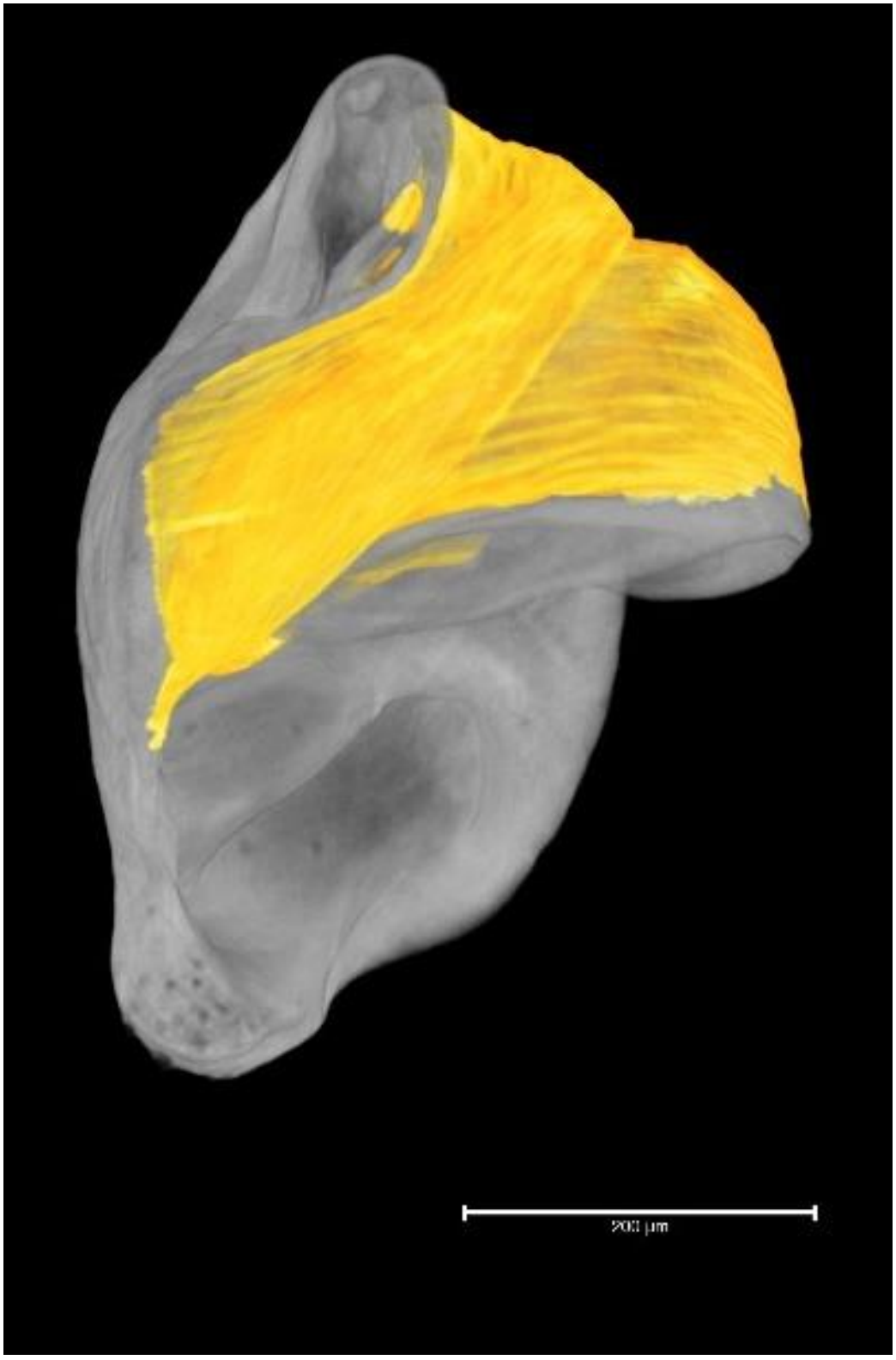

Figure 16. Extension of the basal haematodocha (orange) folded over the subtegulum in resting position. Scale bar: 200 µm.

Figure 17. The moment when the male (left) inserts its pedipalp into the female (right) genital opening and extends the basal haematodocha.

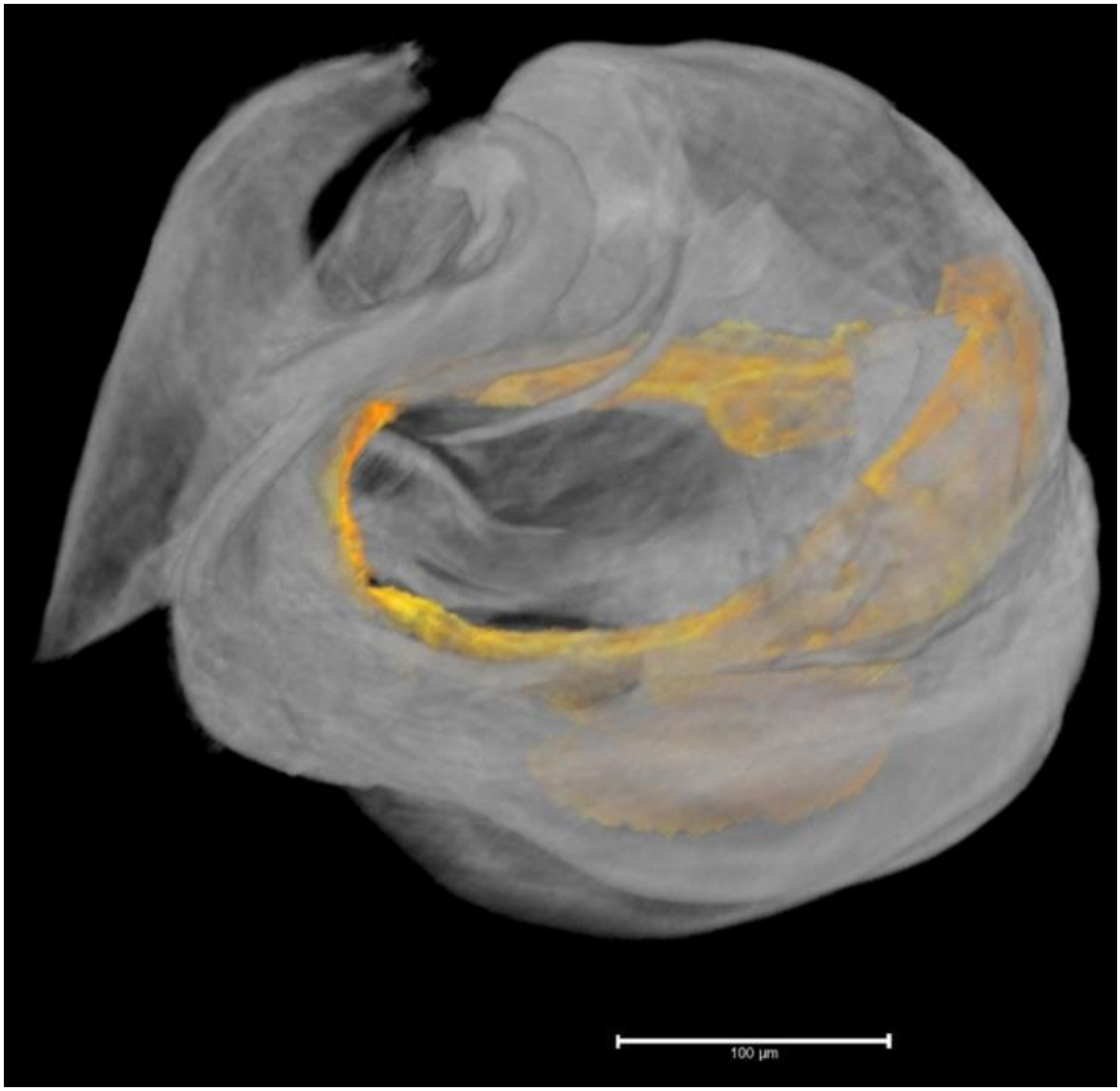

Figure 18. Location of the median haematodocha (orange) that connects subtegulum and tegulum. Scale bar: 100 µm.

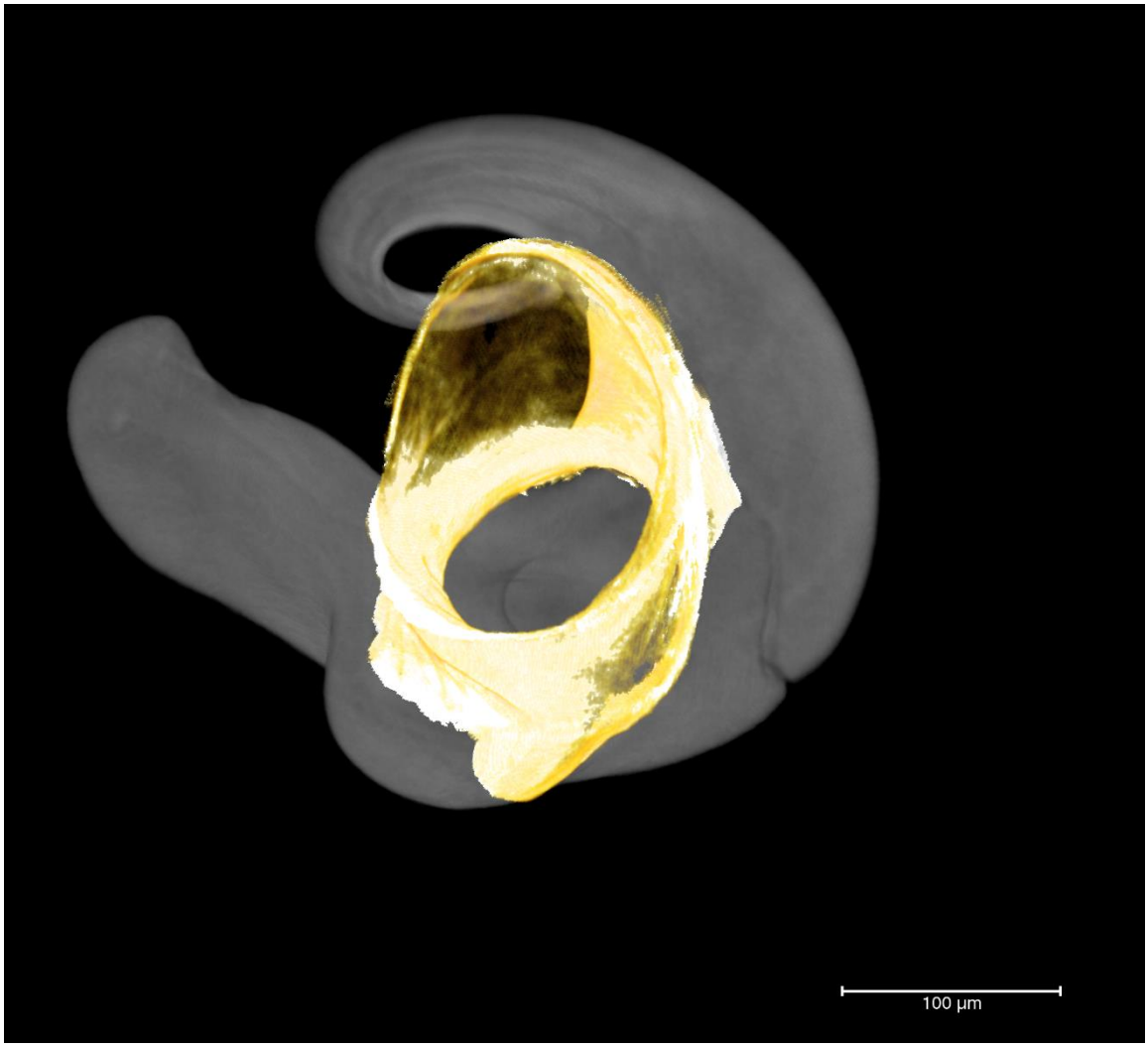

Figure 19. Extension of the embolic membrane (yellow), semi-transparent aspect viewed from proximal. Scale bar: 100 µm.

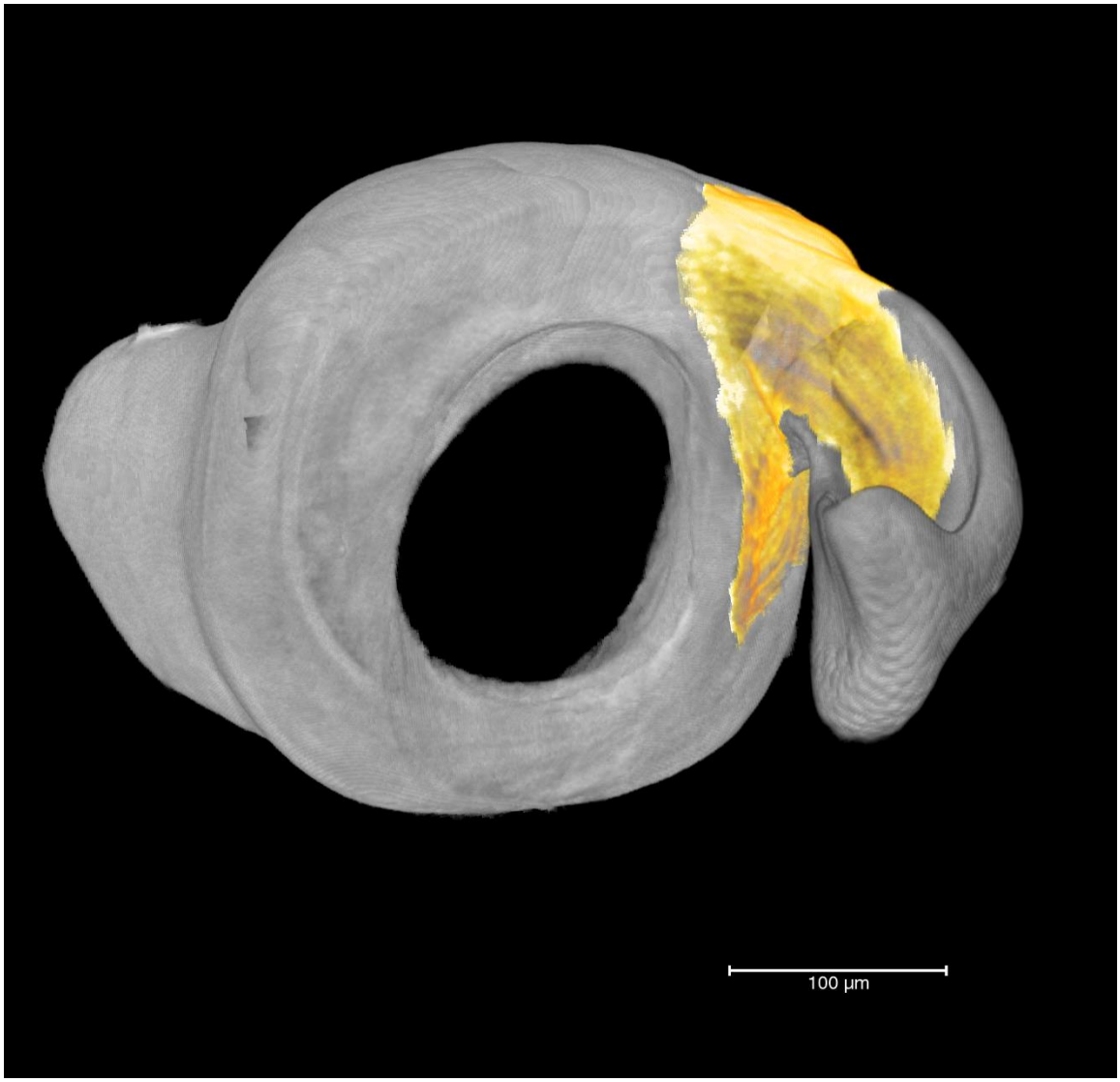

Figure 20. Extension of the embolic membrane (yellow), semi-transparent aspect viewed from distal. A connection with the connective membrane is likely. Scale bar: 100 µm.

Figure 21. Histological section of the conductor. Note the folded connective membrane at the base of the conductor. Scale bar: 50 µm.

Figure 22. Connective membrane (yellow) between conductor and tegulum. Scale bar: 100 µm.

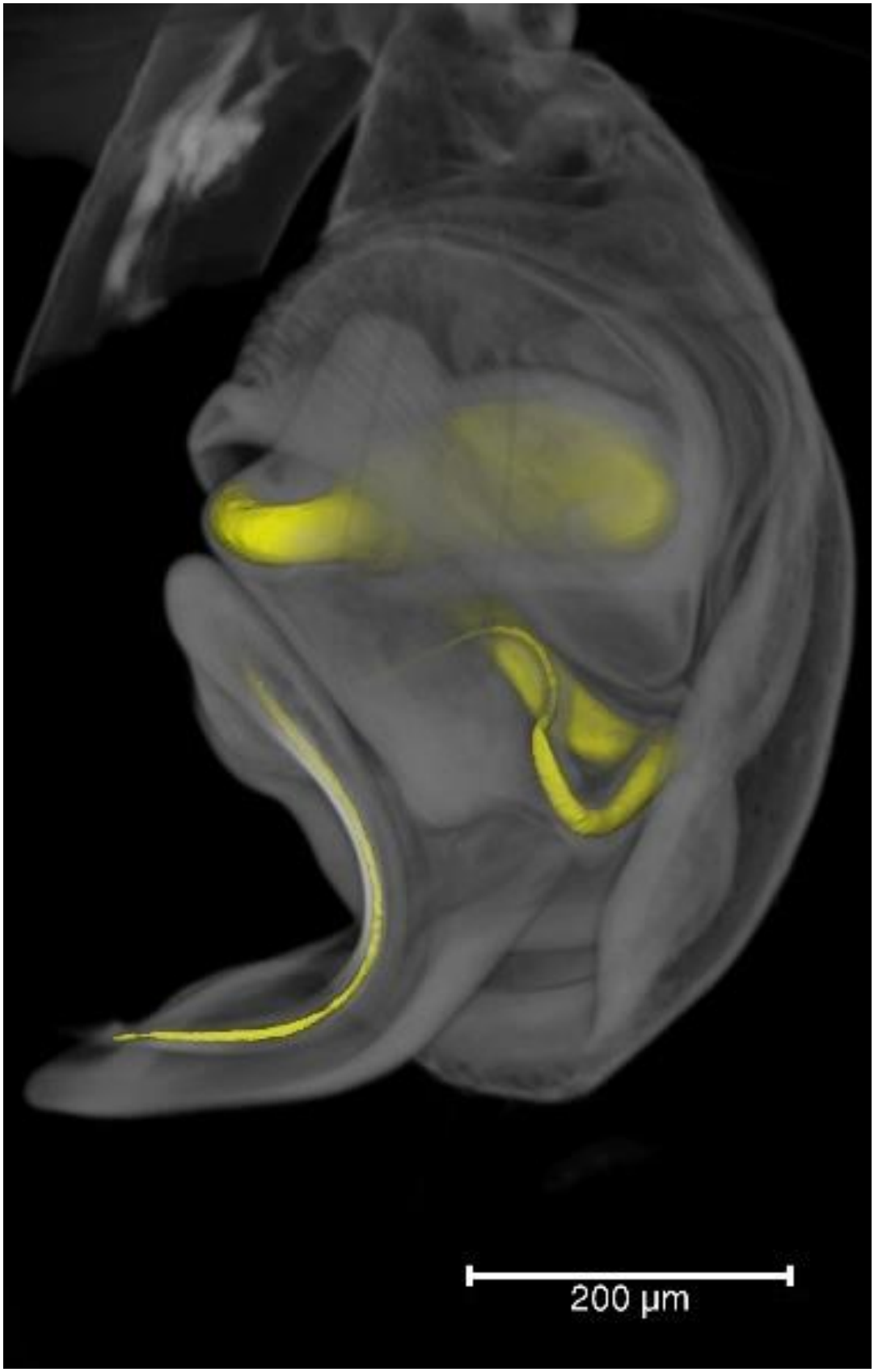

Figure 23. Total reconstruction of the blind sperm duct (yellow) in semi-transparent view to show the position of the duct in the pedipalp tip. Scale bar: 200 µm.

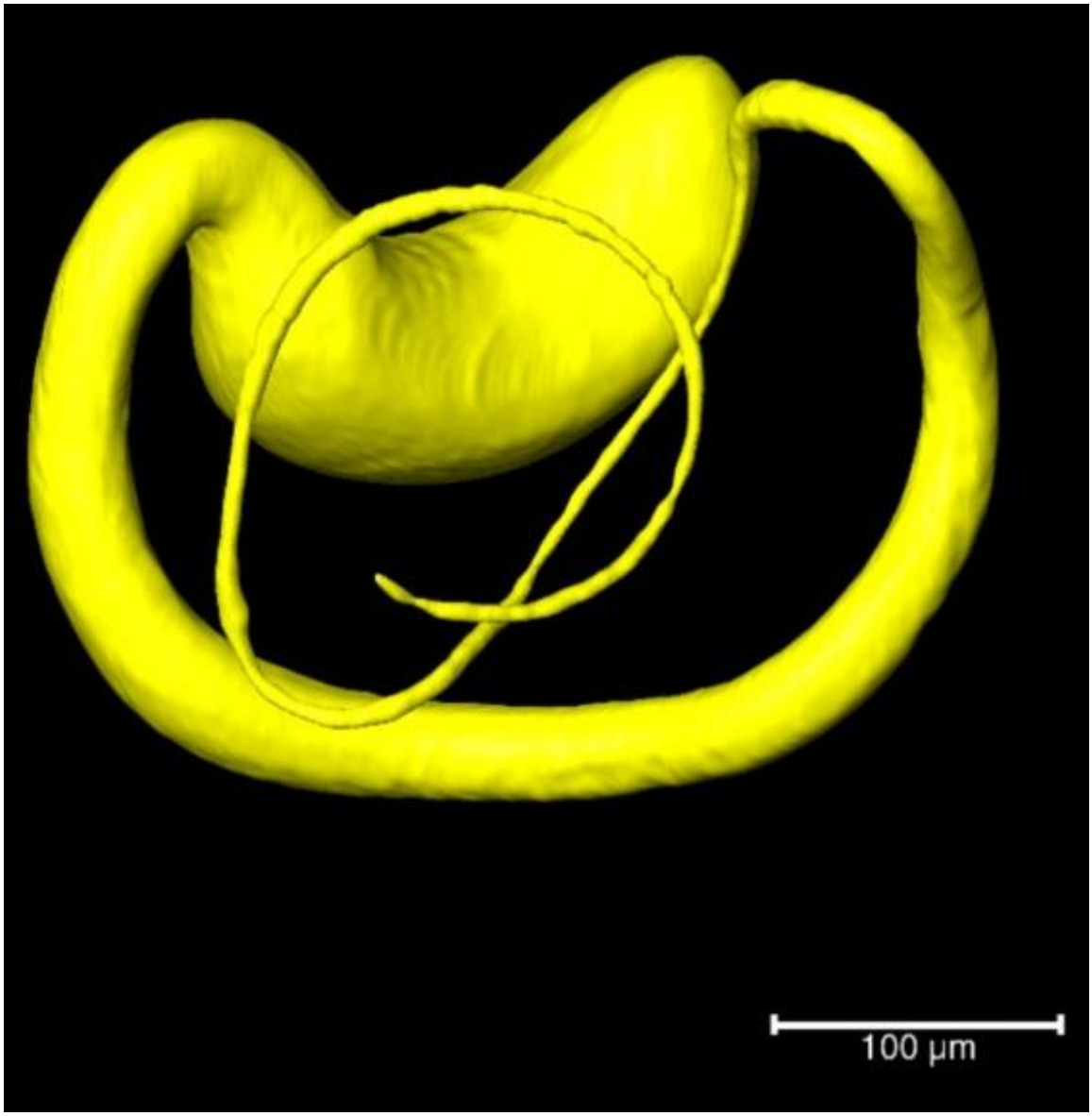

Figure 24. Blind sperm duct viewed from distal. Note the three partite morphology comprising portions of different diameter. Scale bar: 100 µm.

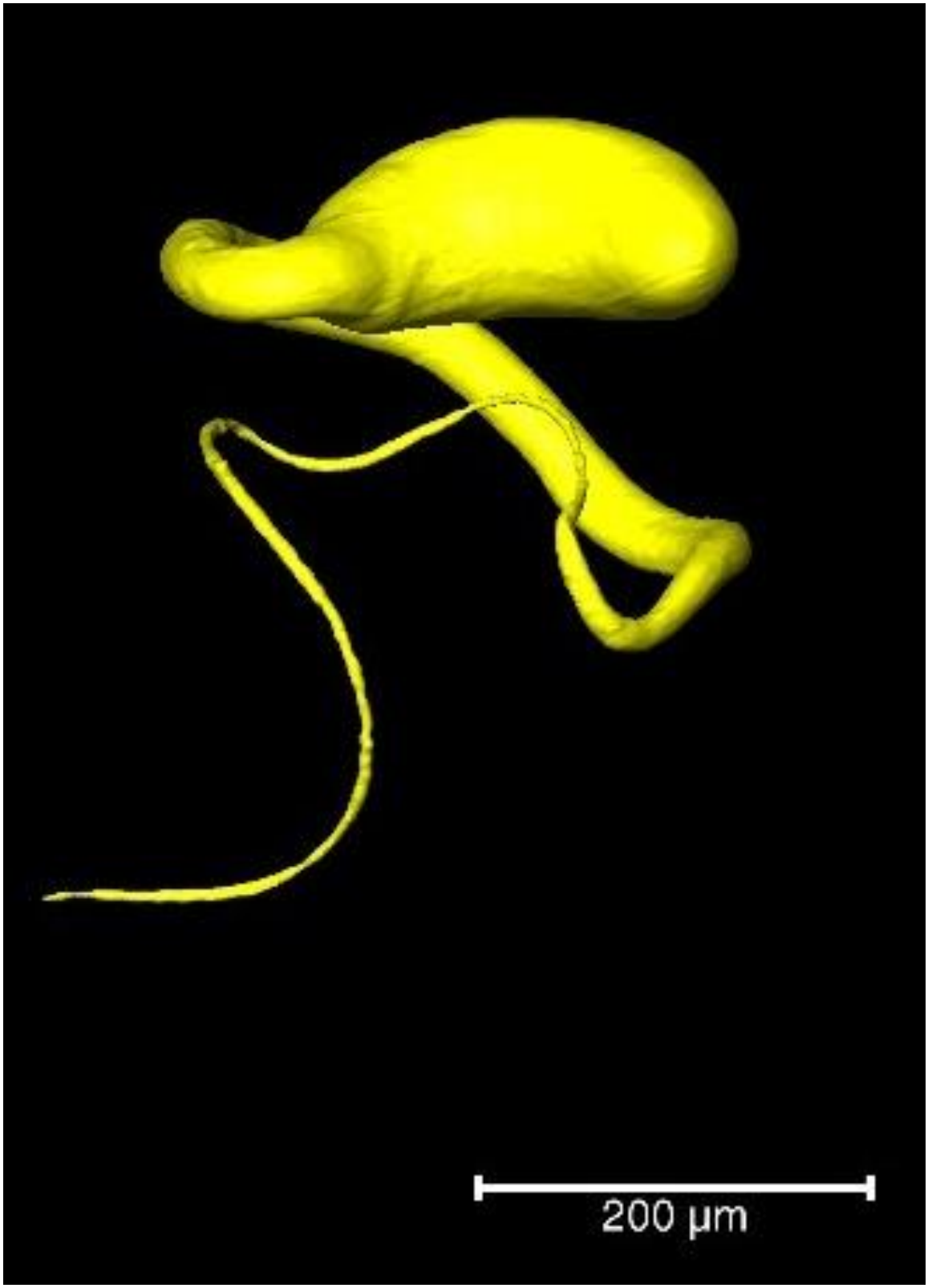

Figure 25. Blind sperm duct viewed from lateral (proximal to the top). Note the three partite morphology comprising portions of different diameter. Scale bar: 200 µm.

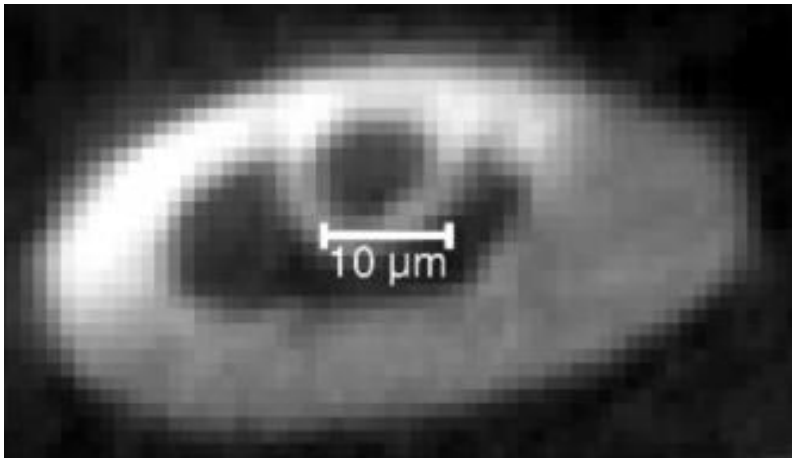

Figure 26. Embolus cross-section taken from µCT microscopy reconstruction. The inner ring is the distal part of the blind sperm duct. The scale bar gives the diameter of the sperm duct at this location.

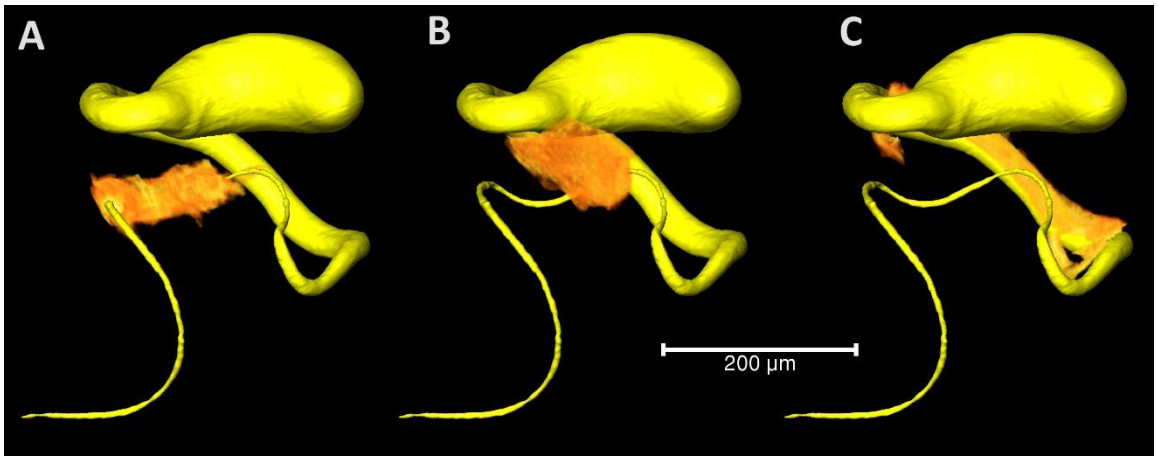

Figure 27. The three glands associated with the blind sperm duct (yellow). The gland tissue is shown in orange. Scale bar: 200 µm for all panels.

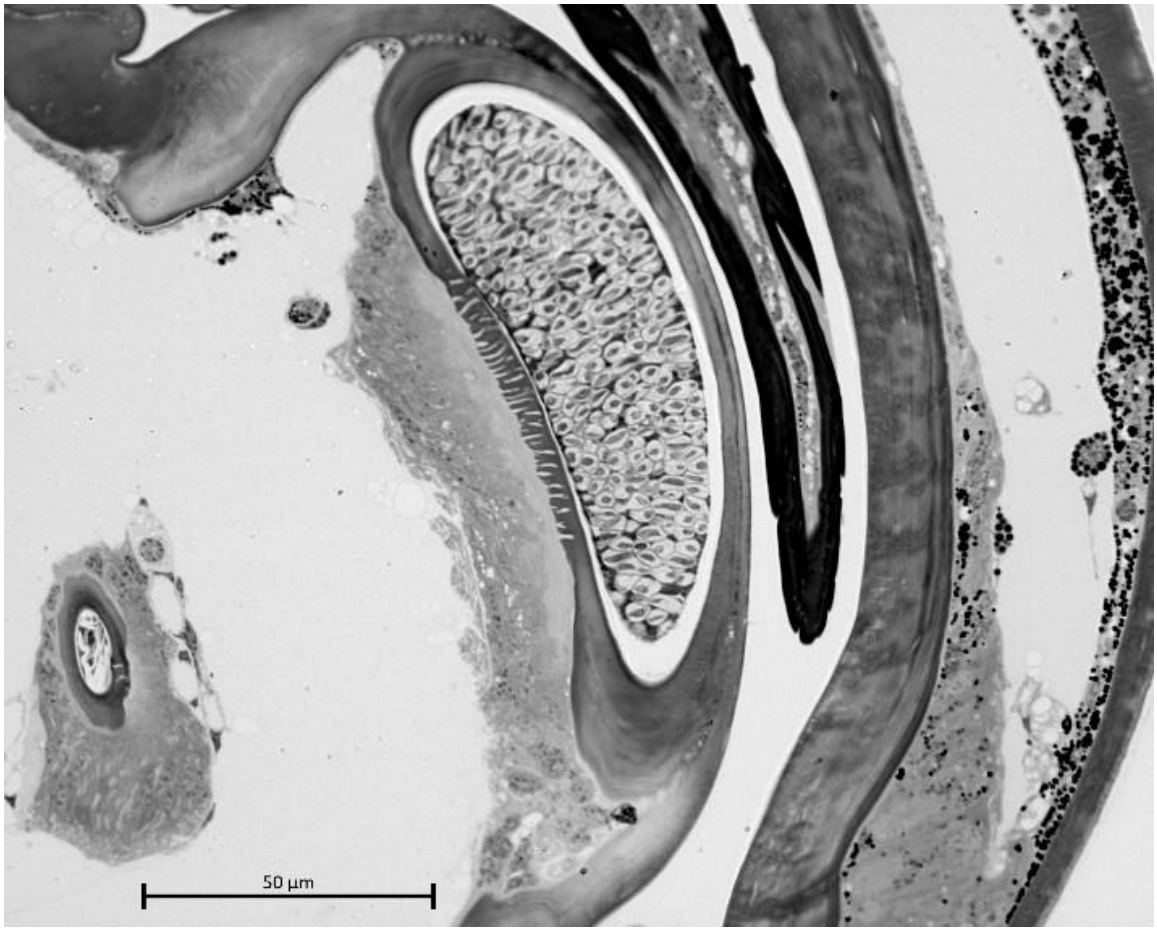
50 µm

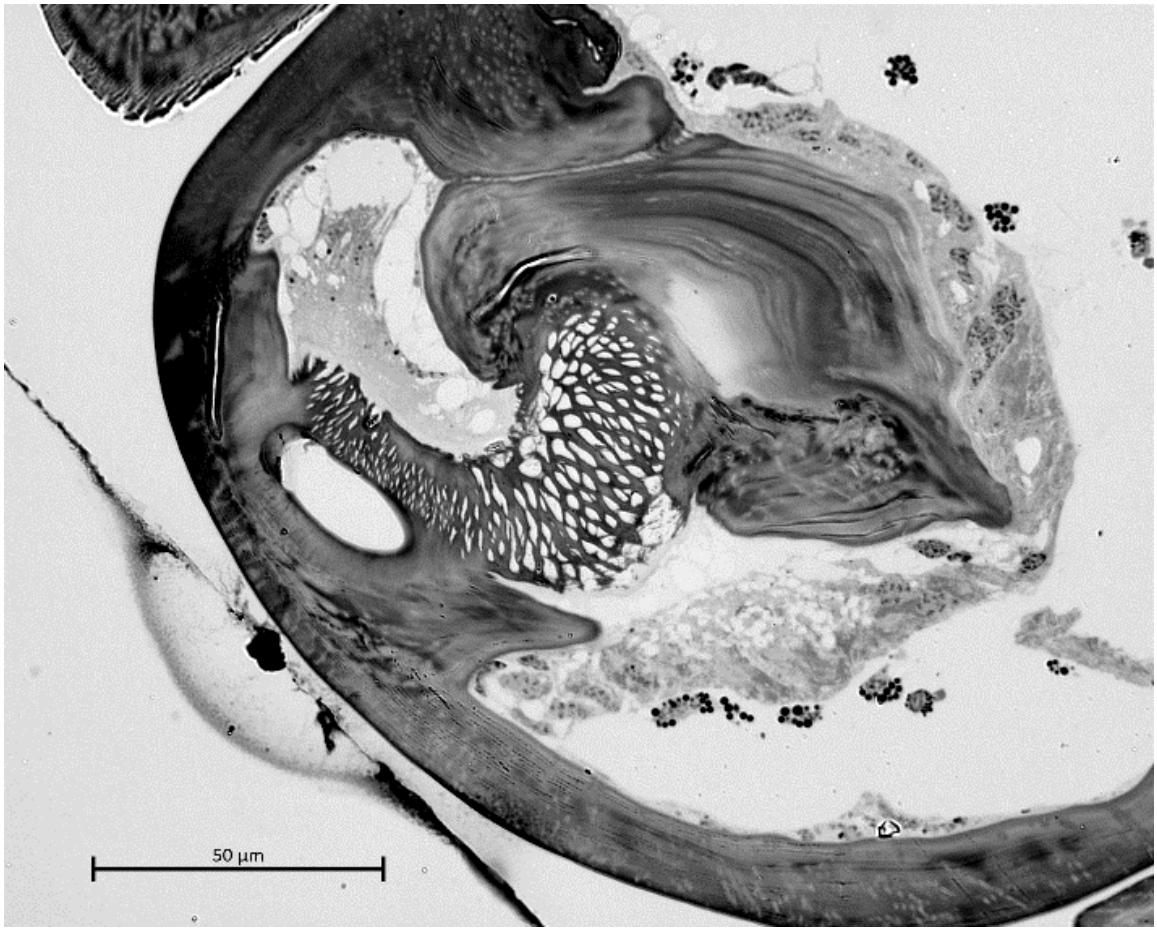

Figures 28 and 29. Cross sections through glandular tissue accompanying the blind sperm duct. Note the sieve-like structure at the transition from gland to duct lumen. Scale bars: 50 µm.

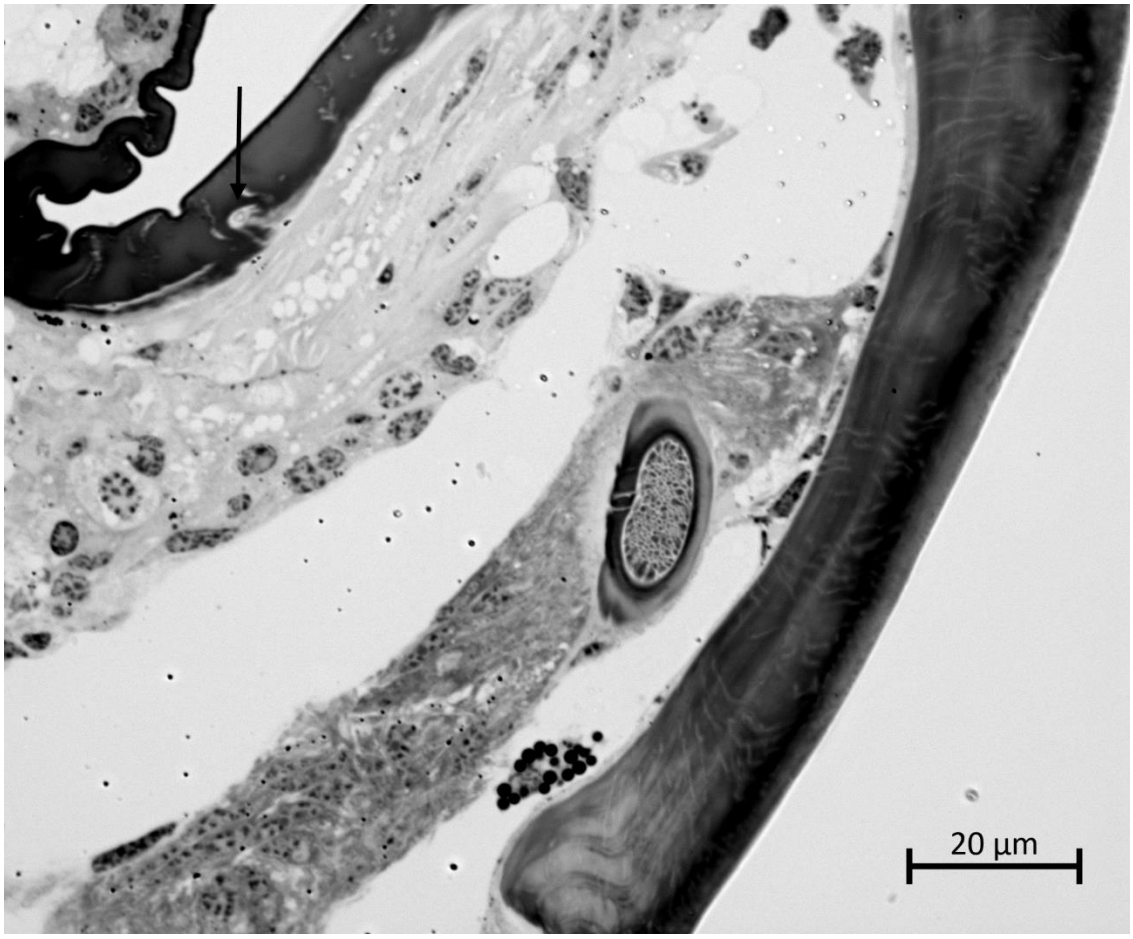

Figure 30. Cross section showing a sensilla embedded in the embolic membrane, arrow. Scale bar: 20 µm.

3.4. Formation and development of the male copulatory organ in the spider *Parasteatoda tepidariorum*

In this chapter the development of the bulbus organ is investigated. The duration of the morphogenesis, the origin of the bulbus organ primordium and the differentiation is described. From these results a staging scheme is developed. Especially interesting is the

Felix Quade, Jana Holtzheimer, Jasper Frohn, Mareike Töpperwien, Tim Salditt, Nikola-Michael Prpic

Author contributions to practical work:

Felix Quade:	Preparation of pedipalps for µCT, reconstruction and segmentation of the µCT-image-stacks, preparation of specimens for confocal-laser-scanning-microscopy (CLSM), imaging and segmentation of CLSM-Data
Jana Holtzheimer:	preparation of specimens for CLSM, imaging and segmentation of CLSM-Data
Jasper Frohn:	Development of the µCT-imaging setup and of the script for µCT-reconstruction
Mareike Töpperwien:	Development of the µCT-imaging setup and of the script for µCT-reconstruction

Status: Submitted to Scientific Reports

Formation and development of the male copulatory organ in the spider *Parasteatoda tepidariorum* involves a metamorphosis-like process

Felix Simon Christian Quade (1,2), Jana Holtzheimer (1,2), Jasper Frohn (3), Mareike Töpperwien (3), Tim Salditt (3), Nikola-Michael Prpic (1,2,4,*)

(1) Georg-August-Universität Göttingen, Johann-Friedrich-Blumenbach-Institut für Zoologie und Anthropologie, Abteilung für Entwicklungsbiologie, Justus-von-Liebig-Weg 11, 37077 Göttingen, Germany

(2) Göttingen Center for Molecular Biosciences (GZMB), Ernst-Caspari-Haus, Justus-von-Liebig-Weg 11, 37077 Göttingen, Germany

(3) Georg-August-Universität Göttingen, Institut für Röntgenphysik, Friedrich-Hund-Platz 1, 37077 Göttingen, Germany

(4) Justus-Liebig-Universität Gießen, Allgemeine Zoologie und Entwicklungsbiologie, Carl-Vogt-Haus, Heinrich-Buff-Ring 38, 35392 Gießen, Germany

(*) Author for correspondence:
Nikola-Michael Prpic
E-mail: nikola-michael.prpic-schaeper@allzool.bio.uni-giessen.de

Abstract

Spiders have evolved a unique male copulatory organ, the pedipalp bulb. The morphology of the bulb is species specific and plays an important role in species recognition and prezygotic reproductive isolation. Despite its importance for spider biodiversity, the mechanisms that control bulb development are virtually unknown. We have used confocal laser scanning microscopy (CLSM) and diffusible iodine-based contrast-enhanced micro computed tomography (dice-µCT) to study bulb development in the spider *Parasteatoda tepidariorum*. These imaging technologies enabled us to study bulb development in situ, without the use of destructive procedures for the first time. We show here that the inflated pedipalp tip in the subadult stage is filled with haemolymph that rapidly coagulates. Coagulation indicates histolytic processes that disintegrate tibia and tarsus, similar to histolytic processes during metamorphosis in holometabolous insects. The coagulated material contains cell inclusions that likely represent the cell source for the re-establishment of tarsus and tibia after histolysis, comparable to the histoblasts in insect metamorphosis. The shape of the coagulated mass prefigures the shape of the adult tarsus (cymbium) like a blueprint for the histoblasts. This suggests a unique role for controlled coagulation after histolysis in the metamorphosis-like morphogenesis of the male pedipalp.

Introduction

With over 1 million described species, arthropods are by far the most speciose group of animals[1]. The arthropods comprise four major groups: Insecta (e.g. beetles, butterflies), Chelicerata (e.g. spiders, mites, scorpions), Myriapoda (e.g. millipeds, centipeds), and Crustacea (e.g. crabs, shrimp). Originally the arthropods are an aquatic (marine) group, but in all four major groups one or several events of terrestrialisation have occurred[2,3]. The conquest of land requires not only the evolution of novel strategies for breathing in air, but also new ways for the safe transfer of sperm from the male to the female. In the aquatic environment, the gametes can simply be released into the water. Under terrestrial conditions a more direct way of gamete delivery is required that also protects the sperm from dehydration. For this purpose, true spiders (Araneae) have evolved a unique copulatory organ in the male, the so-called pedipalp bulb. The pedipalps are a pair of segmented appendages in front of the four pairs of walking legs. In both sexes they serve for sensory perception and feeding, but in males the pedipalps are additionally modified to serve as an intromittent organ. The pedipalps are generally similar to the walking legs, but are shorter and have only six segments, instead of seven in the walking legs (reviewed by Pechmann *et al.*[4]). The last segment of the male pedipalp is scoop-shaped and is termed the cymbium. In the cymbium lies the bulb, which is used by the male to take up its own sperm and safely store it until copulation. During copulation the male uses the pedipalp to reach out for the female genital opening, insert the bulb into it, and then release the stored seminal fluid into the female genital tract. In its simplest form the bulb is a soft, sac-shaped protrusion, but in the majority of species the bulb is additionally equipped with a complex set of strongly sclerotised sclerites[5,6,7]. In these species, the bulb

is not only used for sperm storage and transfer, but the sclerites also ensure a safe locking of the bulb inside of the female genital system to prevent a premature separation and thus sperm loss. The soft portion of the bulb, the so called haematodocha, is inflatable hydraulically (comparable to a balloon). This enables the movements of the sclerites and also provides the necessary flexibility for the entire structure to enter the female genital opening[8,9]. The individual sclerites serve distinct functions during copulation. The ring-shaped tegulum and subtegulum stabilise the soft portions of the bulb and prevent overexpansion. The conductor makes contact to the female body and guides another sclerite, the embolus, into the genital opening. The embolus has at its tip the opening of the blind sperm duct, in which the seminal fluid is stored. The bulbs of some spider groups bear additional sclerites, the so-called apophyses, that play a role in the secure locking of the bulb in the female genitalia[10].

All soft and sclerotised parts of the bulb together form a functional unit, which can be considered as a "key" that is adapted to fit inside the female genital opening (that can be considered as a "lock")[5]. Thus, the bulb of a male spider fits only into the genital opening of a female of the same species. As a consequence, the shape of all bulb components is species specific and, in addition to mate choice and mating behaviour, plays an important role in species recognition and prezygotic reproductive isolation. Accordingly, the bulb is not only crucial for reproduction in spiders, its function in mate recognition also links the bulb directly to gene flow in a population and the process of speciation in spiders. An understanding of the evolutionary changes of its morphology will provide unique insight

into the mechanisms of morphological evolution, especially in co-evolution with the morphology of the female genital system.

The species-specific morphology of an organ or structure is always the result of developmental processes that are in turn controlled by molecular genetic mechanisms. Thus, the evolution of the underlying molecular developmental mechanisms is the basis for morphological evolution. However, very little is known about the development of the male pedipalp and its bulb[11], and the causal molecular and genetic mechanisms are entirely unclear. We have therefore studied the formation and further postembryonic development of the pedipalp bulb in the spider *Parasteatoda tepidariorum*, a member of the cob-web spiders (family Theridiidae). Because the morphogenesis of the bulb takes place hidden below the cuticle of the pedipalp tip, it has previously been studied only in dissected or sectioned material. In the present study we have used confocal laser scanning microscopy (CLSM) and diffusible iodine-based contrast-enhanced micro computed tomography (dice-µCT) to study bulb development in *P. tepidariorum*. These imaging technologies enabled us to visualise the forming bulb primordium *in situ*, and to describe its morphogenesis during postembryonic development of *P. tepidariorum* without the use of destructive procedures.

Results

General sequence and duration of the development of the pedipalp bulb

The postembryonic developmental processes studied in this work take place in the penultimate ("pre-subadult") and the ultimate nymphal instar ("subadult"; see overview in Fig. 1). The primordium of the male pedipalp bulb is first established in the pre-subadult stage (see below), but the majority of developmental processes occur during the subadult stage, i.e. between the penultimate moult and the ultimate moult. In order to measure the duration of the subadult stage we studied altogether 55 individuals that were collected at the pre-subadult stage, were provisionally sexed, and then monitored closely to record the penultimate and ultimate moults (see overview in Supplementary Table S1). The sexing of pre-subadult animals proved difficult, because at this stage external morphological differences between males and females are minimal. However, pre-subadult males show a subtle thickening of the two distal pedipalp segments, and thus could be identified with an error rate of around 10% (similar to the results by Mahmoudi et al.[12]). Only those individuals that were assumed to be males at the pre-subadult stage and were confirmed to be males after the penultimate moult were accounted for, and the dates of their penultimate and ultimate moult were recorded. This resulted in a dataset of altogether 24 males with recorded dates for penultimate and ultimate moult (see Supplementary Table S1). The duration of the subadult stage varied between 10 and 17 days, with an average duration of 12.29 days. Given the fact that all individuals were kept in an incubator with controlled temperature and humidity and were treated according to the same feeding and watering protocol (Supplementary Table S2), this variation strongly suggests intrinsic differences in developmental duration reflecting genetic diversity in

developmental speed. However, we cannot entirely exclude the possibility that the differences in developmental duration were caused by external influences, because we also logged temperature and humidity within the incubator, and this revealed that despite the settings on the incubator, temperature showed a slight circadian oscillation (Supplementary Figure S1) and humidity also undulated more strongly (between 27 % and 45 %) and irregularly over time (Supplementary Figure S2).

Origin of the bulb primordium during the pre-subadult stage

The first external sign of bulb formation is a slight thickening of the two distal segments (tibia and tarsus) of the male pedipalp towards the end of the pre-subadult stage. This minor thickening is caused by the ovoid bulb primordium inside the tarsal segment, and by the formation of wrinkled subadult cuticle (see description below) underneath the cuticle of the pre-subadult. At this time point the bulb primordium is a tiny (ca. 100-150 µm long), oval organ located at the tip of the pedipalp tarsus (Fig. 2A). It is located within the tarsal tip surrounded by the tarsal hypodermis (Fig. 2B), except for the distal end which is located directly beneath the basal plate of the claw of the subadult cuticle (Fig. 2A). Thus, the cells at the tip of the bulb primordium produce the claw of the next instar, whereas the hypodermis surrounding the remainder of the primordium produces the tarsal cuticle of the next instar.

The cuticle of the pre-subadult instar surrounds the entire appendage and is close-fitting the tarsal segment. On the outside it bears a large number of bristles and the claw at its

tip. The cuticle of the subadult instar that is formed beneath this pre-subadult cuticle is similar to the outer pre-subadult cuticle in bearing a large number of bristles and a distal claw. Intriguingly, however, the subadult cuticle at this stage is strongly wrinkled and folded (Fig. 2C). This surface enlargement of the subadult cuticle underneath the pre-subadult cuticle before the penultimate moult is essential for the tremendous and sudden increase of the volume of the distal portion of the male pedipalp after the penultimate moult (see next chapter).

Morphogenesis of the bulb during the subadult stage

After the penultimate moult the male pedipalp shows a strongly swollen distal end (the so-called "club"). As described above, the subadult cuticle is already prepared for this increase of volume at the pre-subadult stage, because it is strongly wrinkled beneath the pre-subadult cuticle. When the pre-subadult cuticle is shed, the subadult cuticle is inflated by haemolymph pressure and is straightened around the inflated distal end of the pedipalp (Fig. 3A). Most of the interior of the pedipalp club is filled with haemolymph, only at the tip of the club, directly below the claw is the primordium of the bulb, which has not significantly changed in shape or size during the moult between the pre-subadult and the subadult stages (Fig. 3A). The bulb primordium is still surrounded by the tarsal hypodermis (Fig. 3B) but sticks out at the distal end where it abuts the basal plate of the claw (Fig. 3A, B). Due to the inflation of the distal portion of the male pedipalp the hypodermis is also stretched and lines the inflated cuticle along the inside of the club. Near the bulb primordium the hypodermis forms a well-ordered epithelium (Fig. 3B, "hy"), but along the inflated cuticle the organisation of the hypodermis is less clear. In the LSM

scans (that predominantly show cuticularized material due to its autofluorescence), the soft hypodermis along the inflated cuticle is hardly visible (Fig. 3, Fig. 4). However, in dice-µCT scans, that are able to better represent soft tissue, it can be seen that much of the hypodermis lines the cuticle in a mesenchymal fashion (Fig. 5A, B, "mes"), indicating the partial disintegration (histolysis) of the hypodermis.

The club is not only a swelling of the tarsus alone, but actually includes two limb segments, the tarsus and the tibia. During further development, it can be seen that the bulb primordium is connected to the patella segment through a long epidermal connection (Fig. 4A, "ec"), and also a bundle of tibial muscles is visible (Fig. 4A, B, "tim"). Inside of the epidermal connection there is a tube-like structure that is likely a primordium of blood vessels and/or nerve tracts. Another internal structure of the bulb primordium is the primordium of the blind sperm duct. In the adult, this duct opens at the tip of the embolus and serves to take up and hold the sperm until copulation. At the subadult stage, however, this duct is still completely closed and shows as a round cavity in cross section (Fig. 5C) or as an elongated cavity in sagittal section (Fig. 5D). A 3D reconstruction of the entire blind sperm duct at the mid subadult stage shows that it has a loop shape (Fig. 5E), thus prefiguring the multiple turn coil it will become in the adult.

The haemolymph filled space between the epithelially organised hypodermis near the bulb primordium and the mesenchymally organised hypodermis along most of the cuticle (Fig. 5B, C, "mes", "epi") increasingly fills with a fine-granular coagulated material that originates from the haemolymph in this cavity (Fig. 4A-C, Fig. 5B, "coa"). Between the

mesenchymal hypodermis and the external side of the coagulated material, a large number of filaments occur that appear to tether and stabilise the forming pedipalp tip within the inflated cuticle (Fig. 4A-C, Fig. 5D). The nature of these filaments is currently unclear. Although they show clearly in LSM scans, they are poorly represented in our dice-µCT scans and therefore are electron-deficient structures after iodine staining. Cells are particularly electron-rich after iodine staining, and this is known to visualise the cellular portion of a wide range of tissue types (e.g. epithelia, muscles, glands, fat tissue, nerves[13]). Therefore, the filaments represent non-cellular structures, likely also from haemolymph coagulates. The coagulated material contains dispersed inclusions that show best in dice-µCT scans (e.g. arrowhead in Fig. 5B). These structures are electron-rich, and this identifies them as cell groups embedded in the matrix of the coagulated material, similar to histoblasts or groups of histoblasts ("histoblast nests"). Figure 6 gives a summary of the main components of the developing pedipalp tip and their fate during postembryonic development. In the pre-subadult, the bulb primordium fills the distal end of the tarsal segment and is partially surrounded by epithelial hypodermis. The entire appendage is surrounded by the pre-subadult cuticle and the wrinkled subadult cuticle that has formed beneath it. After the penultimate moult, in the early subadult, the pedipalp tip is inflated and the bulb primordium is located near the distal tip on the ventral side. It is still surrounded by hypodermal tissue, but most of the hypodermis is now associated with the inflated cuticle and shows mesenchymal rather than epithelial organisation. Later during the subadult stage the cavity that has emerged after the penultimate moult gradually fills with coagulated haemolymph material and filaments.

Differentiation of the sclerites, cymbium and tibia

The hypodermis and the bulb primordium differentiate further during the subadult stage. The most significant change is the compaction of all components by which they attain a shape that comes very close to the final shape of the tarsal tip in the adult, and that detaches the entire tissue from the inflated cuticle of the club (Fig. 4D). The compaction of all components is seen best by the changes in position of important landmarks in the developing pedipalp (please compare coloured landmarks in Fig. 4C and D). In the early bulb primordium (before and shortly after the penultimate moult) no specific substructuring is evident that could be attributed to the forming sclerites. The primordium is oval and has some internal structure, but no outgrowths are yet evident. Later during the subadult stage a small lateral bulge indicates the origin of the embolus (Fig. 4C, orange spot) and the elongated tip of the bulb primordium indicates the growing conductor (Fig. 4C, yellow spot). Both the conductor and the embolus elongate further, but the embolus outgrowth rotates and finally attaches to the outgrowth of the conductor (Fig. 4D, orange spot and yellow spot next to each other). The tibia has a triangular shape from the start, but after compaction this segment is more defined than before (compare purple and green spots in Fig. 4C and D). The cymbium retains a scoop-like shape (see blue spots in Fig. 4C and D which mark the tip of the developing cymbium), but a dramatic change is seen on the opposite side: the ventral portion of the hypodermis is initially similar in shape to the cymbium, but then retracts almost completely from the ventral side (compare the red spot in Fig. 4C and D). At this late subadult stage, a comparison of the structures within the club with the components of the adult male pedipalp shows that all principal components of the adult male pedipalp are already present and have attained almost their final size, shape and correlation within the entire structure (Fig. 7).

A staging scheme for the developing male copulatory organ

In summary, the formation of the bulb starts towards the end of the pre-subadult stage (Fig. 8A). At this stage, the bulb primordium is a small ovoid organ inside the tip of the pedipalp appendage. The penultimate moult leads to a dramatic inflation of the tarsus and tibia, thus leading to the formation of the club, but does not produce major changes in the size or shape of the bulb primordium (Fig. 8B). During the subadult stage the future tibia and cymbium (i.e. the dorsal portion of the tarsus) approach their final size and shape by compaction of the tissue (Fig. 8C-E). The bulb primordium retracts from the location at the tip and grows in size (Fig. 8C). Distally and at the ventral side, protrusions form that indicate the primordia of the sclerites conductor and embolus (Fig. 8D). The embolus primordium rotates so that it finally attaches to the conductor primordium, both now pointing distally (Fig. 8E). The cymbium has attained the scoop-like shape and the bulb primordium is now lying in this concave scoop, being attached to it via a stalk near the junction between tibia and cymbium. And also, the tibia is more compact at this stage, an indication that it has begun attaining its typical bell-cup shape in the adult pedipalp. At this time point all major components and sclerite primordia of the bulb are formed and bulb, tibia and cymbium are maximally compacted and removed from the inflated cuticle of the club. Interestingly, although the entire ensemble of bulb, cymbium and tibia is constantly compacting during development, the outer shape of the club cuticle is not changed. Thus, the size and shape of the outside of the club does not mirror the developmental processes that are taking place inside of the club. In the final phase of the subadult stage, shortly before the ultimate moult, the components of the bulb grow significantly until they fill the entire club (Fig. 8F).

Discussion

The morphology of the copulatory bulb of the male spider pedipalp is essential for the correct fitting inside the female genital opening and thus for the safe transfer of the sperm. Although bulb morphology is thus important for species recognition and prezygotic reproductive isolation in spiders, the mechanisms that control the development and evolutionary diversification of this structure are virtually unknown. The postembryonic development of the male pedipalp including the male copulatory bulb has been studied only in a few spider species so far, and the bulk of these studies dates back to the early 20th century. The first detailed study of the development of the bulb has been performed by Barrows[14] on several spider species with a focus on *Steatoda borealis*, a species that belongs to the Theridiidae and is thus closely related to *P. tepidariorum*. This author argued that the entire bulb develops from the cells that form the claw fundament in females and juvenile males. Barrows argued that the small group of claw fundament cells undergoes hypertrophy in subadult males thus growing rapidly in size forming the soft portion of the bulb. Because the claw fundament cells are able to segregate sclerotized structures (i.e. the claw), he assumed that the bulb (being a hypertrophied claw fundament) can also segregate sclerotized structures that will form the bulb sclerites (conductor, embolus etc.). Harm[15] arrives at a similar conclusion, because she finds (in her study on *Segestria bavarica*) that the sclerotized tip of the bulb of this species (the "stylus") apparently forms at the place where the claw would normally form. However, she stresses that *Segestria bavarica* has a simple bulb, without haematodochae and complex sclerites, and that its morphogenesis might not be representative of spiders with a more complex bulb with several sclerites. Harm[16] has later studied the development of

the bulb of *Evarcha arcuata* (under its synonym *Evarcha marcgravii*) (a jumping spider of the family Salticidae), a species with a more complex bulb. She has confirmed her earlier finding that the distal sclerotized tip of the bulb (the "stylus") appears to be homologous to the claw. However, she cannot identify the primordia of the remaining sclerites in her sectioned material and their origin and homology therefore remains unclear. A separate study was performed by Gassmann[17] on the linyphiid spider *Megalepthyphantes nebulosus* (under its synonym *Lepthyphantes nebulosus*), a species with an extremely complex bulb. In Gassmann´s work, the bulb is also formed at the tip of the pedipalp, i.e. near the claw fundament, but he claims no relationship between claw fundament and bulb. Instead, the primordium of the bulb gradually differentiates and develops the future sclerites as new outgrowths entirely unrelated to the claw. In addition, while Barrows and Harm describe the development of the cymbium from the wall of the tarsus, Gassmann writes that the cymbium develops de novo from "organogenic tissue" that fills the pedipalp tip, and later fuses with the differentiated bulb primordium. Bhatnagar and Rempel[18] have studied another theridiid spider, the black widow *Latrodectus curacaviensis*. They support the conclusions by Barrows and Harm that the bulb develops from a hypertrophied claw fundament, however, their sectioned material shows that the sclerites apparently do not develop from the site of the claw but appear to be new evaginations of the bulb. These contradictory findings could also not be resolved in two subsequent studies[19,20]. In these works, the location of the claw even changed from the tip of the bulb to the tip of the cymbium, suggesting that the sclerites of the bulb are not homologous to the claw.

Our study of the formation and further development of the bulb in *P. tepidariorum* strongly supports the initial findings by Barrows[14] and Harm[15,16]. The bulb primordium forms from cells at the base of the claw of the subadult cuticle, i.e. the primordium comprises those cells that have previously segregated the subadult claw. These cells then form an internalised ovoid organ, that subsequently grows and differentiates the primordia of the bulb sclerites as outgrowths from the main body of the organ. This is strong support for the notion that the bulb sclerites are not an evolutionary novelty of spiders, but instead represent the extremely modified claw of the male adult pedipalp. This makes the bulb sclerites in spiders a unique system to study the mechanisms of evolutionary diversification of a highly modified organ in one sex, and at the same time compare them with the developmental ground-state of the organ (= claw) and its developmental mechanisms which is conserved in the other sex.

Intriguingly, our data show that the strong swelling of the pedipalp in the subadult stage is not caused by the growth of the primordium inside, as previously thought. Instead, the expansion of the cuticle to facilitate the formation of the club is already established at the pre-subadult stage, and the cuticle is then inflated by the influx of haemolymph that rapidly coagulates. The coagulated material, however, does not precipitate irregularly, but it forms a defined structure comprising a central mass and outer filaments. This structure appears to provide a stable framework for the developing bulb, and also serves as a fundament for the morphogenesis of the tibia and the tarsus, because it is partially lined with epithelia and also tethers epithelial connections. Coagulation is a typical physiological response to tissue injury or large-scale tissue degeneration (histolysis). Thus,

coagulation in the pedipalp indicates the presence of histolytic processes that transform the tibia-tarsus morphology of the immature male pedipalp into the derived tibia-cymbium morphology of the adult male, similar to histolytic processes during metamorphosis in holometabolous insects[21]. In addition, the coagulated material in the male pedipalp contains inclusions of cell groups, that very likely represent the cell source for the re-establishment of the cymbium and the tibia after histolysis, comparable to the histoblasts and histoblast nests during insect metamorphosis.

Notably, the morphology of the coagulated mass is virtually constant in all specimens investigated so far, and therefore its formation seems to be the result of a controlled process, rather than irregular precipitation of haemolymph constituents. In fact, the shape of the coagulated mass prefigures the shape of the cymbium and may therefore function as a blueprint for the histoblasts in building the cymbium proper. This indicates that the coagulated mass in the male pedipalp is not merely a general response to histolysis, and thus suggests a unique role for controlled coagulation after histolysis in the metamorphosis-like morphogenesis of the male pedipalp.

Materials and Methods

Parasteatoda tepidariorum husbandry

Our *P. tepidariorum* husbandry is kept at controlled temperature (25 °C) and dark/light cycle (10 hours of light). The animals are kept separate in plastic vials sealed with styrene foam plugs and are supplied regularly with water and food. Juveniles are fed with *Drosophila melanogaster* flies, older stages and adults are fed with larger flies (*Musca domestica* and *Lucilia caesar*) or juvenile crickets (*Acheta domesticus*). Water is provided by humid soil.

Specimen fixation

The spiders to be studied by confocal laser scanning microscopy (CLSM) and diffusible iodine-based contrast-enhanced micro computed tomography (dice-µCT) were anaesthetised at -20°C for 7-10 minutes. Then the opisthosoma was removed and only the prosoma was placed in Karlsson and Schultz phosphate buffer (13mM sodium dihydrogen phosphate monohydrate, 85mM di-sodium hydrogen phosphate dehydrate, 85mmol NaCl, 2,5% glutaraldehyde, 4% formaldehyde in water) at 4°C over night. After fixation, the pedipalps were separated from the spider and the left one was used for CLSM imaging, and the right one was used for dice-µCT imaging. Treatment for CLSM involved bleaching, nucleic acid staining, dehydration and clearing, treatment for dice-µCT involved dehydration, iodine staining and critical point drying (see below).

Bleaching

After fixation, the pedipalps were placed in 15% hydrogen peroxide in PBS-T and were carefully centrifuged to remove gas bubbles from the tissue. The hydrogen peroxide denatures all pigments. After 1 to 2 days, or longer, when there was no O_2 development anymore and the pedipalps were not entirely bleached, the pedipalps were transferred to 30% hydrogen peroxide in PBS-T. When the samples were fully bleached, they were washed twice with PBS-T.

Nucleic acid staining

4′,6-diamidino-2-phenylindole (DAPI) was used for DNA detection, because the wavelength of the fluorescence of DAPI proved to be more different from the wavelength of the autofluorescence of the samples. The staining was performed by transferring the pedipalps into a vial with DAPI (1:1000) for 3 h at room temperature in the dark. DAPI was then removed by several washes in PBS-T.

Dehydration and clearing for CLSM

To dehydrate the pedipalps an ethanol series was performed comprising the following steps for at least 30 min each: 30%, 50%, 70%, 80%, 90%, and 95% ethanol in water. Then the pedipalps were incubated twice in 100% ethanol for half an hour each. After dehydration the ethanol was replaced with 100% methyl salicylate for tissue clearing. Clearing of the pedipalps has been performed as described previously[22] and on the perforated anodised aluminium slide described recently[23].

Confocal laser scanning microscopy (CLSM)

For CLSM scanning a Zeiss LSM 510 microscope was used. An Argon laser with 488 nm wavelength for excitation and a long-pass filter for 505nm wavelength was used for the emitted light. The pinhole was set to 0.81 – 1.0 airy units. The scan size was set to 1024X1024 pixels. The scanning speed was set to 6.4 µs per pixel, line averaging was set to 4. The objectives used were a Zeiss Plan-Neofluar 10x air with a numerical aperture of 0.3 for the whole pedipalp specimen, and a Zeiss Plan-Neofluar 20x air with a numerical aperture of 0.5 to document details.

Dehydration and iodine staining for dice-µCT

An ethanol series was performed comprising the following steps for at least 30 min each: 30%, 50%, 70%, 80%, 90%, and 95% ethanol in water. Then the pedipalps were incubated twice in 100% ethanol for half an hour each. After the dehydration was complete the pedipalps were stained with iodine (in ethanol) to increase contrast. Iodine changes the interaction of the specimen with the x-rays, through an increase of phase shift and absorption. A solution of 1% iodine in ethanol was added to the vial with fully dehydrated samples overnight, then the samples were rinsed three times with 100% ethanol to remove excess iodine.

Critical point drying

An automatic critical point dryer (Leica EM CPD300) was used to perform critical point drying. After the samples were dehydrated and iodine stained, they were transferred into

a microporous container to avoid losing it due to its very small size. These containers were placed into a larger container filled with 100% ethanol and placed in the critical point dryer. 18 cycles of ethanol/liquid carbon dioxide (CO_2) exchange were performed to quantitatively remove the ethanol. The CO_2 was then slowly heated to 31°C with a pressure of 74 bar. It is essential to perform this phase transfer of CO_2 very slowly in order to avoid capillary forces or volume changes that would damage delicate morphological structures inside the forming pedipalps.

Diffusible iodine-based contrast-enhanced micro computed tomography (dice-µCT)

To achieve proper resolution of the soft tissue portions of the samples a self-commissioned laboratory-based X-ray phase-contrast tomography setup was used for dice-µCT imaging[24]. To reach a high resolution of approximately 1 µm despite a relatively high focal spot size of the X-ray source (70 µm) an inverse geometry (source-to sample distance >> sample-to-detector distance) in combination with the high-resolution detector XSight (Rigaku, Prague, Czech Republic) was used. The resolution of this setup is limited to the detector point spread function (0.54 µm) due to negligible optical magnification. The detector´s field of view is 1.8 x 1.4 mm, but we chose as the maximum sample dimensions 0.8 x 0.5 x 0.5 mm, because this makes it much easier to perform tilt corrections in the reconstruction step. A detailed setup description has been published previously[24]. For tomographic reconstruction 25 dark-field images, 25 flat-field images and 1000 projections over 180° were recorded with an exposure time of t = 40 s each. To increase the signal to noise ratio, each empty-beam corrected projection was binned by a factor of 2. To retrieve the phase information the Bronnikov-Aided-Correction algorithm

(BAC) was applied on each projection[25,26]. The tomographic reconstruction was performed with the (cone-beam) filtered back-projection implementation of the ASTRA toolbox[27,28,29].

Image segmentation and processing

dice-µCT and CLSM 3D-stacks were processed in Amira 5.4.1 (FEI SAS, France, www.vsg3d.com). Structures of interest were marked with the brush or magic wand tool in the segment editor. With the brush tool individual or groups of pixels are marked by the user, and the magic wand is a grey value-based region growing algorithm, where the user sets the seeding points and is able to set limit lines to define borders for the growth. To highlight them, the volren-module was connected to the image stack and label field, respectively, then in the port transfer functions two colormaps gray.am and glowred.col were set up with the AlphaScale in gray.am tuned to 20-30%. To assign the glowred.col colormap to the structure of interest the desired colormap was chosen in the material port by selecting the colormap icon. To insert scale bars the module scale was activated and for correct distances the orthographic camera was used in the viewer window. Images for figures were taken with the snapshot tool. Images were then corrected for contrast and colour values and combined into figures using Adobe Photoshop CS5 for Apple Macintosh.

Data availability statement

The datasets generated and analysed during the current study are available from the corresponding author on reasonable request.

References

1. May. R. M. How many species are there on earth? *Science* **241**, 1441-1449 (1988).

2. Budd, G. E. & Telford, M. J. 2009. The origin and evolution of arthropods. *Nature* **457**, 812-817 (2009).

3. Lozano-Fernandez J. et al. 2016. A molecular palaeobiological exploration of arthropod terrestrialization. *Phil. Trans. R. Soc. B* **371**, 20150133; 10.1098/rstb.2015.0133 (2016).

4. Pechmann, M., Khadjeh, S., Sprenger, F. & Prpic, N. M. Patterning mechanisms and morphological diversity of spider appendages and their importance for spider evolution. *Arthropod Struct. & Dev.* **39**, 453-467 (2010).

5. Eberhard, W. G. & Huber, B. A. Spider genitalia. Precise maneuvers with a numb structure in a complex lock in *The evolution of primary sexual characters in animals* (eds. Leonard, J. & Córdoba-Aguilar, A.) 249-284 (Oxford University Press, 2010).

6. Foelix, R. F. *Biology of spiders* (Oxford University Press, 2011).

7. Agnarsson, I., Coddington, J. A. & Knoflach, B. Morphology and evolution of cobweb spider male genitalia (Araneae, Theridiidae). *J. Arachnology* **35**, 334-395 (2007).

8. Loerbroks, A. Mechanik der Kopulationsorgane von *Misumena vatia* (Clerck, 1757) (Arachnida: Araneae: Thomisidae). *Verh. Naturwiss. Ver. Hamburg NF* **27**, 383-403 (1984).

9. Haupt, J. 2004. The palpal organ of male spiders (Arachnida, Araneae) in *European Arachnology 2002* (eds. Samu, F. & Szinetar, C.) 65-71 (Plant Protection Institute & Berzsenyi College Budapest, 2004).

10. Huber, B. A. Functional morphology of the genitalia in the spider *Spermophora senoculata* (Pholcidae, Araneae). *Zool. Anz.* **241**, 105-116 (2002).

11. Coddington, J. A. Ontogeny and homology in the male palpus of orb-weaving spiders and their relatives, with comments on phylogeny (Araneoclada: Araneoidea, Deinopoidea). *Smithsonian Contrib. Zool.* **496**, 1-52 (1990).

12. Mahmoudi, N., Modanu, M., Brandt, Y. & Andrade, M. C. B. Subtle pedipalp dimorphism: a reliable method for sexing juvenile spiders. *J. Arachn.* **36**, 513-517 (2008).

13. Gignac, P. M. *et al.* Diffusible iodine-based contrast-enhanced computed tomography (diceCT): an emerging tool for rapid, high-resolution, 3-D imaging of metazoan soft tissues. *J. Anat.* **228**, 889-909 (2016).

14. Barrows, W. M. Modification and development of the arachnid palpal claw, with especial reference to spiders. *Annals Entomol. Soc. America* **18**, 483-516. Plates 35-43 (1925).

15. Harm, M. Beiträge zur Kenntnis des Baues, der Funktion und der Entwicklung des akzessorischen Kopulationsorgans von *Segestria bavarica* C. L. Koch. *Zeitschr. Morphol. Ökol. Tiere* **22**, 629-670 (1931).

16. Harm, M. Bau, Funktion und Entwicklung des akzessorischen Kopulationsorgans von *Evarcha marcgravi* Sop. *Zeitschr. Wiss. Zool.* **146**, 123-134 (1934).

17. Gassmann, F. Die Entwicklung des männlichen Spinnentasters, dargestellt an *Leptyphantes nebulosus* Sund. *Zoomorphology* **5**, 98-118 (1925).

18. Bhatnagar, R. D. S. & Rempel, J. G. The structure, function, and postembryonic development of the male and female copulatory organs of the black widow spider *Latrodectus curacaviensis* (Müller). *Canad. J. Zool.* **40**, 465-510 (1962).

19. Bhatnagar, R. D. S. & Sadana, G. L. Morphogenesis of the tarsal tissue and the development of the intromittent palpal organs in the wolf-spider *Lycosa chaperi* (Simon) (Araneida: Lycosidae). *Canad. J. Zool.* **49**, 397-400 (1971).

20. Sadana, G. L. Studies on the postembryonic development of the palpal organ of *Lycosa chaperi* Simon (Lycosidae: Araneida). *Zool. Anz.* **186**, 251-258 (1971).

21. Wigglesworth, V. B. *The physiology of insect metamorphosis* (Cambridge University Press, 1954).

22. Smolla, M., Ruchty, M., Nagel, M. & Kleineidam, C. J. Clearing pigmented insect cuticle to investigate small insects' organs in situ using confocal laser-scanning microscopy (CLSM). *Arthropod Struct. Dev.* **43**, 175-181 (2014).

23. Quade, F. S. C., Preitz, B. & Prpic, N. M. A perforated anodised aluminium slide for improved specimen clearing and imaging for confocal laser scanning microscopy. *BMC Res. Notes* **11**, 716; 10.1186/s13104-018-3826-3 (2018).

24. Reichardt, M. et al. Nanoscale holographic tomography of heart tissue with x-ray waveguide optics. *Proc. SPIE* **10391**, 1039105; 10.1117/12.2276648 (2017).

25. De Witte, Y., Boone, M., Vlassenbroeck, J., Dierick, M. & Van Hoorebeke, L. 2009. Bronnikov-aided correction for x-ray computed tomography. *J. Opt. Soc. Am. A* **26**, 890-894 (2009).

26. Töpperwien, M., Krenkel, M., Quade, F. & Salditt, T. Laboratory-based x-ray phase-contrast tomography enables 3D virtual histology. *Proc. SPIE* **9964**, 99640I; 10.1117/12.2246460 (2016).

27. Palenstijn, W. J., Batenburg, K. J. & Sijbers, J. Performance improvements for iterative electron tomography reconstruction using graphics processing units (GPUs). *J. Struct. Biol.* **176**, 250-253 (2011).

28. Van Aarle, W. et al. The ASTRA Toolbox: A platform for advanced algorithm development in electron tomography. *Ultramicroscopy* **157**, 35-47 (2015).

29. Van Aarle, W. et al. 2016. Fast and flexible X-ray tomography using the ASTRA toolbox. *Opt. Express* **24**, 25129-25147 (2016).

Acknowledgements

We thank Beate Preitz for help with CLSM microscopy, and Wiebke Möbius for help with critical point drying. This work was funded by the Deutsche Forschungsgemeinschaft (DFG; grant numbers PR1109/6-1 and PR1109/6-2 (to NMP)). Additional financial backing has been received from the Göttingen Center for Molecular Biosciences (GZMB), Goettingen University (GAU), and Justus-Liebig-University Giessen (JLU). The funders had no role in study design, data collection and analysis, decision to publish, or preparation of the manuscript.

Author contributions

Devised the project: NMP. Planned the experiments: FQ, TS, NMP. Performed the CLSM work: FQ, JH. Performed the µCT work: FQ, JF, MT. Analysed and discussed data: FQ, JH, JF, MT, TS, NMP. Wrote the manuscript: FQ, NMP.

Competing interests' statement

The authors declare no competing interests.

Figures & legends

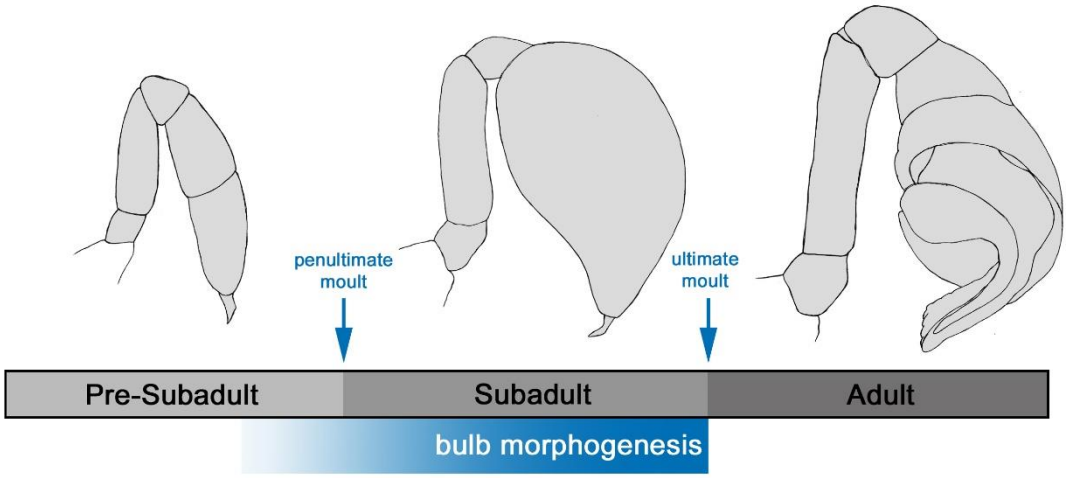

Figure 1. Overview of terminology used in this work. The last two moults subdivide the development of the male pedipalp into a pre-subadult, subadult, and adult stage. Bulb morphogenesis begins at the end of the pre-subadult stage and continues throughout the subadult phase. The drawings depict the typical appearance of the male pedipalp during the three stages.

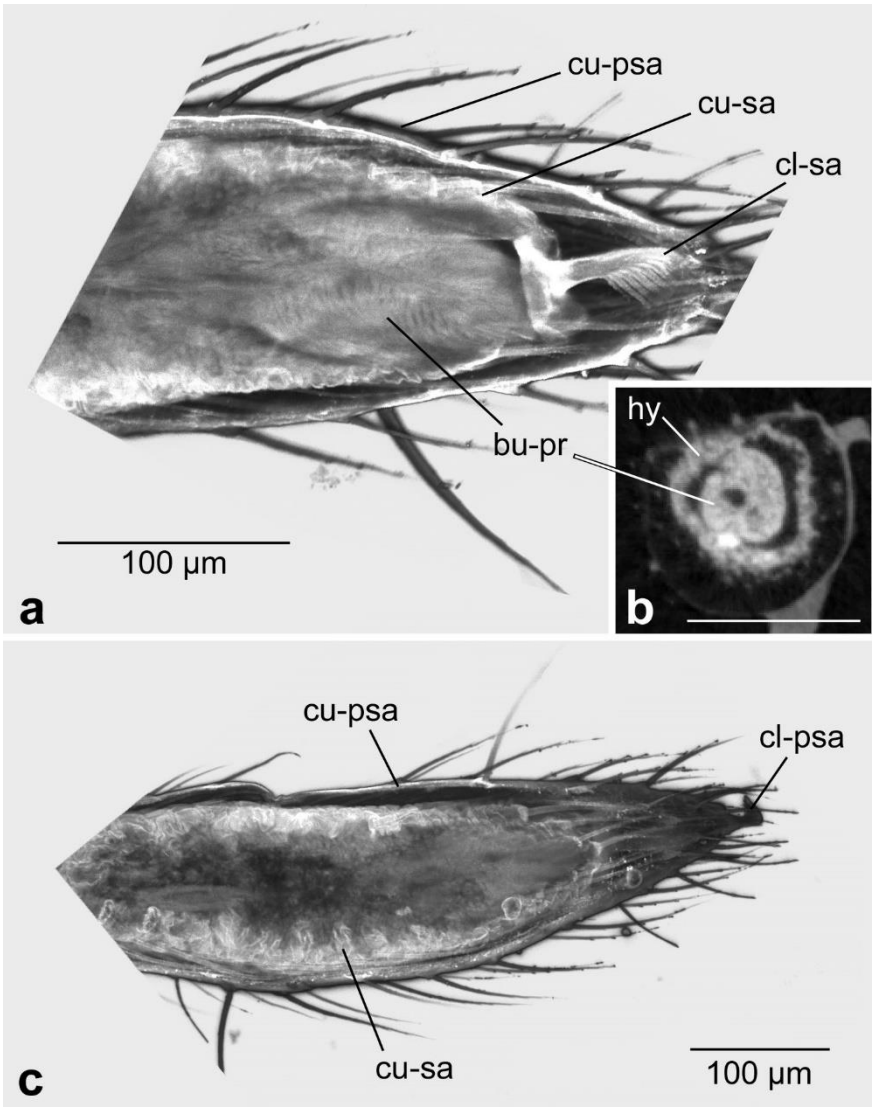

Figure 2. Formation of the bulb primordium at the pre-subadult stage. (a) Confocal LSM scan of the pedipalp tip. Distal is to the right. The ovoid primordium abuts the claw of the subadult cuticle that has already formed below the cuticle of the pre-subadult. (b) dice-µCT scan showing a cross-section roughly at the middle of the ovoid primordium. The primordium is internalised and surrounded by hypodermis. (c) Confocal LSM scan of the tarsus, distal to the right. The focal plane is set so as to show the wrinkled cuticle of the subadult beneath the smooth cuticle of the pre-subadult. Scale bar in all panels: 100 µm. Abbreviations: bu-pr, bulb primordium; cl-psa, claw of the pre-subadult; cl-sa, claw of the

subadult; cu-psa, cuticle of the pre-subadult; cu-sa, cuticle of the subadult; hy, hypodermis.

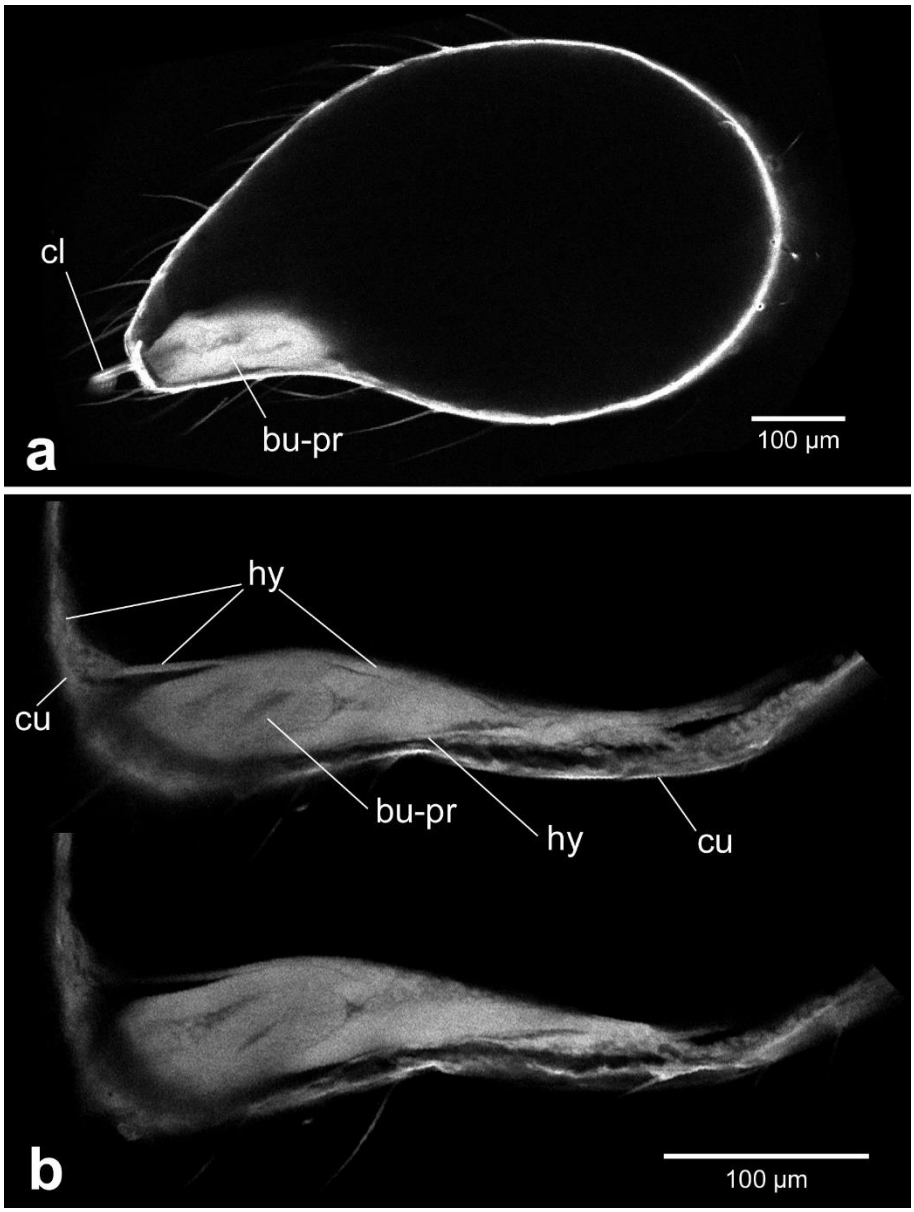

Figure 3. Inflation of the club at the beginning of the subadult stage. (a) Overview of the entire club. Confocal LSM scan. The bulb primordium occupies only a small portion within the club, the remaining club is inflated with haemolymph and this straightens out the

previously wrinkled subadult cuticle. (b) Two different focal planes of CLSM scan showing details of bulb primordium morphology. Distal is to the left in all panels. Scale bar: 100 µm in all panels. Abbreviations: bu-pr, bulb primordium; cl, claw; cu, cuticle; hy, hypodermis.

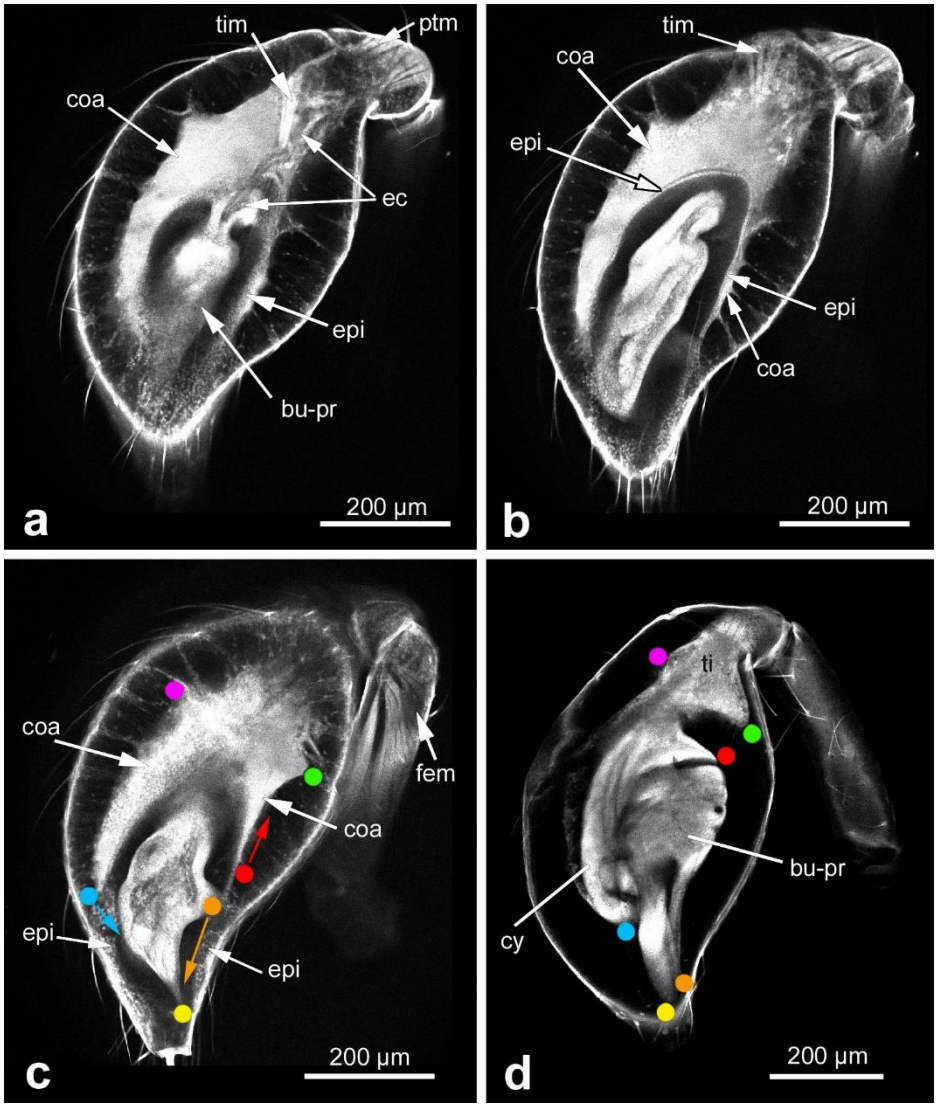

Figure 4. Morphogenesis of the bulb primordium at mid subadult stage. (a-c) Different focal planes of the same CLSM scan to show morphological details inside of the club. The club includes two segments, tibia and tarsus. The primordium undergoes further

differentiation and a structure of coagulated material is evident. (d) Club shortly before the end of the subadult stage. Important landmarks that help to understand morphogenetic movements between c and d are denoted by coloured dots. The most significant movements are indicated by coloured arrows in (c): the tip of the future cymbium rotates towards the bulb primordium (blue arrow), the ventral rim of the future haematodocha retracts proximally (red arrow), whereas the tip of the lateral protrusion (the future embolus) rotates and shifts distally to nestle to the future conductor (orange arrow). Scale bar: 200 µm in all panels. Abbreviations: bu-pr, bulb primordium; coa, coagulated material; cy, cymbium; ec, epidermal connection; epi epithelial hypodermis; fem, femoral muscles; mes, mesenchymal hypodermis; ptm, patellar muscles; ti, tibia; tim, tibial muscle.

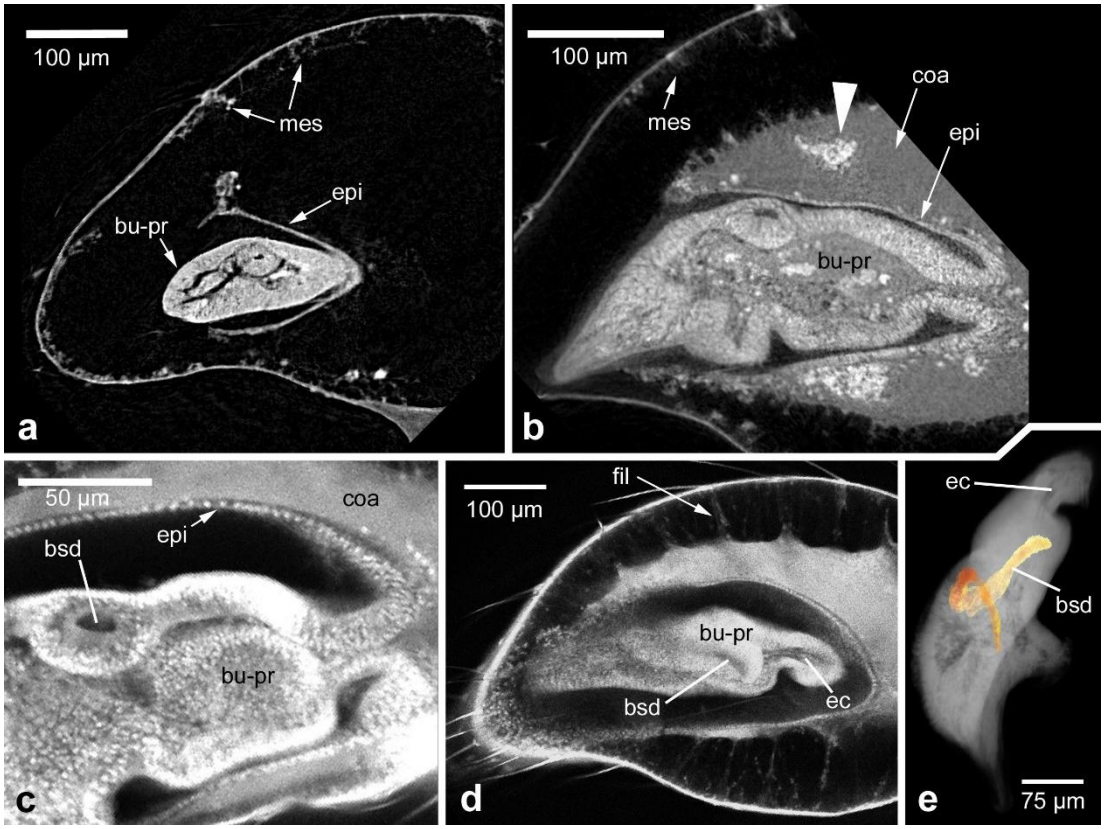

Figure 5. Morphological details within the developing pedipalp and bulb primordium. (a) Early subadult. dice-µCT scan. Distal is to the left in all panels except panel e (proximal up). The hypodermis is epithelial near the bulb primordium, but mesenchymal along the cuticle. (b) Mid subadult. dice-µCT scan. Coagulated material contains inclusions (arrowhead) that likely represent histoblast groups. (c-e) Details of the bulb primordium at mid subadult stage, CLSM scans. (c) Detail of the base of the bulb primordium, showing the epithelial lining below the coagulated material. A part of the blind sperm duct is visible in cross section. (d) Filaments are present between the body of the coagulated material and the mesenchymal hypodermis below the cuticle. The blind sperm duct is seen in sagittal section and a portion of the epidermal connection is visible (that leads through to the tibia, not included in this focal plane). (e) 3D reconstruction of the blind sperm duct

within the bulb primordium (coloured in orange). The other cavity that is visible is a portion of the epidermal connection to the tibia. Scale bars: 100 µm in a, b, d; 50 µm in c; 75 µm in e. Abbreviations: bsd, blind sperm duct; bu-pr, bulb primordium; coa, coagulated material; ec, epidermal connection; fil, filaments; epi, epithelial hypodermis; mes, mesenchymal hypodermis.

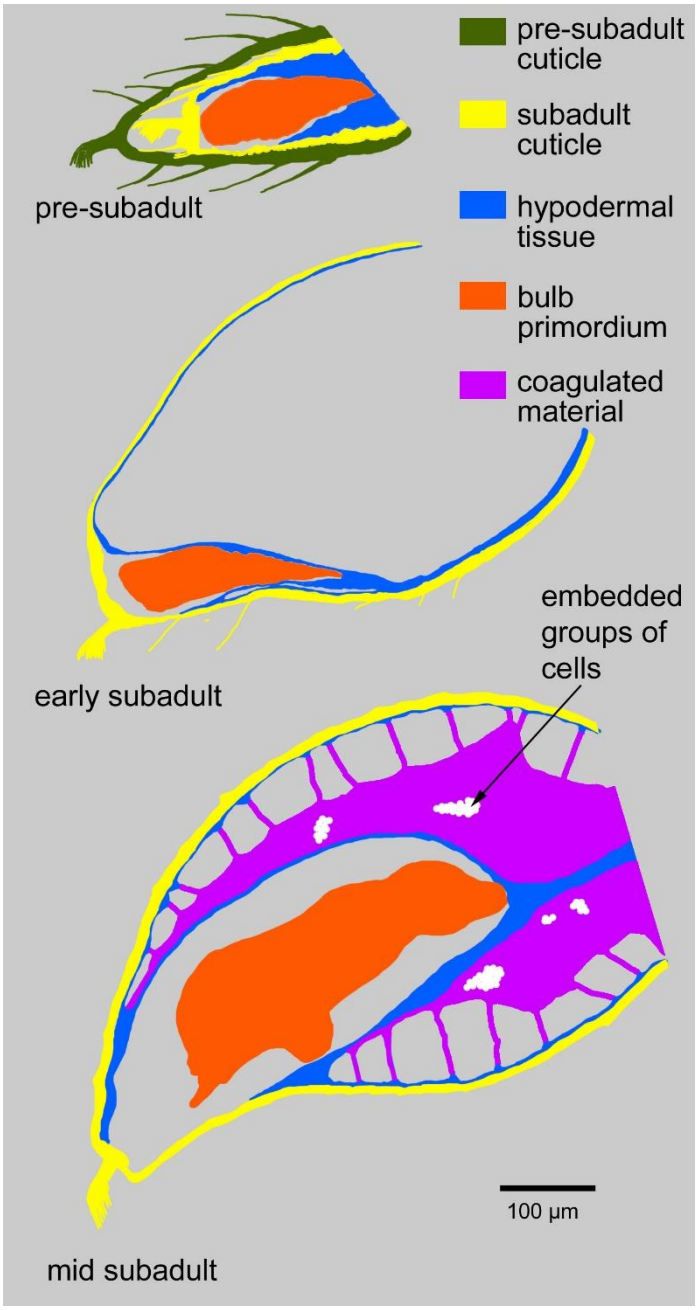

Figure 6. Schematic overview of the organisation of the distal end of the male pedipalp at the pre-subadult, early and mid subadult. Colours are explained in the figure. Scale bar: 100 µm.

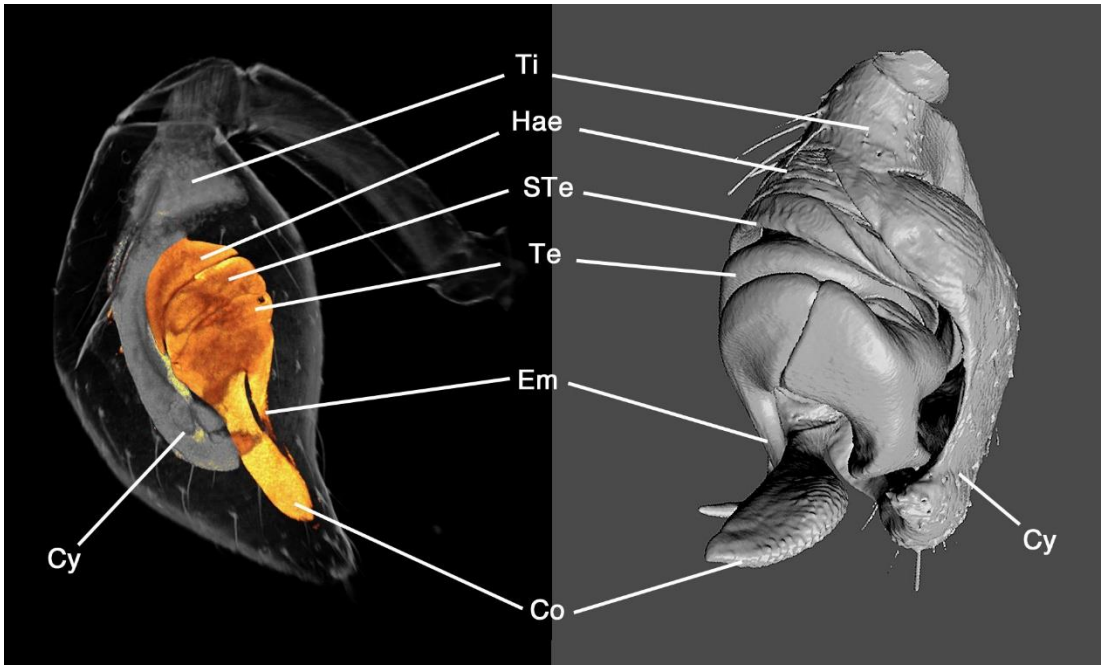

Figure 7. All principal components of the bulb are present at the late subadult stage. Left: Pedipalp club at the late subadult stage, CLSM scan. The bulb primordium is denoted in orange. Right: Adult pedipalp tip with bulb sclerites, 3D reconstruction of a CLSM surface scan. Lines connect corresponding structures. Abbreviations: Co, conductor; Cy, cymbium; Em, embolus; Hae, haematodocha; STe, Subtegulum; Te, tegulum; Ti, tibia.

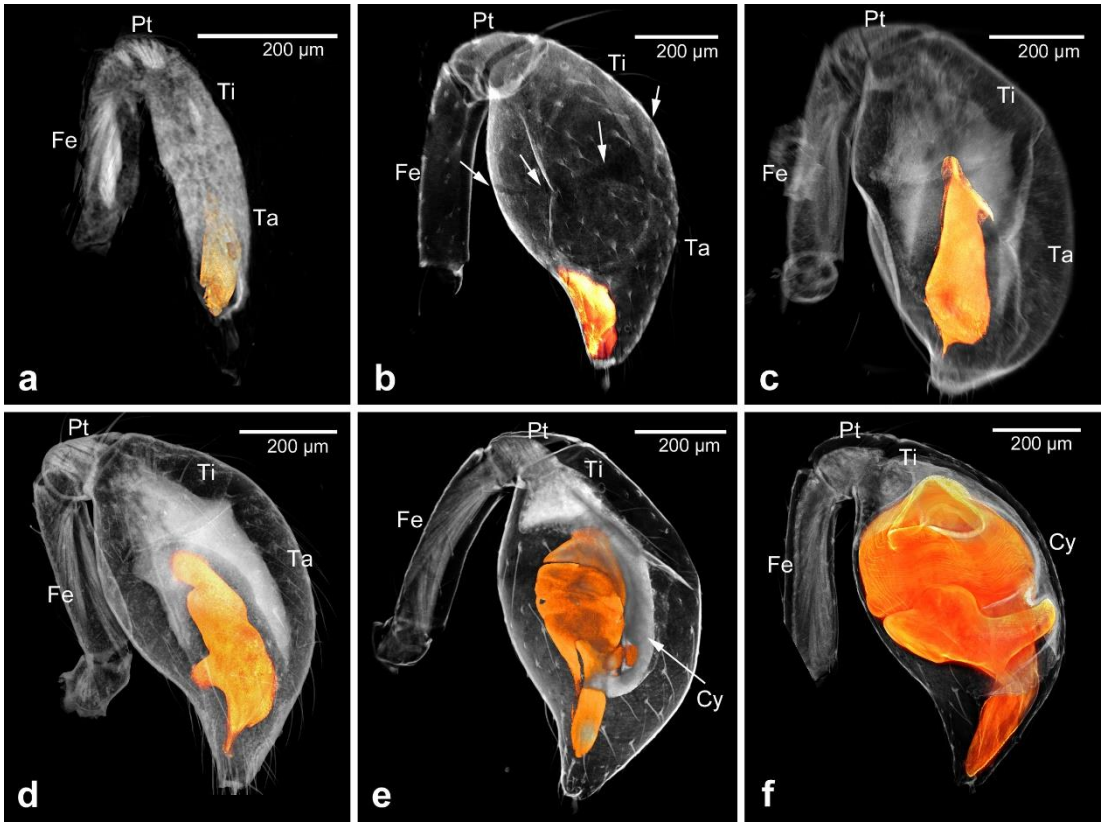

Figure 8. A staging scheme for the developing male copulatory organ. Confocal LSM scans; the bulb primordium is highlighted in orange in all panels. (a) Pre-subadult stage. (b) Early subadult stage. The arrows point to the remnant of the tibiotarsal joint in the inflated cuticle. (c, d) Successive mid subadult stage pedipalps. (e) Late subadult stage. (f) Subadult shortly before the ultimate moult. Scale bars: 200 µm in all panels. Abbreviations: Cy, cymbium; Fe, femur; Pt, patella; Ta, tarsus; Ti, tibia.

4. Discussion

Spiders are an interesting object for research into morphological diversity, because their body plan includes several unique and highly diverse morphological features and thus spiders provide many opportunities to study morphological novelties. Tracing from marine ancestors, spiders have adapted to a terrestrial lifestyle independent from the insects. Many of the adaptations of spiders to life on land involve the shape and function of their appendages. From these appendage modifications, the transformation of the tarsal tip of the male pedipalp into an intromittent organ, the bulbus organ, is particularly interesting. Being an autapomorphy for spiders (*i.e.* a distinctive feature that is unique to a given taxon) the bulbus' role as intromittent organ for sperm transfer on land accounts for a large part of their evolutionary success. It is derived from a system of spermatophor transfer which is still visible in the coenospermia in recent basal branching taxa (Alberti and Michalik 2004). As described in the introduction, the bulbus organ made sperm transfer more reliable, faster and introduced a prezygotic isolation which could accelerate speciation.

Despite the interest in the evolution of the bulbus organ, no consistent hypothesis for the origin and evolution could be proposed yet. A reason for this seems to be the lack of detailed morphological data for the full ontogenesis, covering the beginning of bulbus development until the adult structure. In addition to this lack of data, the shape of the sclerites of the male pedipalp bulbus organ is species-specific, at least in higher spiders. Therefore, their morphology and function is highly diverse, and this makes homology statements between the sclerites of different spider groups quite difficult. In this study I devised a combination of modern three-dimensional imaging and classic histological techniques to investigate the full ontogenesis of the bulbus organ of *P. tepidariorum* in detail. During my work it became clear

that understanding the adult morphology is prerequisite for comprehending postembryonic development. With *P. tepidariorum* being an emerging model system, the data aquired in the present study will allow the first investigations of the developmental genetics of the bulbus organ.

Summary adult morphology

My data on the adult morphology of the bulbus organ of *P. tepidariorum* showed that the fundament of the pedipalp tip is the cymbium that gives rise to the bulbus organ and that at the same time holds this organ in place when not in use. The bulbus itself comprises a "fleshy" portion that is sac-shaped and supports a number of heavily-sclerotised sclerites on its surface. Generally, it has a tripartite structure which is built of the subtegulum, tegulum and the embolic section. The embolic section gives rise to the sclerites which are involved in the connection and penetration of the female during the copulatory act. The sclerites are namely the embolus, the theridioid tegular apophysis and the median apophysis. As discussed in chapter 3.4., the present study revealed that for two sclerites the homology hypotheses by Agnarsson and colleagues (2007) are likely to be incorrect. In this study the proper homology hypotheses have been stated and given the correct terms based on the nomenclature introduced by Agnarsson and colleagues (2007). The formerly named conductor is in fact the theridioid tegular apophysis, and the proximal embolus is really the median apophysis. All these sclerites are linked by four connective membranes, the basal and median haematodocha, the embolic membrane and a connective membrane. Inside of the bulbus organ I identified a spiral-shaped blind sperm duct accompanied by three glands, which are presumed to play a role during sperm ejaculation and nutrition (Foelix 2010). Especially interesting is the innervation of the bulbus organ of *P. tepidariorum*. A small nerve bundle

enters the bulb joined by a single blood vessel. This bundle projects into the tegulum were it builds one ganglion near the gland of the blind sperm duct and a second ganglion on the embolus base where it innervates at least one sensillum in the embolic membrane. This pattern is similar to the one described for *Philodromus cespitum* (Sentenská et al. 2017) and together with the innervation described for the bulbus organ of *Hickmania troglodytes* (Lipke et al. 2015) unequivocally rebuts the former assumption that the bulbus organ is a numb structure (Eberhard and Huber 2010).

Summary development

My investigations on the development of the bulbus organ of *P. tepidariorum* showed that the primordium of the bulbus organ is already built in the stage before the penultimate moult. The bulbus primordium forms from cells at the base of the claw of the subadult cuticle, *i.e.* the primordium comprises those cells that have previously segregated the subadult claw. In contrast to bulbus formation, cymbium and tibia are built differently in a process firstly described by us. In this process haemolymph coagulates roughly into the shape of the cymbium and tibia and subsquently contracts into a more defined form. Histoblast-like cell clusters seem to reorganize this material into the two segments in a processes similar to metamorphosis of insects. Therefore, formation and further development of the bulbus in *P. tepidariorum* strongly support the initial findings by Barrows (Barrows 1925) and Harm (Harm 1931; Harm 1934) that the bulbus originates from the so called claw fundament.

Hypothesis on the origin and evolution of the bulbus organ

The present study revealed that the bulbus primordium is built from the claw fundament and that the sensory organ in the adult bulbus lies in the embolic membrane. The combination of these two important findings led me to the reasoning that the whole tarsal tip and not only the claws (in the literature sometimes also called pretarsus) need to be taken into account when discussing the bulbus' evolutionary origin. The tarsal tip is built up by the claws and an arthrodial membrane. This arthrodial membrane encloses the proximal plate of the claw and allows it to move flexible in its articulation while preventing haemolymph outflow. In legs of the spider *Cupiennius salei* the tarsal tip's arthrodial membrane is equipped with sensory organs (Speck and Barth 1982; Seyfarth et al. 1985). According to Seyfarth and colleagues these sensory organs are a type of "internal joint receptors" lying beneath the membrane. These receptors serve as vibration- and proprioreceptors which give information about the position of the claws. Every joint of spider appendages is equipped with arthrodial membranes and some of these membranes are reinforced with so called arcuate sclerites (Clarke 1986). Legs of spiders are moved not only by muscles but additionally by haemolymph pressure (Anderson and Prestwich 1975). The reinforcement by arcuate sclerites probably plays an important role in these hydraulic systems (pers. comm. Jens Runge, Universität Rostock).

During the evolution of spiders the pedipalp was first used to directly transmit the spermophor into the female genital opening. It gradually transformed into a pipette aspirating sperm, storing it, penetrating the female genital opening and ejacultate the sperm into the spermatheca. In my hypothesis the claw evolved into the embolus and the arthodial membrane was enlarged. The evolution of sclerites, similar to the arcuate sclerites of leg joints of spiders, made the membranous sac more rigid and facillitated the evolution of a complex

hydraulic system. This hydraulic system allows directed movement of the sclerites to each other, thereby pushing the embolus into the female genital opening. These sclerites became the tegulum and subtegulum. The rest of the tarsus evolved into the cymbium, assuring the pedipalp's function prey handling and sensory perception remains intact, but also taking up an additional role by protecting the intricate copulatory organ while not in use. Evidence for this theory are the sensillae in the embolus membrane of *Philodromus cespitum* (Sentenská et al. 2017) and in *P. tepidariorum* which would be homologous to the proprioreceptors R19 or R20 in the tarsal membrane of the spider *Cupiennius salei* (Speck and Barth 1982; Seyfarth et al. 1985).

5. Outlook

My research on the development and adult morphology of the bulbus organ of *P. tepidariorum* has answered fundamental questions. The data on the development showed that the bulbus originates in the claw fundament, while tibia and cymbium are built from scratch through a newly discovered mechanism. This involves coagulation of haemolymph and reorganisation of the coagulated material by histoblast-like cell clusters. It was confirmed that the adult bulbus is built up in a tripartite way, as described by Agnarsson and colleagues (2007). The hitherto existing homology statements for two sclerites were corrected and the correct terms discussed. Furthermore, an innervation was found and a sensilla, which appears to be similar to that in the bulbus of *Philodromus cespitum* (Sentenská et al. 2017). Together these findings clearly show that a comprehensive analysis of the morphology over its ontogenesis yields deep insights. However, at the same time new questions arose which now must be answered with future research endeavours.

Serial-Block-Face-Imaging

Based on numerous histological studies it was assumed that the bulbus is a numb structure (Eberhard and Huber 2010). Since the configuration of the male and female copulatory organs is quite complex and they work comparable to a key-lock-system, it was argued that the alignment during sex without sensory feedback is quite complicated. Because of this, different researchers tried to identify an innervation (Osterloh 1922; Harm 1931; Lamoral 1973; Eberhard and Huber 1998) but nevertheless failed. The reason for this misinterpretation could be the complicated three-dimensional morphology of the bulbus, that the histological stains capable of differentiating nerve cells have failed to do so and that fixative does not infiltrate

easily into the bulbus (Eberhard and Huber 2010; Sentenská et al. 2017). However, detailed morphological analyses of the bulbus organ showed in contrast to former investigations that it is innervated, and sensory organs are indeed present (Lipke et al. 2015; Sentenská et al. 2017 and present study). During our investigation of the adult morphology of the bulbus of *P. tepidariorum* we realized that our sophisticated approaches to generate a high-resolution dataset were not able to resolve the full innervation scheme and some other remaining questions of microstructure, *e.g.* the microstructure of the glands. Serial-Block-Face-Imaging in a scanning-electron-microscope would be the technique of choice to tackle these problems. Investigations on the three-dimensional structure of spider spermatozoa of 3 µm diameter have shown results of stunning detail (Lipke, Hörnschemeyer, et al. 2014; Lipke, Ramírez, et al. 2014). In this technique a sample is prepared similar to samples for transmission-electron-microscopy (TEM) and the resulting resin block then mounted into a scanning-electron-microscope equipped with an ultramicrotome. The resin block face is imaged in high-detail followed by removal of an ultra-thin slice by the microtome in a recurring sequence. This setup allowed us to create a three-dimensional dataset with a voxel size of 32x32x80nm with around 7500 serial sections in collaboration with Dr. Jan Hegermann and Dr. Christoph Wrede of the Zentrale Forschungseinrichtung Elektronenmikroskopie, Medizinische Hochschule Hannover. Since the dataset was created in the end of 2018, I was not able to analyse and integrate it into my here represented work. However, superficial analyses already showed that it will give us deep insights into the microstructure of the bulbus and resolve the full innervation pattern.

Intraspecific variability

Spider copulatory organs are species-specific. They fit into each other in a very tight manner and therefore play an important role in prezygotic isolation (Eberhard and Huber 2010). Consequently, the shape of sclerites which connect to the female copulatory structures need to have a specific form which cannot be too variable. With this in mind, the question arises how spiders can speciate if there is so little space for variation. However, if variation exists it may serve as basis for speciation. Until now there has been no research if there is any variation of the male bulbus' sclerites or their female counterparts in or between populations. In my study on the copulatory organ of male *P. tepidariorum*, I show that we can capture the three-dimensional shape of these sclerites in high resolution with dice-CT. This method is non-destructive and can be applied to valuable museum and collection specimens without damage (Lenihan et al. 2014). To get population material, I was able to lend specimens of male *P. tepidariorum* from the arachnological collections of the CeNaK (Centrum für Naturkunde), Hamburg, curator Danilo Harms; the Museum für Naturkunde, Berlin, curator Jason Dunlop; and the Forschungsmuseum Koenig, Bonn, curator Bernhard Huber. These specimens originate from populations in Germany, Austria, Poland, Portugal and Brasil and where collected between 1895 and 2014. In most cases there has been only one male sampled per location, but escpecially the Poland, Portugal and Brasil samples comprise four or even more males. The provided samples represent a great variety of populations, different timepoints and geographical localities, and will give an impression of the morphologic variability of natural populations of male *P. tepidariorum*. The inbred laboratory line of *P. tepidariorum* available in our laboratory does not contain significant genetic variability, *i.e.* is almost isogenic, and therefore should not show variability of the bulbus sclerites. Therefore, it can serve as a control for statistical comparison with the specimens of natural populations, where

genetic variability is considerably higher. Moreover, I was able to get male specimens of the closely-related spiders *Parasteatoda lunata* and *P. simulans*, which will serve as outgroups in the shape analysis.

Most methods of shape analysis of phenotypic data rely on measurements or markers chosen and applied by researchers ("landmarks"). They are known under the term morphometry or geometric morphometry. Additionally, they use two-dimensional representations like photo- or micrographs as data and therefore have an inbuilt bias. During data acquisition it is nearly impossible to avoid or correct for tilt or problems of projection. Despite modern advances now make it possible to use three-dimensional data, these methods still rely on humans to choose and place the markers, so bias in form of human recognition of shape remains. Spherical harmonics (SPHARM) is a method to mathematically model three-dimensional shapes of morphological structures captured, *e.g.* by µCT (Shen et al. 2009). These mathematical models can then be analysed statistically with methods like principal component analysis (PCA), to extract the main components of shape change between samples. One major advantage of this method is that it relies only on few homologous landmarks to register the objects relative to each other (Shen et al. 2009). Moreover, the analysis can be performed in a free software suite (http://www.enallagma.com/SPHARM.php). This method has been successfully applied to analyse complex morphological structures, like damselfly genitalia, sinus-cavities of carnivores or pectoral girdles of fish (McPeek et al. 2009; Curtis and Van Valkenburgh 2014; Standen et al. 2014). With my ability to three-dimensionally capture the sclerites of the bulbus in high resolution, the acquired specimens from multiple populations and two outgroups, and SPHARM as readily available method, I will be able to analyse the intraspecific variability of the bulbus sclerites of *P. tepidariorum.*

Genetic mechanisms of the postembryonic development

The genetic mechanisms of the postembryonic development of the bulbus are virtually unknown. A differential transcriptome analysis revealed a set of candidate genes which showed a specific and high expression in the developing subadult male pedipalps, including a set of transcription factors with known roles in appendage or sex-specific development (Schomburg 2017). But how genetic networks pattern the primordium built in the presubadult stage or when and in which processes the revealed candidate genes are used is still not investigated.

For *P. tepidariorum* gene expression can be studied mainly by in-situ hybridisation. Because the development of the bulbus happens postembryonically, the tissues involved are built up of much more layers then embryos. Due to this fact I assume that classical staining with NBT/BCIP with subsequent transmission light microscopy will be insufficient to satisfactorily analyse the gene expression pattern. Therefore, I started to improve and optimize a protocol for fluorescent in-situ hybridisation. With this technique it is possible to hybridize at least two different gene products (mRNAs) with labelled RNA-probes which can then be marked with fluorescent tags of different colours. After tissue clearing these fluorescent tags can be three-dimensionally imaged with a confocal laser scanning microscope, revealing which cells express the investigated genes.

The function of the proposed candidate genes can be studied by a technique called RNA-interference (RNAi). This method uses an innate mechanism (also present in our spider model) that is important in the immune response to viruses and other foreign genetic material. It works systemically and can be used to efficiently knock-down gene products in juvenile

spiders. The resulting phenotype gives information on the function of the gene of interest during bulbus development.

6. References

Agnarsson I. 2004. Morphological phylogeny of cobweb spiders and their relatives (Araneae, Araneoidea, Theridiidae). Zool. J. Linn. Soc. 141:447–626.

Agnarsson I, Coddington JA, Knoflach B. 2007. Morphology and Evolution of Cobweb Spider Male Genitalia (Araneae, Theridiidae). J. Arachnol. 35:334–395.

Alberti G, Michalik P. 2004. Feinstrukturelle Aspekte der Fortpflanzungssysteme von Spinnentieren (Arachnida). Denisia 0012:1–62.

Albo MJ, Costa FG. 2017. Female wolf spiders exert cryptic control drastically reducing ejaculate size.Hebets E, editor. Ethology 123:659–666.

Anderson JF, Prestwich KN. 1975. The fluid pressure pumps of spiders (Chelicerata, Araneae). Zeitschrift für Morphol. der Tiere 81:257–277.

Angelini DR, Kaufman TC. 2005. Insect appendages and comparative ontogenetics. Dev. Biol.

Austad SN. 1984. Evolution of sperm priority patterns in spiders. In: Smith RL, editor. Sperm Competition and the Evolution of Animal Mating Systems. Academic Press Inc. p. 223–250.

Barrows WM. 1925. Modification and Development of the Arachnid Palpal Claw, with Especial Reference to Spiders. Ann. Entomol. Soc. Am. 18:483–525.

Bhatnagar RDS, Rempel JG. 1962. Structure, function, and postembryonic development of male and female copulatory organs of black widow spider Latrodectus Curacaviensis (Müller). Can. J. Zool. 40:465–510.

Bhatnagar RDS, Sadana GL. 1971. Morphogenesis of the tarsal tissue and the development of the intromittent palpal organs in the wolf-spider Lycosa chaperi (Simon) (Araneida: Lycosidae). Can. J. Zool. 49:397–400.

Clarke J. 1986. The comparative functional morphology of the leg Joints and Muscles of Five Spiders. Bull. Br. Arachnol. Soc. 7:37–47.

Coddington JA. 1990. Ontogeny and Homology in the Male Palpus of Orb Weaving Spiders and their Relatives, with Comments on Phylogeny (Araneoclada: Araneoidea, Deinopoidea). Smithson. Contrib. to Zool. 496:1–52.

Curtis AA, Van Valkenburgh B. 2014. Beyond the Sniffer: Frontal Sinuses in Carnivora. Anat. Rec. 297:2047–2064.

References

Dunlop JA, Webster M. 1999. Fossil evidence, terrestrialization and arachnid phylogeny. J. Arachnol. 27:86–93.

Eberhard WG, Huber BA. 1998. Possible links between embryology, lack of innervation, and the evolution of male genitalia in spiders. Bull. Br. Arachnol. Soc. 11:73–80.

Eberhard WG, Huber BA. 2010. Spider Genitalia - Precise Maneuvers with a Numb Structure in a Complex Lock. In: Leonard J, Cordoba-Aguilar A, editors. The Evolution of Primary Sexual Characters in Animals. New York: Oxford University Press. p. 249–284.

Foelix R. 2010. The Biology of Spiders. Third edit. Oxford University Press

Gassmann F. 1925. Die Entwicklung des Männlichen Spinnentasters, dargestellt an Leptyphantes nebulosus Sund. Zeitschrift für Morphol. und Ökologie der Tiere 5:98–118.

Harm M. 1931. Beiträge zur Kenntnis des Baues, der Funktion und der Entwicklung des akzessorischen Kopulationsorgans von Segestria bavarica c. l. koch. Zeitschrift für Morphol. und Ökologie der Tiere 22:629–670.

Harm M. 1934. Bau, Funktion und Entwicklung des akzessorischen Kopulationsorgans von Evarcha marcgravi Scop. Zeitschrift Für Wissenschaftliche Zool. 146:123–134.

Haupt J. 2002. The palpal organ of male spiders (Arachnida, Araneae). Eur. Arachnol.:65–71.

Hoekstra RF. 1987. The evolution of sexes. In: Stearns Stephen C., editor. The Evolution of Sex and its Consequences. Basel: Birkhäuser Basel. p. 59–91.

Huber BA. 1994. Funktion und Evolution komplexer Kopulationsorgane. Eine Analyse von Schnittserien durch in copula schockfixierte Spinnen. Mitt. dtsch. Ges. allg. angew. Entomol. 9:2–4.

Huber BA. 2004. Evolutionary transformation from muscular to hydraulic movements in spider (Arachnida, Araneae) genitalia: a study based on histological serial sections. J. Morphol. 261:364–376.

Lamoral BH. 1973. On the morphology, anatomy, histology and function of the tarsal organ on the pedipalpi of Palystes castaneus (Sparassidae, Araneida). Ann. Natal Museum 21:609–648.

Lasker R, Theilacker GH. 1962. Oxygen Consumption and Osmoregulation by Single Pacific Sardine Eggs and Larvae (Sardinops caerulea girard). ICES J. Mar. Sci. 27:25–33.

Lenihan J, Kvist S, Fernández R, Giribet G, Ziegler A. 2014. A dataset comprising four micro-computed tomography scans of freshly fixed and museum earthworm specimens. Gigascience 3:6.

References

Lipke E, Hammel JU, Michalik P. 2015. First evidence of neurons in the male copulatory organ of a spider (Arachnida, Araneae). Biol. Lett. 11:20150465.

Lipke E, Hörnschemeyer T, Pakzad A, Booth CR, Michalik P. 2014. Serial Block-Face Imaging and its Potential for Reconstructing Diminutive Cell Systems: A Case Study from Arthropods. Microsc. Microanal.:1–10.

Lipke E, Ramírez MJ, Michalik P. 2014. Ultrastructure of spermatozoa of orsolobidae (Haplogynae, Araneae) with implications on the evolution of sperm transfer forms in Dysderoidea. J. Morphol. 275:1238–1257.

McPeek MA, Shen L, Farid H. 2009. The correlated evolution of three-dimensional reproductive structures between male and female damselflies. Evolution (N. Y). 63:73–83.

Michalik P, Aisenberg A, Postiglioni R, Lipke E. 2013. Spermatozoa and spermiogenesis of the wolf spider Schizocosa malitiosa (Lycosidae, Araneae) and its functional and phylogenetic implications. Zoomorphology 132:11–21.

Osterloh A. 1922. Beiträge zur Kenntnis des Kopulationsapparates einiger Spinnen. Zeitschrift Für Wissenschaftliche Zool. 119:326–421.

Parker GA. 1984. Sperm Competition and the Evolution of Animal Mating Strategies. In: Robert L. Smith, editor. Sperm Competition and the Evolution of Animal Mating Systems. Elsevier. p. 1–60.

Parker GA. 2011. The origin and maintenance of two sexes (anisogamy), and their gamete sizes by gamete competition. In: Togashi T, Cox PA, editors. The Evolution of Anisogamy: A Fundamental Phenomenon Underlying Sexual Selection. Cambridge: Cambridge University Press. p. 17–74.

Parker GA, Baker RR, Smith VGF. 1972. The origin and evolution of gamete dimorphism and the male-female phenomenon. J. Theor. Biol. 36:529–553.

Pechmann M, Khadjeh S, Sprenger F, Prpic N-M. 2010. Patterning mechanisms and morphological diversity of spider appendages and their importance for spider evolution. Arthropod Struct. Dev. 39:453–467.

Pechmann M, Prpic N-M. 2009. Appendage patterning in the South American bird spider Acanthoscurria geniculata (Araneae: Mygalomorphae). Dev. Genes Evol. 219:189–198.

Prpic N-M, Damen WGM. 2004. Expression patterns of leg genes in the mouthparts of the spider Cupiennius salei (Chelicerata: Arachnida). Dev. Genes Evol. 214:296–302.

References

Prpic N-M, Damen WGM. 2008. Arthropod appendages: a prime example for the evolution of morphological diversity and innovation. In: Minelli A, Fusco G, editors. Evolving Pathways: Key Themes in Evolutionary Developmental Biology. Cambridge: Cambridge University Press. p. 381–398.

Prpic N-M, Damen WGM. 2009. Notch-mediated segmentation of the appendages is a molecular phylotypic trait of the arthropods. Dev. Biol. 326:262–271.

Sadana GL. 1971. Studies in the Postembryonic Development of the Palpal Organ of Lycosa chaperi Simon (Lycosidae : Araneida). Zool. Anz. 186:251–258.

Schomburg C. 2017. Developmental Studies on Eye Types and Pedipalps in Parasteatoda tepidariorum.

Sentenská L, Müller CHG, Pekár S, Uhl G. 2017. Neurons and a sensory organ in the pedipalps of male spiders reveal that it is not a numb structure. Sci. Rep. 7:12209.

Seyfarth EA, Eckweiler W, Hammer K. 1985. Proprioceptors and sensory nerves in the legs of a spider, Cupiennius salei (Arachnida, Araneida). Zoomorphology 105:190–196.

Sharma PP. 2018. Chelicerates. Curr. Biol. 28:R774–R778.

Sharma PP, Kaluziak ST, Pérez-Porro AR, González VL, Hormiga G, Wheeler WC, Giribet G. 2014. Phylogenomic interrogation of arachnida reveals systemic conflicts in phylogenetic signal. Mol. Biol. Evol. 31:2963–2984.

Shen L, Farid H, McPeek MA. 2009. Modeling three-dimensional morphological structures using spherical harmonics. Evolution (N. Y). 63:1003–1016.

Speck J, Barth FG. 1982. Vibration sensitivity of pretarsal slit sensilla in the spider leg. J. Comp. Physiol. A 148:187–194.

Standen EM, Du TY, Larsson HCE. 2014. Developmental plasticity and the origin of tetrapods. Nature 513:54–58.

Thomas RH, Zeh DW. 1984. Sperm Transfer and Utilization Strategies in Arachnids: Ecological and Morphological Constraints. In: Smith R, editor. Sperm Competition and the Evolution of Animal Mating Systems. Elsevier. p. 179–221.

Töpperwien M, Krenkel M, Quade FSC, Salditt T. 2016. Laboratory-based x-ray phase-contrast tomography enables 3D virtual histology.Khounsary AM, van Dorssen GE, editors. Proc. SPIE 9964:99640I.

References

Uhl G. 1993. Sperm storage and repeated egg production in female Pholcus phalangioides Fuesslin (Araneae). Bull. la Société neuchâteloise des Sci. Nat. 116:245–252.

Vöcking O, Uhl G, Michalik P. 2013. Sperm Dynamics in Spiders (Araneae): Ultrastructural Analysis of the Sperm Activation Process in the Garden Spider Argiope bruennichi (Scopoli, 1772). PLoS One 8:e72660.

World Spider Catalog (2018). World Spider Catalog. Version 19.5. Natural History Museum Bern, online at http://wsc.nmbe.ch, accessed on December 2018. doi: 10.24436/2